MICROWAVE PHOTONIC FILTER DESIGN VIA OPTICAL FREQUENCY COMB SHAPING

A Dissertation

Submitted to the Faculty

of

Purdue University

by

Minhyup Song

In Partial Fulfillment of the

Requirements for the Degree

of

Doctor of Philosophy

December 2012

Purdue University

West Lafayette, Indiana

This dissertation is dedicated to my parents, to my parents in law, to my dear children, and to my lovely wife.

ACKNOWLEDGMENTS

Firstly, I would like to express my deepest appreciation to my advisor Professor Andrew M. Weiner for his guidance, encouragement, and support throughout my graduate study at Purdue. Without his guidance I would not get a chance to work in the exciting area of microwave photonics and realize any of research achievements reported in this dissertation. I also would like to thank my committee members, Professor Minghao Qi, Professor Dimitrios Peroulis, and Professor Alexandra Boltasseva for their support during the course of this research.

I am deeply thankful to my former and current colleagues in Ultrafast Optics and Optical Fiber Communication Laboratory. Dr. Daniel E. Leaird helped me to start the lab work and gave me technical support with valuable discussions. Dr. Chris M. Long and Dr. Ehsan Hamidi taught me a lot when I joined the group and first started the microwave photonic filtering research. My special thanks go to Dr. Victor Torres-Company and Dr. Dongsun Seo for their collaborations and generous discussions on various topics. I also acknowledge a lot of fruitful discussions with Santiago Tainta, Jian Wang, Rui Wu, Joseph Lukens, Amir Rashidinejad, Pei-Hsun Wang, Andrew J. Metcalf, and Yihan Li.

Finally, I would be grateful to my family and my friends for their continuous support and understanding.

TABLE OF CONTENTS

Page

Page

LIST OF TABLES

Table Page

LIST OF FIGURES

Figure Page

Figure Page

Figure Page

Figure Page

Figure Page

LIST OF ABBREVIATIONS

ASE: Amplified spontaneous emission
AWG: Arbitrary waveform generator
BER: Bit error rate
BW: Bandwidth
CFBG: Chirped fiber Bragg grating
CW: Continuous wave
DCF: Dispersion compensating fiber
DPSK: Differential phase shift keying
EDFA: Erbium doped fiber amplifier
FIR: Finite impulse response
FT: Fourier transform
FSR: Free spectral range
FWHM: Full width at half maximum
GDR: Group delay ripple
HNLF: Highly non-linear fiber
IF: Intermediate frequency
IM: Intensity modulator
LCM: Liquid crystal modulator
MWP: Microwave photonics
MZ: Mach-Zehnder
O/E: Optical-to-electrical
OFC: Optical frequency combs
OSA: Optical spectrum analyzer
PD: Photo detector, or Photodiode
PM: Phase modulator
RF: Radio frequency
SLM: Spatial light modulator
SLS: Sidelobe suppression

SMF: Single mode fiber
SNR: Signal-to-noise ratio
SSB: Single sideband
TBWP: Time-bandwidth product
UWB: Ultra-wideband
VIPA: Virtually imaged phased array
VNA: Vector network analyzer

ABSTRACT

Song, Minhyup. Ph.D., Purdue University, December 2012. Microwave Photonic Filter Design via Optical Frequency Comb Shaping. Major Professor: Andrew M. Weiner.

The field of microwave photonics (MWP), where the wideband and low-loss capability in optics is utilized to enhance the performance of radio frequency (RF) systems, has been significantly explored over the last decades. This perspective offers benefits that are unattainable with conventional electronics solutions, such as ultra-broad bandwidth, insensitivity to electromagnetic interference, transport through optical fiber networks, easy tuning control, or programmability. One important application of microwave photonics is the implementation of microwave filters for high carrier frequency and wide bandwidth RF waveform. In this thesis, MWP filters based on an optical frequency combs (OFCs) and a dispersive medium are presented. First, noise evaluation of MWP filters based on OFCs is explored to show the potential of optical frequency comb technology to operate over large distances in MWP filter links. Then, amplitude and phase control complex coefficient taps MWP filters are presented. We demonstrate reconfigurable and tunable flat-top MWP filters by applying positive and negative weights across the comb lines and adding a phase ramp onto the tap weights. Furthermore the application of this technique to phase filtering operation over an ultra-wide bandwidth will be demonstrated through high-speed real-time measurement. We present the implementation of matched filter to compress the chirped pulses to their bandwidth limited duration. We also explore the group delay ripple (GDR) compensation of chirped fiber Bragg grating (CFBG) which would reduce the delay of MWP filter links.

1. INTRODUCTION

1.1. Overview

Microwave photonic techniques have been developed to enhance the performance of ultra-broadband radio-frequency system [1]. The use and advantages of microwave photonics have been described in various references in the literature [1-4]. The idea of photonic processing is based on optical processing of broadband analog RF signals in optical domain [1]. Here, the RF input signal is modulated onto the optical source, and the signal processing takes place in the optical domain. After optical-to-electrical (O/E) conversion in a photodetector (PD), the optical source will be detected, resulting in output RF signal. In the last few years, extensive efforts of microwave photonic researches have been directed to the implementation of broad bandwidth microwave signal processing especially to filter design [2]. Our research till date has focused on development work on microwave photonic amplitude and phase control filter designs, which are the main theme of this dissertation. In order to understand our original approach for the process of microwave photonic filters, it is necessary to have an understanding of optical frequency combs (OFCs) and pulse shaping.

Microwave photonic filters are mainly focused on a multi-tap geometry based on the notions of finite impulse response digital filter design [5]. On the other hand, thanks to their ultra-low phase-noise performance, optical frequency combs are becoming ubiquitous tools in precise optical metrology applications like spectroscopy, etc. High-repetition rate optical frequency combs which have discrete spectral lines with fixed frequency positions are chosen as multi-wavelength optical source for microwave photonic filters. To this effect, we will briefly talk about optical frequency combs in section 1.2. In section 1.3 we will describe in detail the principles of spectral line-by-line pulse shaping which enables the synthesis of complex coefficient taps by programming

amplitude and phase of each line, which is a topic that is gaining increasing attention. We also will briefly describe the theoretical principle and configuration of multi tap microwave photonic filters in section 1.4 so that any future reference to it will be clearer. Section 1.5 provides a general organization of this dissertation.

1.2. Optical Frequency Combs (OFCs)

An optical frequency comb is a pulsed laser source producing periodic optical pulses with a stabilized repetition rate [6,7]. The spectrum of such a pulse train is a discrete set of frequencies spaced by a constant repetition rate (the inverse of the pulse train period). This series of sharp spectral lines is called a frequency comb. Such combs have enabled new signal processing application in microwave photonics [1], optical arbitrary waveform generation [8], and optical communications [9].

Traditionally, optical frequency combs have been derived from mode-locked lasers which emit a series of short pulses separated in time by the round trip time of the laser cavity. Figure 1.1(a) shows an ideal comb: all lines are having the same amplitude and phase with an infinite bandwidth. Mode locked laser combs have Gaussian envelope due to the gain profile, as shown in Fig. 1.1(b), with all the lines in phase. Figure 1.1(c) shows the corresponding time domain trace to the comb. In reality, comb lines are not exact multiples of the repetition rate due to the difference between phase and group velocities within the laser media, resulting in a frequency offset illustrated in Fig. 1.1(b). The realistic comb lines are given by the equation [6]

$$f_m = mf_{rep} + \varepsilon \tag{1.1}$$

where $m f_{rep}$ is multiples of the laser repetition rate and ε is known as the carrier envelope offset frequency, whose value can undergo large fluctuation without stabilization mechanisms.

However, the mode-locked frequency comb has limited tuning ability, complicated feedback control, and frequency instability at relatively high repetition rates. Due to this reason, there has been significant development of alternative frequency comb sources [10-14]. Applying a strong sinusoidal phase modulation to a CW laser can generate multiple sidebands, leading to generation of a frequency comb [10-12]. When an input

pulse is applied to a strong and quadratically varying temporal phase, it undergoes time-to-frequency mapping, so that the shape of the spectrum becomes a scaled replica of the temporal intensity profile of the input waveform.

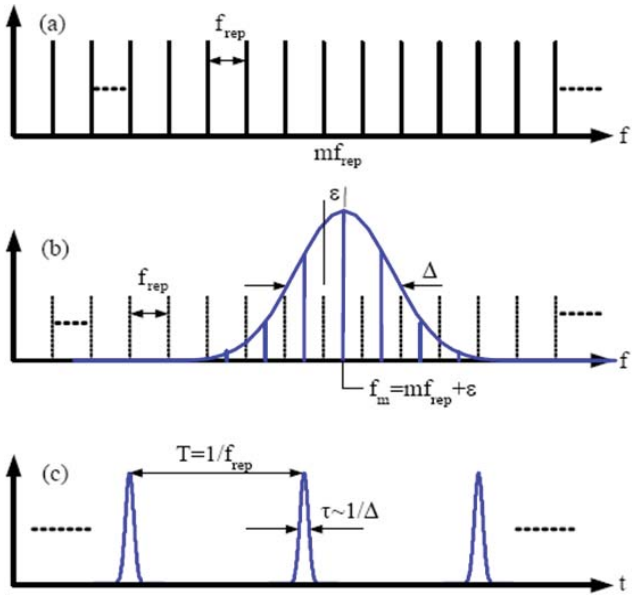

Fig. 1.1 (a) Ideal frequency comb, (b) Frequency comb from a mode locked laser with a Gaussian envelope, (c) Time domain pulse from a mode locked laser

Figure 1.2 shows the process to generate flat optical frequency combs from a continuous-wave laser. An intensity modulator driven with a sinusoid generates flat-topped pulse, and it is subjected to a strong sinusoidal phase modulation by phase modulator, which results in a flat comb due to the flat topped pulse input. Advantage of this frequency combs include the ability to create high repetition rate (for e.g. 10s of GHz corresponding to the interesting data rates regime in optical communication) combs with stable optical center frequencies and convenient tuning of the repetition rate and optical center frequency. In this dissertation, all the frequency comb sources which we use in our work are obtained by phase modulating a continuous wave laser (PMCW).

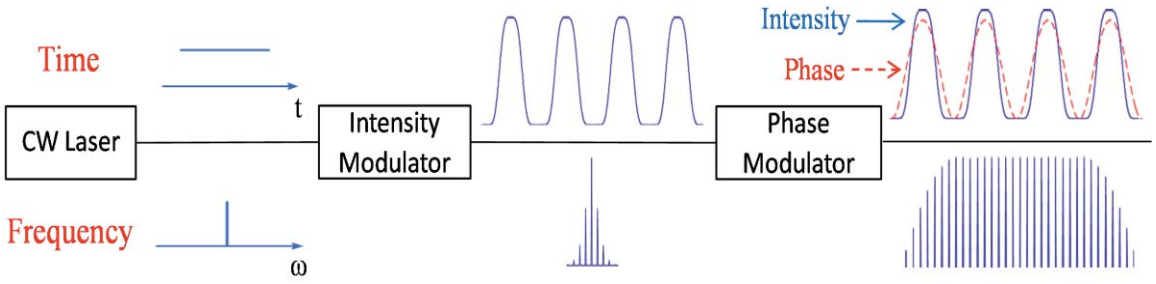

Fig. 1.2 Schematic of frequency combs generated by phase modulation using the cascaded intensity modulator (IM) and phase modulator (PM) (adapted from [12])

1.3. Spectral Line-by-line Pulse Shaping

As we described in the previous section, an optical comb consists of an equally spaced set of narrow-linewidth optical taps, in which both the frequency spacing and the absolute frequencies remain approximately constant. By using an optical comb, we are able to exploit pulse shaping to address the amplitudes and phase of comb lines. Current pulse shaping can be divided into two approaches: Direct space-to-time (DST) pulse shaping and Fourier transform (FT) pulse shaping. In DST pulse shaping [15,16], output waveforms are directly scaled by applied spatial masks. In FT pulse shaping case, output waveforms are Fourier transform of shaped optical spectra [17]. Figure 1.3(a) shows the basic FT pulse shaping apparatus which consist of spectral dispersers (for e.g. diffraction gratings), lenses, a mask, and a modulator array. The individual frequency components are spread angularly by the first diffraction grating, and then focused at the back focal plane of the first lens to spatially separate them in one dimension. Then the amplitude and phase of the spatially dispersed frequency components are manipulated by the modulator array. After the optical frequencies are recombined by the second lens and grating, the shaped output pulse is obtained. The Fourier transform of the complex pattern transferred by the masks onto the optical spectrum result in programmable user-defined waveforms.

To realize microwave photonic filters composed of complex coefficient taps, independent amplitude and phase control of each taps in OFCs is required. However, due to difficulty in building a pulse shaper capable of resolving each spectral line at <1 GHz repetition rate of optical combs generated by mode-locked lasers, taps are manipulated as groups of spectral lines. In achieving line-by-line control, pulse shaper design also needs

great care for spectral resolution improvement. Figure 1.3(b) schematically shows the line by-line pulse shaping regime, which is experimentally demonstrated [18]. Potential applications of line-by-line pulse shaping include microwave photonics as well as optical arbitrary waveform generation (OAWG) [19].

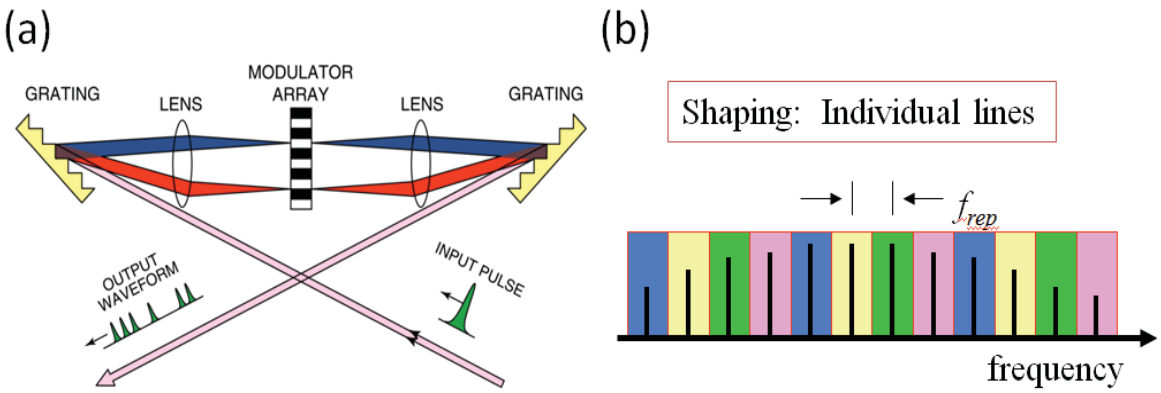

Fig. 1.3 (a) FT pulse shaper based on diffraction gratings (adapted from [17]), (b) Pulse shaping in line-by-line regime (adapted from [18])

1.4. Multi-tap Microwave Photonic (MWP) Filters

Microwave filter design has been conventionally focused on implementation of electrical filters in communication and radar systems. Here we briefly review the current microwave filter technology.

Most microwave filters are made up of one or more coupled resonators, and the high suppression, sharp filters require high order filter which results in high loss. In order to overcome high loss, the high temperature superconductors have applied to implement low loss, highly selective filters [20]. The tunable microwave filters have been achieved by applying Micro-Electro-Mechanical Systems (MEMS) technology. Since the mechanical varactor shows higher quality factors than electrical varactor, highly selective, tunable filters can be obtained with small number of poles through MEMS technique [21].

Although there have been significant advances, still there are desired filter properties such as filter selectivity, tunability, programmability, and noise figure that can't be achieved simultaneously. Microwave photonic filters offer such properties over a large

bandwidth compared to conventional RF filters [3]. In contrast to recent work on microwave photonic filters based on coherent optical filters [22,23], most microwave photonic filters are based on a multi-tap delay line scheme. Tapped-delay-line microwave photonic filters are based on the concept of discrete finite impulse response (FIR) filter [5]. Conventionally, there are two possible approaches to making multi-tap delay lines: those which a continuous wave (CW) laser source with a number of delay lines and those which multiple different wavelength optical sources with a single dispersive delay line [3]. Much of the early work used multiple physical delay lines, which is difficult to control and program. As a result, there has been increasing interest in implementing filters using the second approach. By equally spacing of the carriers in frequency, taps with equal delay spacing will be obtained after a dispersive medium [24].

Fig. 1.4 shows the overall configuration of multi-tap microwave photonic (MWP) filters based on second approach. The RF signal (red line) is modulated over an optical source comprising multiple optical frequencies (blue line) and passed through a pulse shaper to program amplitude and phase of each tap, which are proportional to the corresponding carrier. Each optical carrier experiences a frequency dependent delay by the medium dispersion, resulting in multiple optical delay lines. By applying equally spaced carriers in frequency and a linear dispersion medium, taps with equal delay spacing will be obtained. The output of the delay line is connected to a photodiode to convert the optical signal to an electrical signal. According to FIR digital filter design algorithm, a finite number of delay taps shows the periodic filter response in frequency domain [5]. The resulting filter impulse response can be written as

$$h(t) = \sum_{n=0}^{N-1} a_n \, \delta(t - nT) \tag{1.2}$$

where a_n's are the taps complex coefficients, and T is the differential delay between taps, determined by the group delay dispersion and the frequency spacing between optical carriers. By Fourier transformation of the impulse response we obtain the frequency response of the filter as

$$H(\omega) = \sum_{n=0}^{N-1} a_n \exp\left[-j\, n\, \omega T\right] \tag{1.3}$$

From (1.3) the filter transfer function has a periodic spectral characteristic as shown in Fig 1.5. The filter period known as free spectral range (FSR) is inversely proportional to the tap delay spacing T and the filter bandpass shape governed by adjusting the taps' weights. Figure 1.5 shows the approximately Gaussian shape passband derived by the Fourier transform of the Gaussian shape impulse response shown in Fig. 1.4. The filter sidelobe suppression (SLS) showing the filter rejection of nonadjacent channels is mainly affected by the shape and fluctuation of taps. We will introduce various multi-tap microwave photonic filters such as programmable tunable amplitude-control and phase-control filters in chapter 3 and chapter 4 respectively.

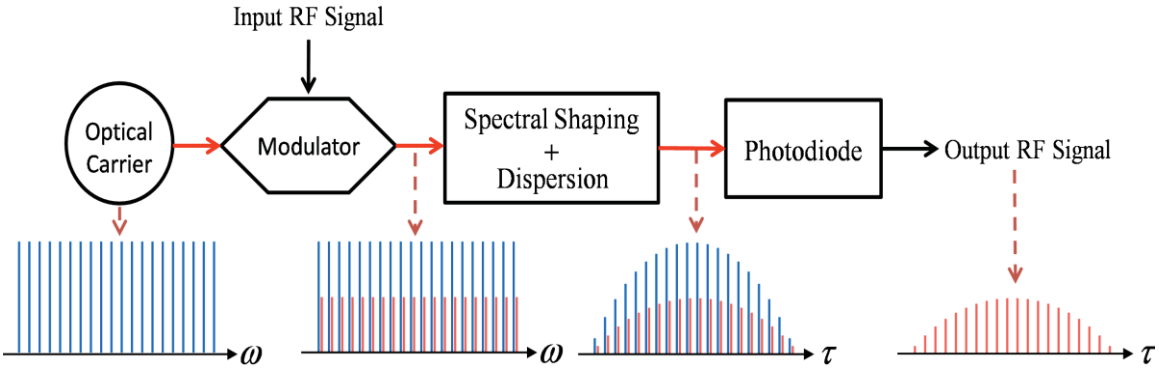

Fig. 1.4 Configuration of a multi-tap microwave photonic (MWP) filters

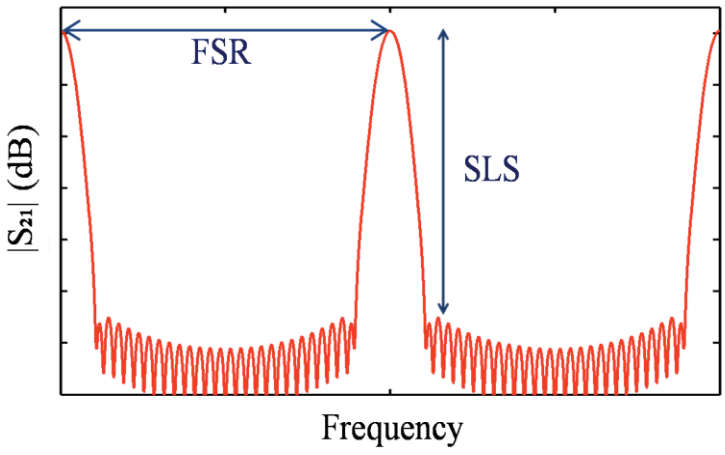

Fig. 1.5 A multi-tap microwave photonic filter transfer function. FSR: free spectral range, SLS: sidelobe suppression

1.5. Thesis Outline

The dissertation is organized into the following chapters. In Chapter 2, we experimentally investigate the noise characteristic of microwave photonic filter based on OFCs. We compare microwave photonic filter links based on OFCs and amplified spontaneous emission (ASE) sources within same structure to prove the great noise properties of OFCs based MWP filters. In Chapter 3, we will demonstrate reconfigurable and tunable flat-top microwave photonic filters based on an OFCs and a dispersive medium. Complex taps allowing flexible and tunable filter characteristics are implemented by programming the amplitude and phase of individual comb lines using an optical pulse shaper. First, we implement a flat top filter by applying positive and negative weights across the comb lines, then tune the filter center frequency by adding a phase ramp onto the tap weights. In Chapter 4, programmable multi-tap microwave photonic phase filters operating over an ultra-wide bandwidth are explored. Complex programmability over dozens or hundreds of taps is achieved by optical line-by-line pulse shaping on Gaussian shaped, flat, or ultra-broadband OFCs using an interferometric scheme. Through high-speed real-time measurements using arbitrary waveform generator (AWG) and real time scope, we show programmable chirp control. In Chapter 5, the phase control of taps by a pulse shaper is utilized to compensate the group delay ripple (GDR) of chirped fiber Bragg grating (CFBG) which can give many advantages (low loss, small volumes, a small filter delay time, much shorter than dispersion compensating fiber (DCF), etc.) to our microwave photonic filter configuration. Finally, in Chapter 6, we summarize the thesis and suggest a few possible directions for future research.

2. NOISE EVALUATION OF MICROWAVE PHOTONIC FILTERS BASED ON OPTICAL FREQUENCY COMBS

2.1. Preface

In this chapter we will demonstrate that a filtered microwave photonic link implemented with an optical frequency comb as multi-tap optical source offers a significant improvement in noise characteristics when compared to sliced incoherent light sources. We provide a comparative study of the noise performance of microwave photonic filtered links based on these two light sources (incoherent spectral slicing and EO frequency comb generators). Specifically, we show that high-speed data can be transmitted with minimum degradation through the EO frequency-comb based filtered link, whereas the incoherent optical source needs to have a very broad spectrum to transmit the same data with error-free performance. In section 2.2 we introduce the multi-tap microwave photonic filters which have been achieved by different optical sources especially sliced broadband incoherent sources and OFCs. The noise performance of MWP filter links are studied in two different scenarios. In section 2.3 we first compare the filtering characteristics when using a frequency comb and an amplified spontaneous emission (ASE) source having identical bandwidths and tap delays. In section 2.4 we consider an ASE source broader than the comb source while showing the same filter transfer function. By measuring the eye diagram, bit-error-rate (BER), and single-sideband (SSB) spectrum of a clock source transferred through a filtered MWP links, we experimentally demonstrate that microwave photonic filters implemented with optical frequency combs have a significantly better noise performance and effective wavelength allocation when compared to ASE sources. The contents of Chapter 2 have been presented in our publication [25].

2.2. Introduction

As we discussed in section 1.4, in multi-tap microwave photonic filter scheme, the optical source consists of an array of spectral lines or optical taps. After being modulated by the microwave signal to filter, transmitted through a dispersive medium and photodetected, each optical tap provides a delayed and weighted copy of the input electrical signal. It is well known that this scheme must operate in the incoherent regime, i.e., in order to establish a linear relation between the input and output electrical signals, the optical tap summation must be performed in intensity. This can be achieved either by using an optical source with a coherence time shorter than the tap delay or by separating away the optical taps to avoid interference beats in the photodiode. The latter option has been widely explored by several microwave photonic filtering schemes, with the optical taps implemented by wavelength multiplexing a discrete array of narrow-linewidth tunable lasers as shown in Fig. 2.1(a) [26]. Although being reconfigurable and flexible, there is a clear limitation in terms of complexity, since the number of taps is given by the number of available lasers. On the other hand, the former incoherence option shown in Fig. 2.1(b) enables a cheaper solution, since the optical taps can be alternatively generated by spectrally carving a broadband incoherent source [27-29] (so-called spectral slicing techniques). When combined with an optical pulse shaper as optical filters, this approach provides a great number of controllable optical taps [30]. However, the stochastic nature of the optical source leads to degradation (i.e., the intensity and phase noise) of the filter's performance [31-33]. Intensity noise is the frequency domain representation to show the effect of the fluctuation in the amplitude of the source, and phase noise caused by time domain instabilities (timing jitter) is the noise power at a given offset frequency from the carrier. Among them, since the phase noise characteristics is important for many applications which require a careful control over signal temporal characteristics, phase noise in optical links has been investigated, e.g., Chromatic dispersion effects on phase noise [34], the amplified spontaneous emission (ASE) noise of an eribium-doped fiber amplifiers (EDFA) [35], or an external modulator effects on phase noise [36]. Several efforts have been explored to mitigate this issue,

including optimizing the bandwidth of the spectral slices [31] or using balanced photodetection [37].

Recently, our group has explored the use of high-repetition-rate optical frequency combs (shown in Fig. 2.1(c)) as multi-tap optical sources in delay-line MWP filters [38]. While being similar in concept to mode-locked lasers [39], the possibility of tuning in an independent manner both the repetition rate and optical carrier frequency in optical frequency combs provides greater flexibility in tuning the synthesized microwave band pass, even at sub-microsecond speeds [40]. When combined with optical pulse shaping techniques, this approach enables reconfigurable complex filtering with hundreds of optical taps available [8] while using a single narrowband cw laser. In this contribution, we show that microwave photonic filters implemented with optical frequency combs yet have another desired attribute, namely, a significantly better noise performance when compared to sliced spectrally incoherent sources. It is theoretically proved that a low-coherence optical source will bring noticeable noise deterioration to the generated signal [36]. The noise performance of MWP filter links are studied in two different scenarios. In section 2.3, we first experimentally compare the filtering characteristics when using a frequency comb and an ASE source having identical bandwidths and tap delays. In section 2.4, we consider an ASE broader than the comb source while showing the same filter transfer function.

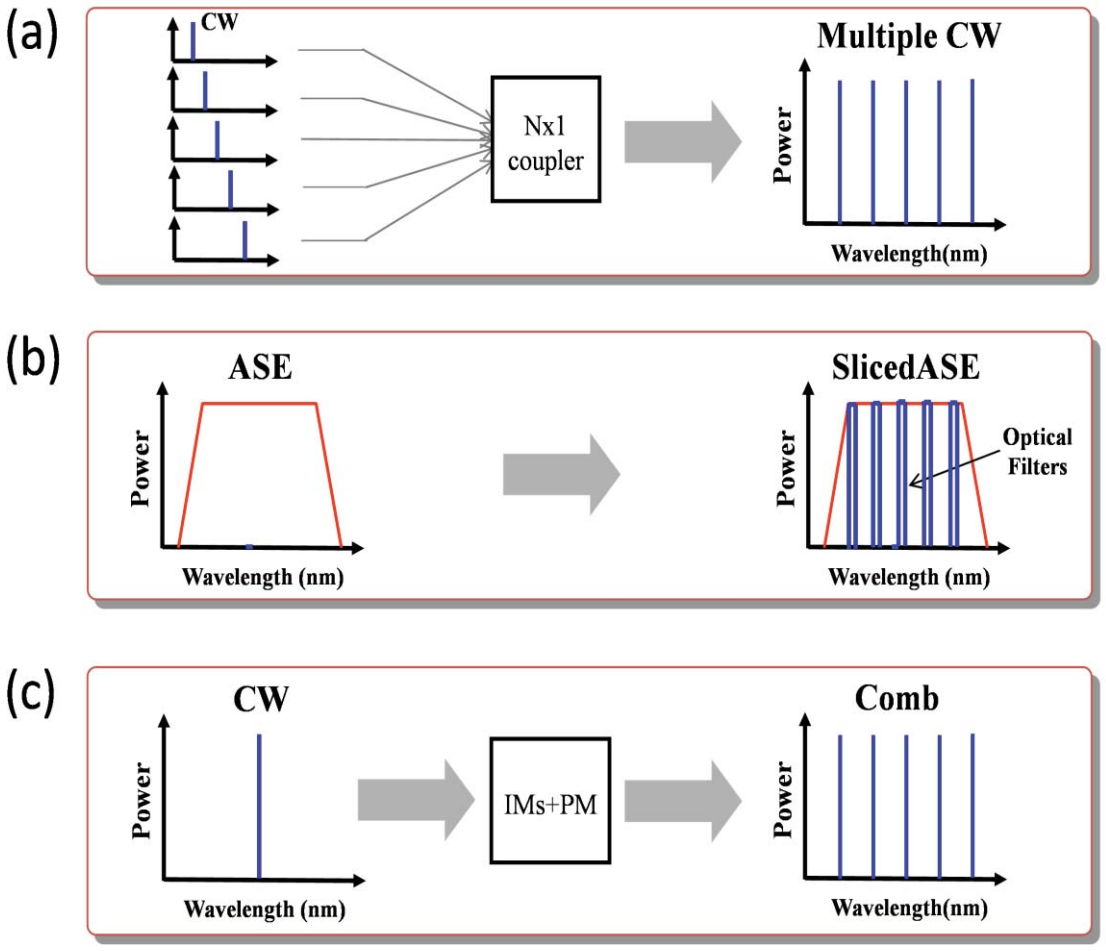

Fig. 2.1 Schemes to generate array of spectral lines, (a) Combination of different wavelength of cw lasers, (b) Sliced broadband incoherent source by optical filters, (c) Optical frequency combs

2.3. Optical Frequency Combs vs. Equivalently Sliced ASE Source

Figure 2.2 shows the schematic of our experiment setup, which is a typical positive-only-tap MWP filter configuration [41]. After amplification through an EDFA (Erbium Doped Fiber Amplifier), the optical source (either the OFCs or ASE) is modulated by the electrical signal to be filtered using a dual-drive Mach-Zehnder modulator biased at quadrature point (half power point). The two input RF ports have 90 degree phase difference, featuring optical single-sideband (OSSB) modulation [42]. We use a 90 degree hybrid coupler with a bandwidth of 1 to 12.4 GHz and a maximum phase imbalance of ±7 degrees to apply the pair of RF signals to the modulator [42]. The

modulated light is sent to a dispersive medium (a dispersion compensating module that has -1259.54 ps/nm dispersion at 1550 nm with relative dispersion slope 0.00455/nm) and subsequently detected by a 22 GHz bandwidth photodiode (PD). The filter transfer function (S21 parameter) is measured by a network analyzer.

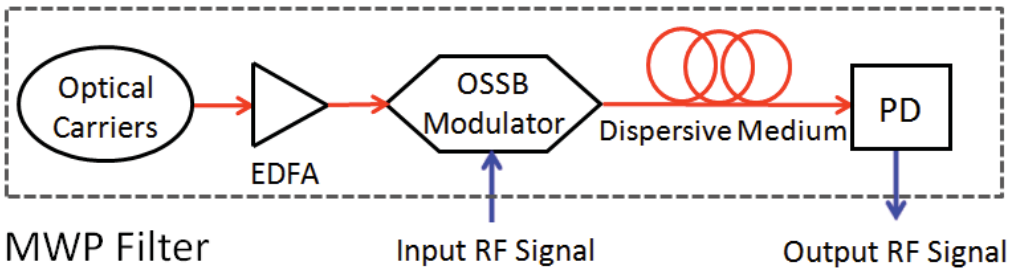

Fig. 2.2 Experiment set up of multi-tap microwave photonic filters

Fig. 2.3(a) and (b) show the experimental configuration and optical spectrum measured by optical spectrum analyzer (OSA) with 0.01 nm resolution for coherent and incoherent multiple optical carriers. ASE an optical broadband source sliced with a periodic optical filter having an interferometer with 100 psec relative delay. It has deep nulls in its transmission response with 10 GHz periodicity as shown in Fig. 2.3(a), and this device is commonly used for differential phase shift keying (DPSK) demodulation at 10 Gb/s. A tunable narrow bandwidth optical bandpass filter (0.3 nm 3dB bandwidth) is applied to shape the envelope. The OFCs shown in Fig. 2.3(b) is composed by cascading an intensity and phase modulator driven by a 10 GHz clock signal [13]. The bias point and phase shift are adjusted to provide a pseudo-flat-top envelope, and the clock frequency is selected to match the ASE spectral period. A 10 GHz repetition rate comb is further apodized by optical pulse shaper (Finisar Waveshaper 1000s) to match the envelope shape to Fig. 2.3(a) as shown in Fig. 2.3(b). As a result, identically apodized >25 taps are achieved by coherent and incoherent optical sources. The standard deviation between OFCs and ASE is 0.01 dB.

The extinction ratio of DPSK is >18 dB, but optical spectrum measured by OSA shows 11 dB extinction ratio at peak as shown in Fig. 2.3(a) because it is blurred due to

the limited resolution bandwidth (RBW). The optical power of DPSK demodulator is given by

$$P(\omega) \propto (\varepsilon - 1)\cos\left(\frac{2\pi\omega}{\Delta\omega}\right) + (\varepsilon + 1) \tag{2.1}$$

where ε is the ratio of the nulls' amplitude to the peaks' amplitude of demodulator interferometer in terms of power transmission, or in other words $-10\log_{10}\varepsilon$ (dB) is the degree of extinction with which the demodulator interferometer suppress the carriers. $\Delta\omega$ is the periodicity of DPSK demodulator, which is 0.08 nm (100 ps delay between arms). Figure 2.4 shows he numerically calculated optical power spectrum of DPSK demodulator. The ideal spectrum of DPSK is shown in blue when the extinction ratio is 18 dB. By applying RBW (for which we used 0.01nm Gaussian window function) of OSA, the extinction ratio is reduced to ~12 dB (red), which is close to the extinction ratio of the measured optical spectrum.

Fig. 2.3 (c) shows the measured (solid) and simulated (dash) transfer functions of the MWP filters achieved when using the spectrally sliced source (red) or the OFC (blue). The dispersion compensating module (Dispersion compensating fiber (DCF)) with -1259.54 ps/nm results in delay difference of 96 ps between adjacent 10 GHz taps. The free spectral range (FSR) of the filter is 10.4 GHz, equal to the reciprocal of the 96 ps delay increment. The measured filter responses closely match the predicted ones, showing a bandwidth of ~620 MHz at 3 dB and > 30 dB sidelobe suppression in baseband. The attenuation of the band-pass with the ASE source is likely due to a high-frequency roll-off caused by the finite bandwidth of the spectral slices.

Despite the similarity in their transfer functions, the above filters have a radically different behavior in noise performance. To illustrate this, we send 2^{31}-1 bit length of on-off keyed non-return-to-zero (NRZ) modulated data at 1Gbps generated by a pattern generator (Agilent Technologies N4901B SerialBERT) through the MWP filter link implemented with either optical source. As can be seen from Fig. 2.5(a), after amplification, eye diagrams are measured by digital serial analyzer (Tektronix DSA 8200). As can be observed from Fig. 2.5(b), after 4 GHz low-pass filtering and amplification, the comb based MWP filter (left) shows the clearly open eyes with sharp

rise-fall transitions, but the ASE based MWP filter (right) shows the closed eyes corresponding to big signal distortion due to noise. The dramatic reduction in SNR with the ASE is due to the thermal-like statistics of this light source. The above results have an important consequence. The fact that the comb-based MWP filters keep the quality of the input microwave signal implies that higher data rates can be transmitted through the link. Nevertheless, as shall be explored in the next section, the SNR can be increased with broader optical bandwidth ASE sources, which is well-known in WDM communication systems working with spectrally sliced light sources [43].

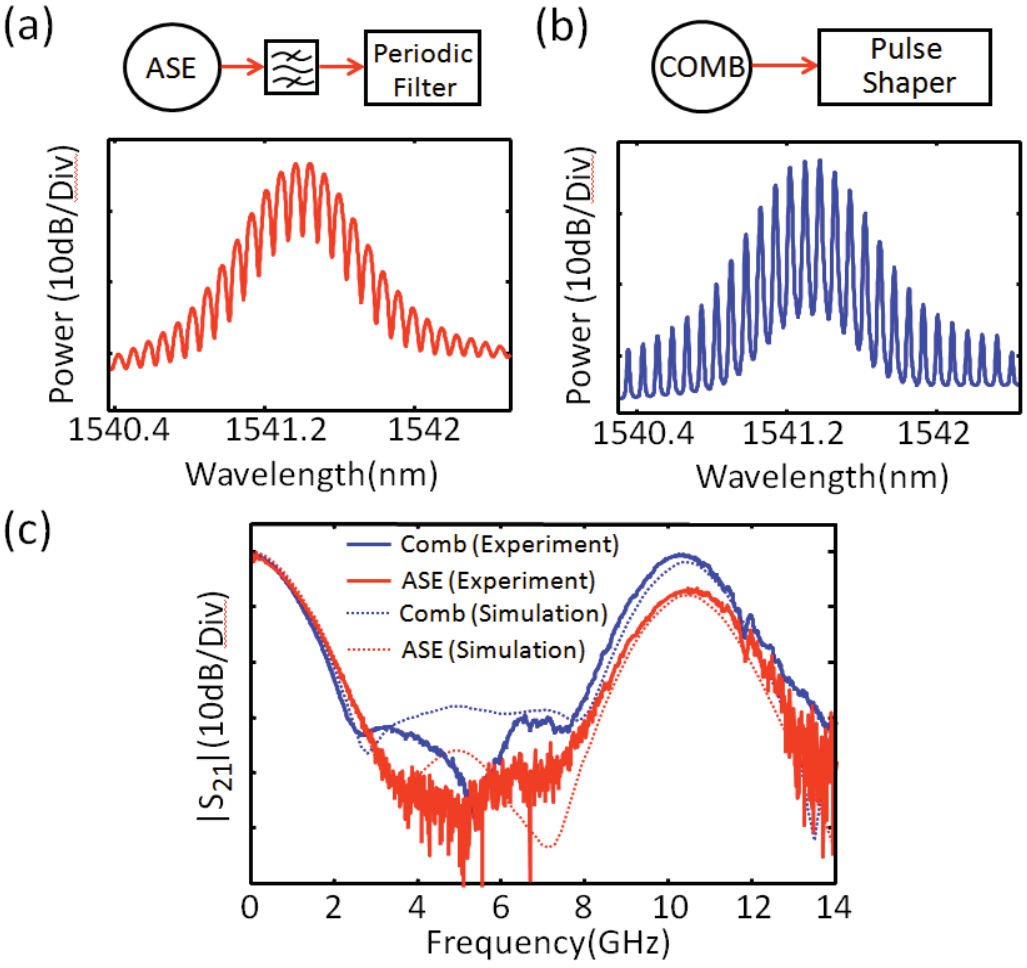

Fig. 2.3 Experimental configuration and optical spectrum measurement of shaped multi-tap optical carriers based on (a) spectrally incoherent and (b) coherent light sources, (c) Measured (solid) and simulated (dotted) filter transfer function of MWP filter based on coherent (blue) and incoherent(red) optical carriers, respectively

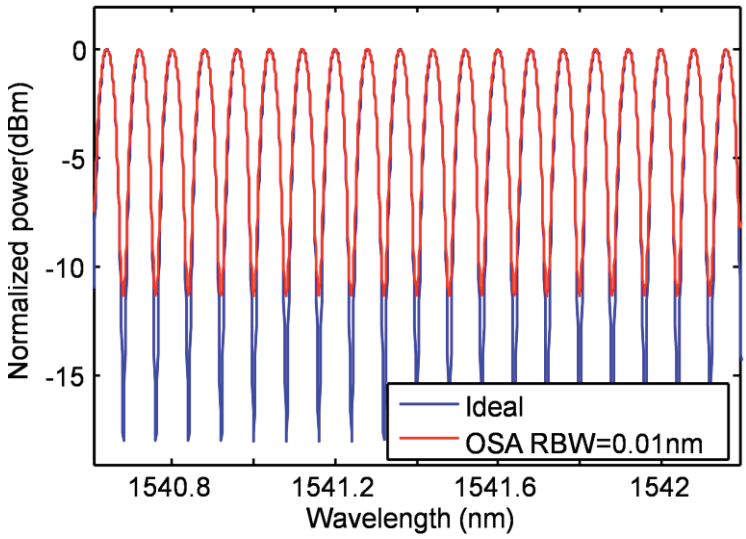

Fig. 2.4 Simulated optical power spectrum of DPSK demodulator

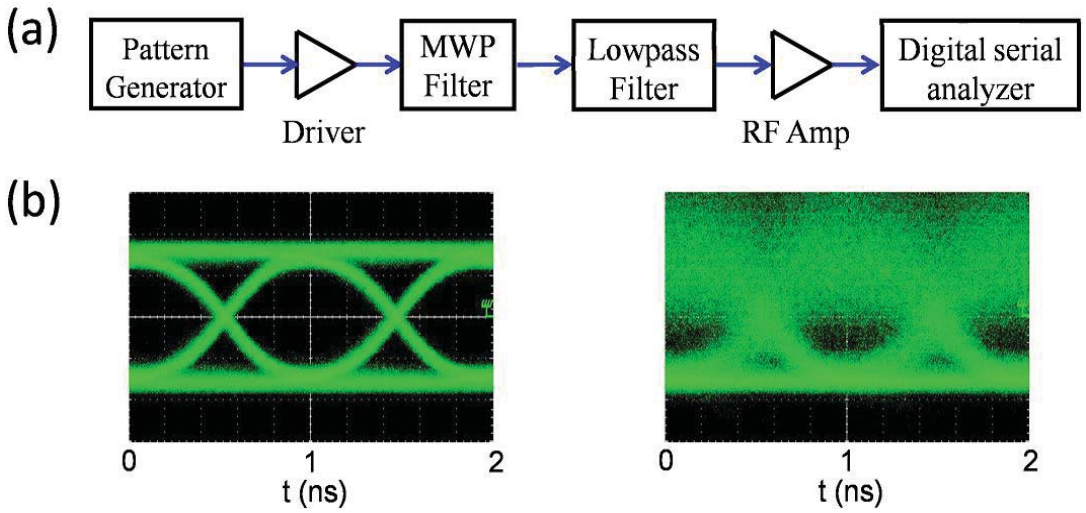

Fig. 2.5 (a) Noise performance measurement set up, (b) Measured eye diagrams of a 1Gbs NRZ signal at the output of the MWP link implemented with a frequency comb (left) and spectrally sliced ASE (right)

2.4. Optical Frequency Combs vs. ASE Source Having Broader Bandwidth

The noise performance of microwave filter links is next studied with an optical frequency comb and a broad linewidth of sliced ASE source devised to reduce noise in spectrum slicing system. We now allocate 20× larger bandwidth to the ASE, so that it

spans most of the C band. We have verified experimentally that when broader bandwidth is allocated to the ASE, it can achieve better data transmission performance than when it has the same bandwidth as the optical frequency comb generator. Figure 2.6(a) shows the two Gaussian-shaped spectra apodized with the pulse shaper. The spectral slices of ASE (left) are shaped as cosine square with 200 GHz spectral period in order to keep the same number of taps as the comb (right), resulting in 25 nm bandwidth at 10 dB (i.e., 20 times larger than the OFCs). Both, OFCs and ASE are apodized by a pulse shaper (Finisar Waveshaper 1000S), so that both sources have the same Gaussian tap weights.

Fig. 2.6(b) shows the measured (solid) and simulated (dash) transfer functions of the MWP filters achieved when using the spectrally sliced source (red) or the optical frequency comb (blue), which is implemented with the setup in Fig. 2.2. For the OFCs, the modulated light is passed through a dispersion compensating fiber (DCF) module with -1259.54 ps/nm dispersion at 1550 nm, resulting in a tap delay of 96 ps between adjacent spectral lines. For the ASE, the length of dispersion is reduced accordingly (3.5km single-mode fiber) to match the tap delay of the comb. The measured filter responses closely match the predicted ones, and the both measured filter shapes are almost identical. They show bandwidths of ~410 MHz at 3 dB and > 24 dB sidelobe suppression in baseband.

The eye diagrams measured by the set up in Fig. 2.5(a) are shown in Fig. 2.7 when optical power at PD is -12 dBm. Figure 2.7(a) and (b) show the measured eye diagrams when CW laser is applied with and without dispersion, respectively. Clearly open eyes in Fig. 2.7(c) and (d) are when the comb-based MWP link is provided with and without dispersion (i.e., with and without any RF filtering effect). Compared to Fig. 2.7(b), the eye shape is changed by applying dispersion as shown in Fig. 2.7(d), since the shape is affected by the filter passband shape. The ASE-based link also brings open eye diagrams, as shown in Fig. 2.7(e) and (f), with an SNR slightly lower than the comb. However, in order to get this SNR with incoherent light, the optical bandwidth had to be 20× larger. This is likely due to the intensity noise, intersymbol interference, and the dispersion induced amplitude noise of the ASE source [31].

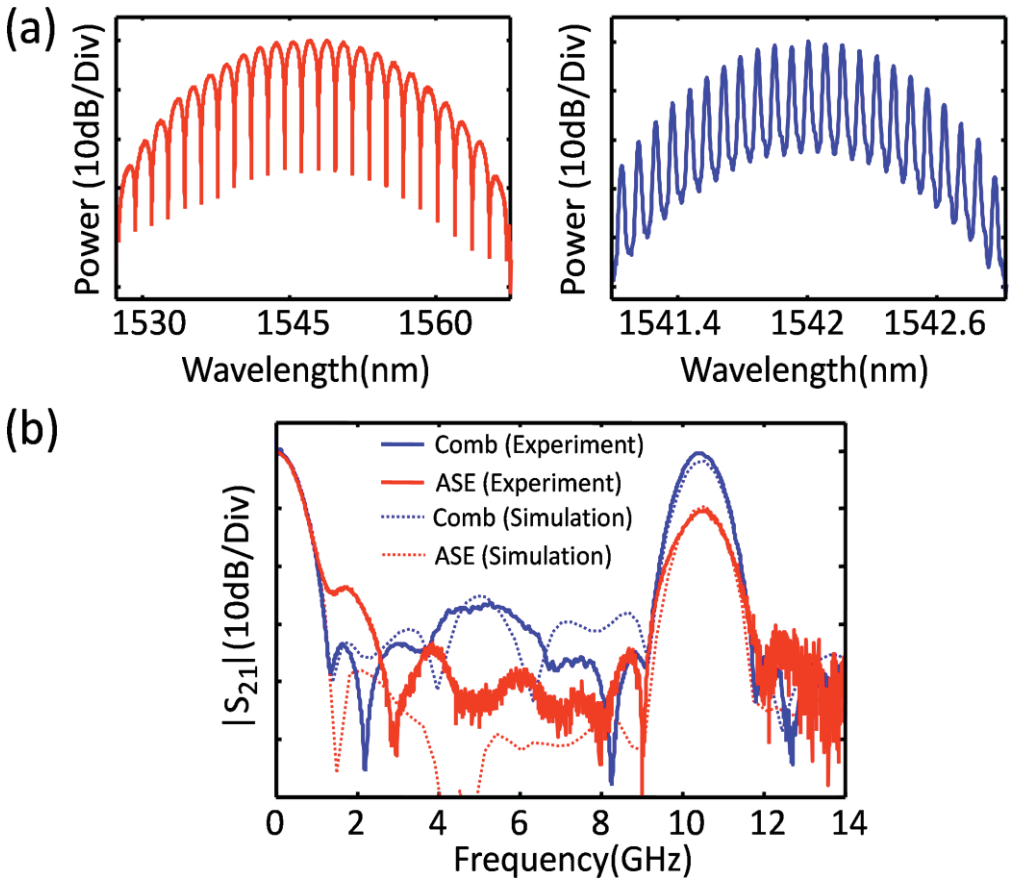

Fig. 2.6 (a) Measured Gaussian shaped multi-tap optical carriers based on the combs (right) and widely sliced incoherent light sources (left), (b) Measured (solid) and simulated (dotted) filter response based on the OFCs (blue) and the ASE (red) respectively

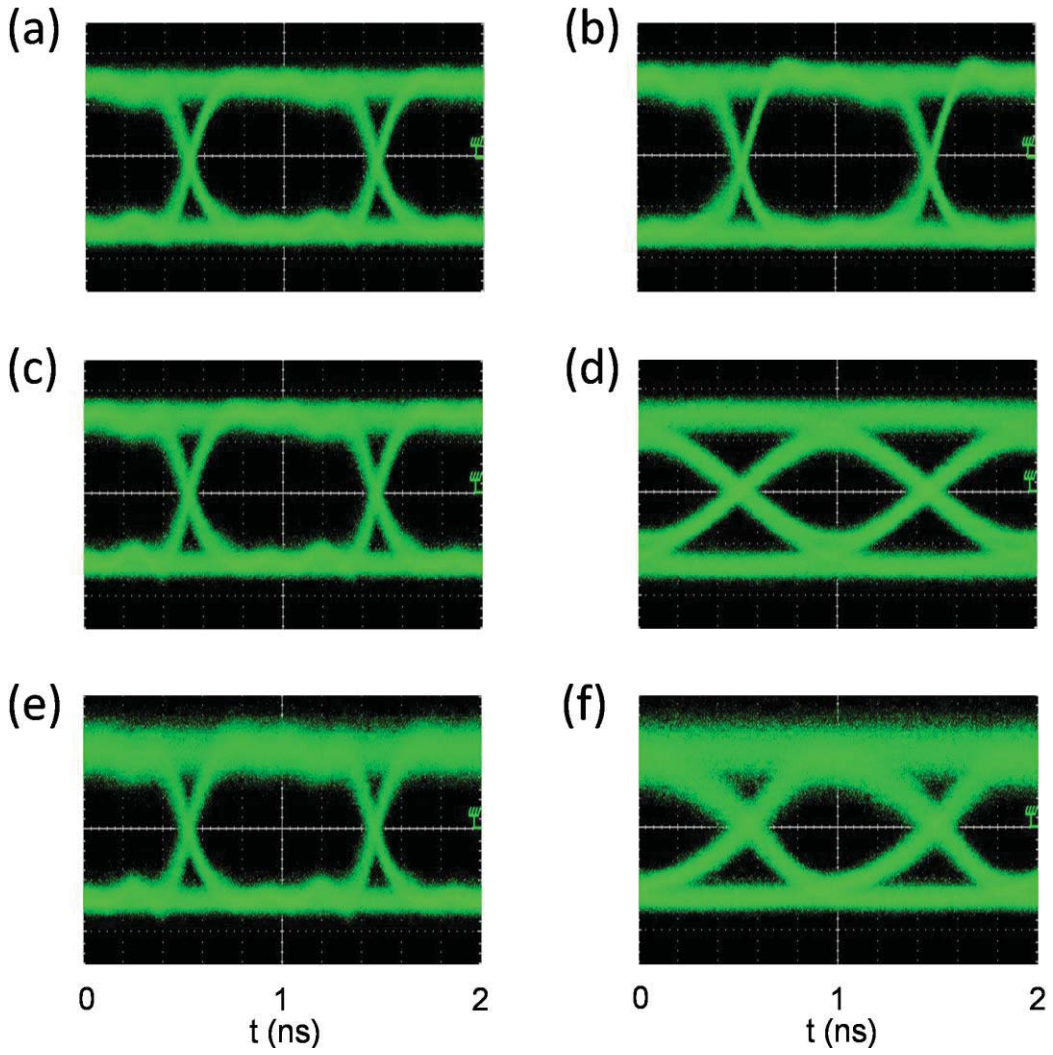

Fig. 2.7 Measured eye diagrams of a 1Gbs NRZ signal with (right) and without (left) dispersion in the MWP link implemented with (a) (b) CW, (c) (d) OFC, and (e) (f) spectrally sliced ASE respectively

To check the difference of noise performance more specifically, we measured bit-error-rates (BERs). Figure 2.8 shows measured BERs with corresponding linear fitting lines (dotted) at 1Gbps when implemented with CW laser, OFC, or sliced ASE. Without dispersion, the BER curve for the OFC is essentially identical compared to that with a CW laser when BER is 10^{-9}. In contrast, the BER-curve for the sliced ASE without dispersion shows 1.79 dB power penalty relative to the CW, which is caused by the increased intensity noise of the ASE source. With the dispersive fiber the BER curve with

the OFC shows 1.87 dB power penalty relative to CW, which is caused since the resulting baseband RF filter is narrower than the RF modulation bandwidth. The ASE-based filter now shows an additional 5.29 dB power penalty relative to CW (3.42 dB relative to ASE without dispersion). This penalty is higher than expected assuming the amplitude noise and filtering penalties were additive. This is likely due to the dispersion-induced amplitude noise contributed by the spectral linewidth of the ASE taps [43].

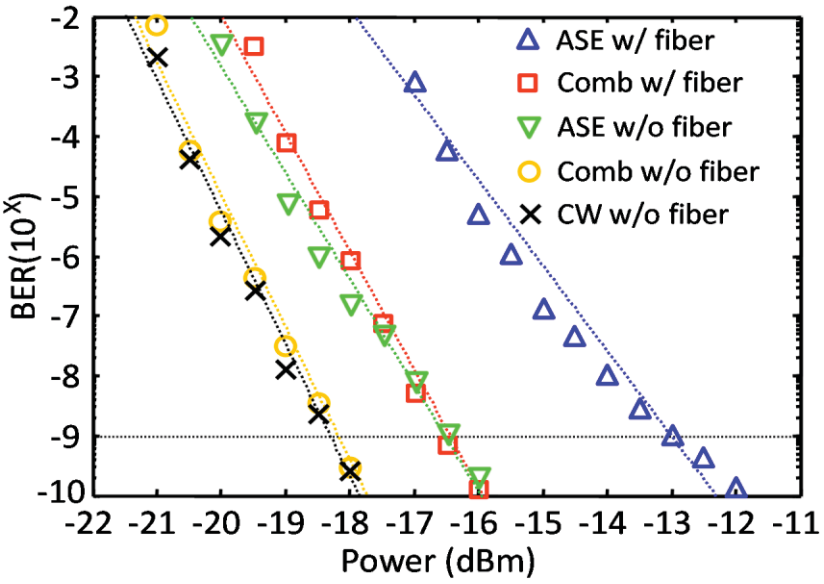

Fig. 2.8 Measured BER with corresponding linear fitting lines at 1 Gbps NRZ signal at the output of the MWP link

Microwave photonic filter links are interesting for simultaneous transmission and demultiplexing of multiple RF channels because the filter's free spectral range changes inversely proportional to the dispersion amount, which is controlled by the length of the fiber links [44]. The OFCs achieve a better noise performance while using significantly narrower optical bandwidth, which permits to achieve larger distances in the MWP filter link to maintain the same tap delay. As in the previous case, the optical source will be responsible for the noise characteristics in the bandpass response. In order to assess this, we consider the Gaussian apodized sources in Fig. 2.6(a), and ~ 1.35 times larger

dispersion is applied to both filters to shift the FSR to 8 GHz. The measured transfer functions corresponding to the OFCs (solid) and ASE (dash) are shown in Fig. 2.9(a). We then send an 8 GHz clock signal to the filters, and measure the single-sideband (SSB) power spectral density at the output of the link. As can be seen from Fig. 2.9(b), the SSB spectrum of the transmitted clock signal at 1 kHz offset is ~-96 dBc/Hz for the comb and ~-90dBc/Hz for the ASE source. The situation gets worse at higher frequencies, where the differences approach ~20dB at 1 MHz offset.

In conclusion, we have performed a comparative study of the noise performance of two microwave photonic filter links using two different multi-wavelength sources: a spectrally coherent opto-electronic frequency comb and a spectrally sliced incoherent ASE source. We precisely tailored both sources by applying a pulse shaper so that the filter transfer function of the microwave link looks essentially identical. Even if they have similar filter response, our experiment results (eye diagram, bit-error-rate (BER), and single-sideband (SSB) spectrum) show that their noise characteristics are completely different. Although the SNR of MWP filters links can be increased with broader bandwidth ASE sources, this comes at the expense of an inefficient use of bandwidth and a shortage in fiber-link reach due to dispersive effects. On the other hand, opto-electronic frequency comb generators offer minimum penalty transmission with respect to a CW-based MWP fiber link, make a better use of the available optical bandwidth, and allow to transmit RF clock source with essentially no distortion in its single-sideband RF spectrum. These results highlight the potential of opto-electronic frequency combs generators as multi-wavelength light sources for MWP applications in radio-over-fiber communications.

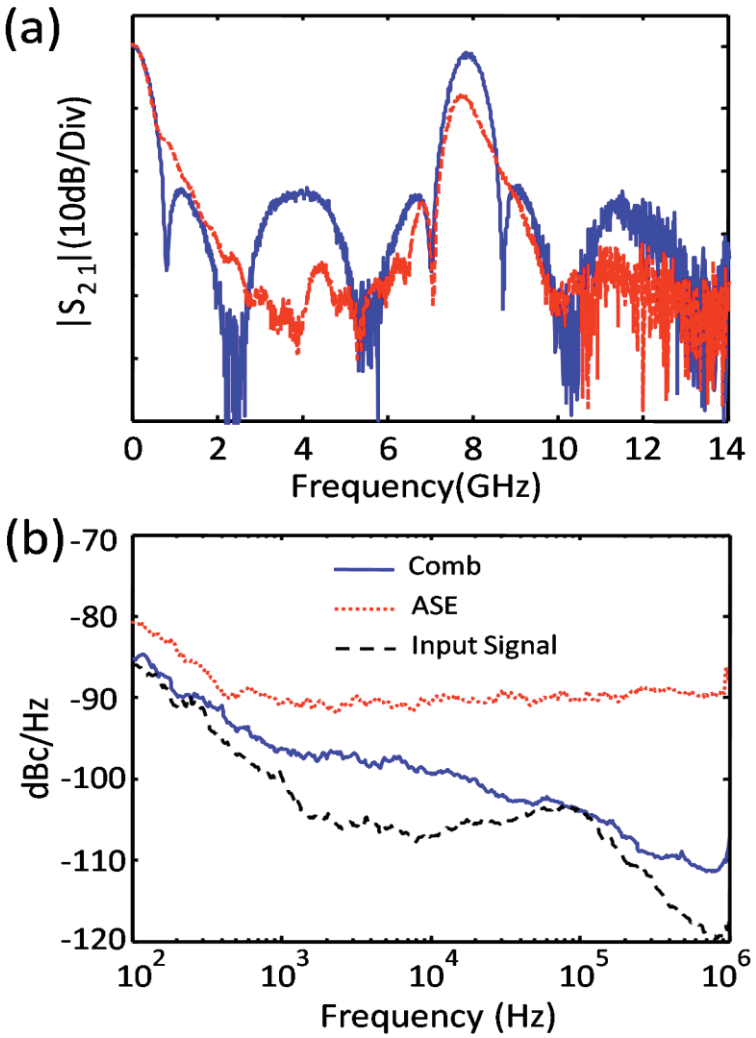

Fig. 2.9 (a) Measured filter transfer function based on coherent (solid) and incoherent (dash) optical carriers when ~ 1.35 times larger dispersion is applied than those in Fig. 2.6(b), (b) SSB RF spectrum of a 8GHz clock signal (dash line) transmitted through a MWP filter link implemented with a frequency comb (solid line) and spectrally sliced ASE (dotted line)

3. RECONFIGURABLE AND TUNABLE FLAT TOP MICROWAVE PHOTONIC FILTERS UTILIZING OPTICAL FREQUENCY COMB SOURCES

3.1. Preface

In this chapter we will demonstrate a new complex coefficient taps microwave photonic filter configuration which utilizes an optical comb source, and a pulse shaper in an interferometric configuration. This configuration enables us to achieve flat top microwave photonic filters with reconfigurable bandwidth and tunable center frequency. Specifically, we implement various bandwidths of flat top filters by applying positive and negative weights across the comb lines, then tune the filter center frequency by adding a phase ramp onto the tap weights. In section 3.2 we will discuss the concept of finite impulse response (FIR) flat top filter designed by windowing method. Simulation results for the flat top filter with different window function show that if the bandwidth, transition band, and number of taps are assumed to be same, a sinc function impulse response multiplied by a Kaiser window shows highest sidelobe suppression and minimum passband ripple. In section 3.3 we will describe the experimental set up of programmable and tunable microwave photonic filters based on an evenly spaced set of optical frequency comb and a dispersive medium. We adopt line-by-line pulse shaping in an interferometric configuration to realize amplitude and phase control of individual taps. In sections 3.4 and 3.5 we will describe the experimental result to the programmable control of both the flat top filter bandwidth and center frequency by using this scheme. 1.5 to 3 GHz 3 dB bandwidth of flat-topped filters with mostly greater than 27-dB stopband loss are demonstrated using 32 taps with both positive and negative tap coefficients. We also apply a linear phase to the comb using a pulse shaper to achieve filter tuning without changing filter shape. By increasing the slope of linearly increasing phase, we

demonstrate the filter passband shifts from 3.2 to 6.8 GHz. The work on the reconfigurable and tunable MWP flat top filter has been presented in our publication [45].

3.2. Finite Impulse Response (FIR) Flat-top Filter Design

A filter having flat top passband bandwidth and fast rolloff on band edge is preferred for signal fidelity and tolerance of signal frequency drift. Therefore, it is desirable to design a filter with flat top spectral response. Ideal rectangular filters have infinite impulse responses with sinc function envelopes consisting of both positive and negative tap values. As is well known in digital filtering, a flat top filter which is similar to an ideal rectangle filter can be obtained utilizing a finite number of taps by multiplying an infinite sinc function with a window function [46]. Fig 3.1 shows a sinc function impulse response multiplied by a window function and its filter transfer function obtained by Fourier transform. The finite sinc function impulse response show the flat top filter which is similar to ideal rectangular filter, but it includes passband and stopband ripples.

The desirable flat top filter should have small passband ripple, high sidelobe suppression, and narrow transition band. According to our simulation, different window functions show different filter properties as shown in Table 3.1. Table 3.1 shows the well-known window examples and their window functions w(n) [46]; N represents the width, in samples, of a discrete time window function, and n is an integer, which shows the time shifted forms of the windows. In the Kaiser window function, I_0 is the zero-th order modified Bessel function of the first kind, and coefficient α is usually 3. For simulation, the number of taps sets as 64, and the bandwidth of rectangular filter set as 2.5GHz. The simulated sidelobe suppression and passband ripple of each window cases are shown in Table 2.1. Here we use a Kaiser window for our experiment which offers desirable filter properties such as highest sidelobe suppression and minimum passband ripple. Figure 3.2(a) and (b) shows the simulated filter response obtained with the Kaiser window, which shows 55 dB sidelobe suppression and 0.022 dB passband ripple when implemented with 64 taps.

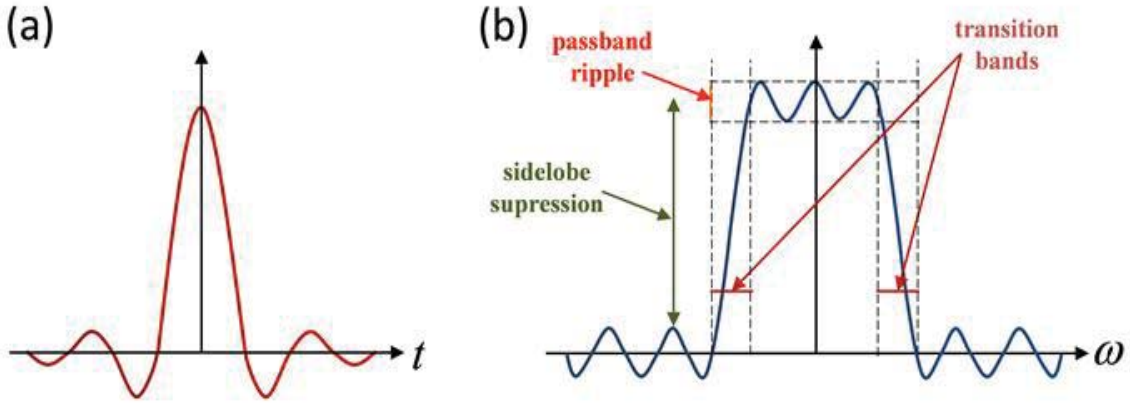

Fig. 3.1 (a) Sinc function impulse response multiplied by a window function, its corresponding filter response is shown in (b)

Table. 3.1 Window type examples and their window functions. Both simulated sidelobe suppression and passband ripple of flat top passband are given in dB scale when the number and the delay of taps, bandwidth of passband, and transition band are assumed as 64, 96 ps, 2.5 GHz, and 500 MHz, respectively.

Window Type	$w(n) \quad (0 \le n \le N-1)$	Sidelobe Suppression (dB)	Passband ripple (dB)
Kaiser	$I_0\left(\alpha\sqrt{1-\left(\frac{n}{N}\right)^2}\right)\Big/ I_0(\alpha) \quad I_0(x)=1+\sum_{r=1}^{\infty}\left(\frac{(x/2)^r}{r!}\right)^2$	55	0.022
Bartlett	$1-\frac{\lvert n\rvert}{N+1}$	27	0.290
Hanning	$\frac{1}{2}\left[1+\cos\frac{2\pi n}{2N+1}\right]$	44	0.071
Hamming	$0.54+0.46\cos\frac{2\pi n}{2N+1}$	52	0.035
Blackman	$0.42+0.5\cos\frac{2\pi n}{2N+1}+0.08\cos\frac{4\pi n}{2N+1}$	31	0.255

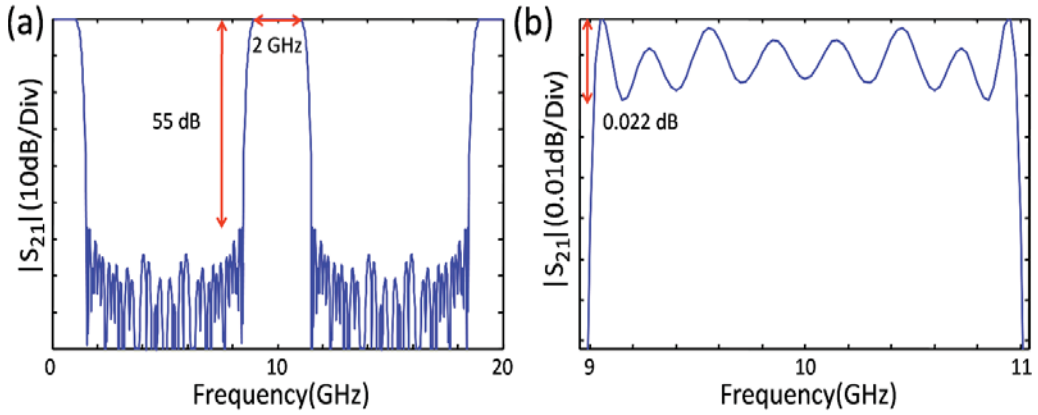

Fig. 3.2 (a) Simulated filter transfer function when a Kaiser window is applied, (b) Zoom-in view of the passband of (a)

3.3. Complex Coefficient Taps Microwave Photonic Filters

As mentioned in chapter 2, tapped delay line microwave photonic filters are based on the concept of discrete time finite impulse response filter [5]. However, based on digital signal processing theory, a delay line filter with positive taps can only function as low-pass filters [47]. There is also quite limitation in the range of transfer functions that can be implemented with all-positive coefficients [47]. This results in a limitation on the functionalities of the microwave photonic filters. To overcome this limitation, there have been several implementations in the last few years to generate negative coefficients and hence to achieve arbitrarily shaped flexible filters and bandpass filters [30, 47-50]. On the other hand, it is also desirable that the photonic microwave filters are tunable. Various techniques have been proposed for the implementation of tunable microwave photonic filters, which are usually achieved by adjusting the time delay difference [51-54]. However, these schemes have been based on adjusting the time delay difference, resulting in the changes of filter free spectral range (FSR). However, these schemes would lead to the changes of bandpass shape by changing FSR. For many applications, it is highly desirable to change only the center frequency of the passband while keeping the shape of the frequency response unchanged. Some other techniques can achieve tunability without bandpass shape changes. There have been implementations based on stimulated Brillouin scattering [55], a phase spatial light modulator used in a cross-

polarized carrier-sideband geometry [56], a pulse shaper capable of resolving and applying different phases to optical carriers and sidebands [57], and a phase shifted fiber Bragg grating [58]. However, these techniques were demonstrated only for a small number of taps.

Our work employs optical frequency combs, which can practically scale to much larger number of taps compared to multiple lasers, while providing optical frequency stability and coherence not available from amplified spontaneous emission (ASE) or typical harmonically mode-locked laser sources. The attribute enables line-by-line pulse shaping [18] in an interferometric configuration [38], which we adopt here to realize amplitude and phase control of individual taps. Microwave photonic filters based on optical frequency combs have recently been shown to produce low sidelobes when implemented with a large number of taps [38]. However, the range of frequency responses that can be implemented is limited if only positive taps are available. In section 3.4 and 3.5, we experimentally demonstrate the ability to program dozens of complex taps to implement flat-top microwave photonic filters with reconfigurable bandwidth and tunable center frequency, respectively.

3.4. Programmable Flat-top Microwave Photonic Filters

Fig 3.3 shows the suggested microwave photonic filter configuration to implement large number of complex tap weights. We consider a configuration with a single sideband modulator placed into one arm of an optical interferometer. The pulse shaper is arm #2 to give a programmable amplitude and phase difference between the two interferometer arms. A comb with 10 GHz repetition rate and nearly flat power spectrum is divided into two paths through a 3-dB optical splitter. After amplification through an EDFA, path 2 passes through a commercially available optical pulse shaper (Finisar WaveShaper 1000s) based on FT pulse shaping [17] in which we program the amplitude and phase of comb lines to control the complex tap weights. In path 1, the individual comb lines are single-sideband modulated with a dual drive Mach-Zehnder (MZ) modulator biased at a quadrature point [42], and the modulator output is sent to a periodic optical filter implemented by 10 Gb/s DPSK demodulator which has deep nulls in its transmission response with 10 GHz periodicity. The nulls are tuned to remove the original comb lines

by matching its frequency nulls to the comb carrier frequencies, leaving only sidebands. The two paths are aligned in polarization by using a polarizer controller in one arm, and combined in a 3-dB coupler, so that the shaped optical comb is mixed with a comb of sidebands without altering the amplitudes and phases. The coupler output is passed through a dispersion compensating fiber (DCF) that has -1259.54 ps/nm at 1550 nm, resulting in delay difference of 96 ps between adjacent 10 GHz comb lines. The optical signal is detected by a 22 GHz bandwidth photodiode (PD) and the transfer function (S21) is measured by a network analyzer. The reason why we choose 3-dB splitter and couplers is to maximize the power of filter response. The filter transfer function generated at the PD is proportional to [38]

$$H(\omega_{RF}) \propto \sqrt{\alpha(1-\alpha)\beta(1-\beta)} \tag{3.1}$$

where α and β are the splitter and coupler coupling coefficients in terms of power. As we can see in Eq. (3.1) the filter transfer function is maximized when α and β are chosen equal to 0.5, in other words when we choose 3-dB splitter and couplers.

For this configuration, we can write the filter transfer function as

$$H(\omega_{RF}) \propto \sum_n \sqrt{p_{1n} p_{2n}} \exp[\, jnD\Delta\omega(\omega_{RF} + \tau/D) - j\Phi_n] \tag{3.2}$$

where p_{1n} and p_{2n} are the powers of the n^{th} comb line in the two paths of interferometer, D the fiber dispersion, Δω the repetition frequency of optical frequency comb, τ the amount of relative delay between two interferometer paths, and Φ_n the additional phase applied to the n^{th} comb line by the pulse shaper. Tuning of the frequency response can be achieved either by varying the optical delay τ of the delay stage or by programming the Φ_n for a linear phase function. By inverse Fourier transformation of the filter response of the filter, we obtain the impulse response as

$$h(t) \propto \sum_n \sqrt{p_{1n} p_{2n}} \exp[\, jn\Delta\omega\tau - j\Phi_n]\delta\left(t - nD\Delta\omega\right) \tag{3.3}$$

The electrical signal generated after optoelectronic conversion is composed by a sum of beating terms between each of the RF sidebands from path 1 and the nearest shaped comb line from path 2. As a result, both amplitude and phase for each individual tap can

be controlled in a user-defined fashion. As seen from (3.2), both apodized negative and positive taps can be achieved by controlling tap amplitudes $\sqrt{p_{2n}}$ and phases Φ_n via line-by-line pulse shaper.

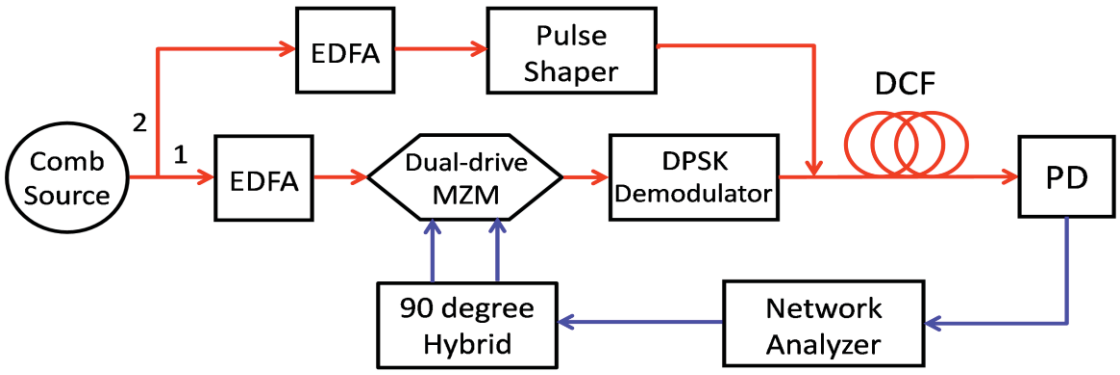

Fig. 3.3 Suggested microwave photonic filter architecture to implement complex tap weights, EDFA : Erbium doped fiber amplifier, MZM : Mach-Zehnder modulator, DPSK : Differential phase shift keying, DCF : Dispersion compensating fiber, PD : Photodiode

Fig. 3.4(a) shows an optical comb measured using an optical spectrum analyzer, which has been shaped to match a sinc function impulse response (for a 3-dB bandwidth of 2.5 GHz) apodized by a Kaiser window. There are 32 taps composed of 16 positive and 16 negative taps as shown on the top of Fig 3.4(a). Using the pulse shaper, phase of 0 was applied for the positive taps, and a phase of π for the negative taps. The system shows weak coupling between the amplitude and phase. To get desired amplitude and phase, we perform experimental adjustments for both amplitude and phase (we iteratively adjust both values in experiment). By checking the interference between neighboring spectral lines in time domain, we could confirm that the desired phase was applied to the corresponding tap. The red plot in Fig. 3.4(a) is our flat comb before shaping, and the blue plot is the shaped comb according to a Kaiser window. The measured peaks deviate from the ideal peaks (not shown) by 0.28 dB in terms of the standard deviation. Fig. 3.4(b) shows the measured and simulated RF filter transfer functions corresponding to Fig. 3.4(a). The passband is centered at 7 GHz, and the FSR (free spectral range, not

shown) is 10.4 GHz, which is equal to the inverse of the 96 ps tap delay. The black and red plots in Fig. 3.4(b) shows the simulated filter transfer function using the ideal (not shown) and measured (in Figs. 3.4(a)) optical comb profiles and equation (3.2). The simulated response based on the measured comb closely matches the predicted response based on the ideal comb with regards to the transition band (530 MHz), sidelode suppression (33 dB), 3dB passband bandwidth (2.5 GHz), and passband ripple (0.4 dB), but differ in the shape of the sidelobes. The slight difference can be attributed to the small errors in the tap weights. The measured filter transfer function is shown in blue in Fig. 3.4(b). As we can see there is a close agreement between simulated and measured filter transfer function. The measured filter shows 27 dB sidelobe suppression and 3 dB passband ripple. Although the passband ripple is larger than simulation, the stop-band attenuation and the transition band of measured plot are close to simulation.

As a comparison we also show an example of a finite impulse response filter obtained through the equiripple filter design method [59]. For the equiripple filter function method, the ripple of passband and stopband of a filter will be minimized when they have same amount of ripples [59]. To find this equiripple filter solution, Parks Mcclellan filter function uses the polynomial interpolation method [60]. Figure 3.4(c) and (d) show the shaped comb and its corresponding measured and simulated filter responses for tap amplitudes chosen according to an equiripple filter design algorithm, respectively. The passband is centered at 7.9 GHz, and the deviation between the measured optical spectrum and the ideal apodization (not shown) is 0.35 dB. The simulated response based on the measured comb closely matches the predicted response with regards to the transition band (530MHz), 3dB passband bandwidth (2.5 GHz), and passband ripple (1.5dB), but shows ~ 16 dB degradation in sidelode suppression (30 and 46 dB SLS with measured (red) and ideal (black) comb respectively). The measured filter shows 22 dB sidelobe suppression and 3.2 dB passband ripple.

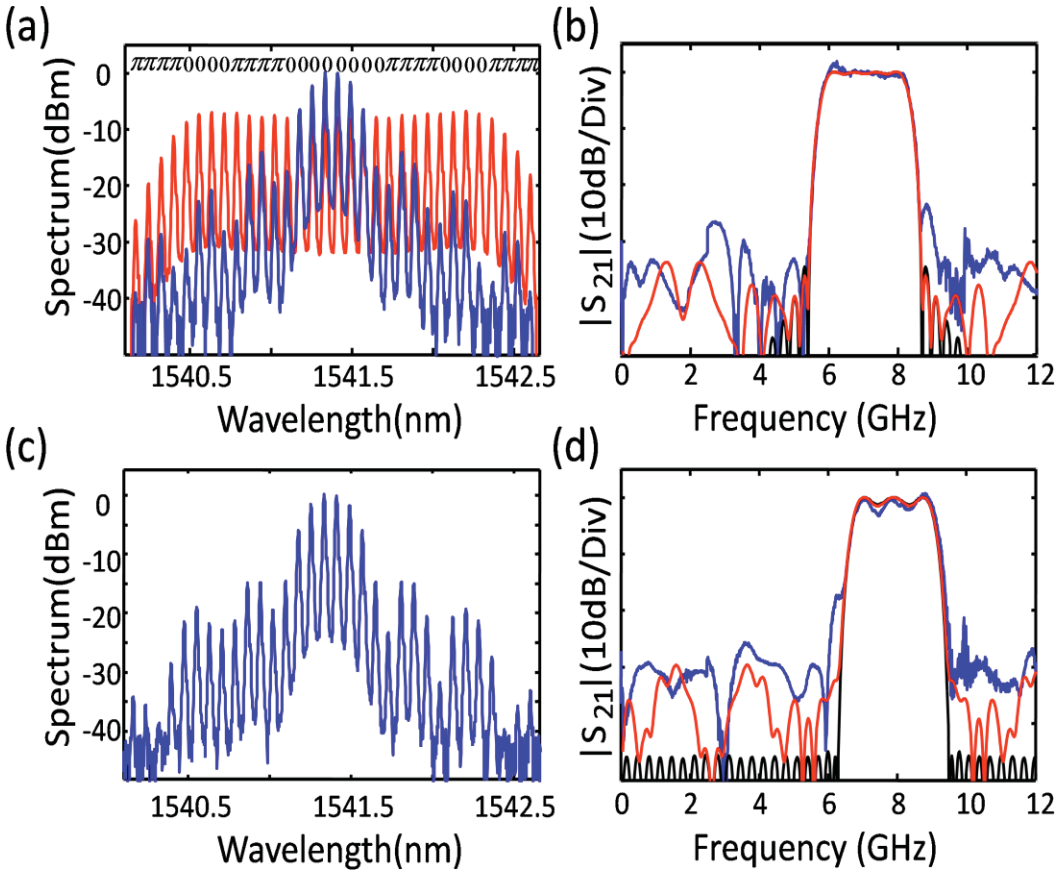

Fig. 3.4 (a) Measured optical spectra from an OSA of the two spectral profiles interfering: the single sideband, suppressed carrier at arm 1 having a flat spectral shape (red), and the 2nd arm spectrum shaped in amplitude to get the flat top profile according to a Kaiser window (blue) of which phases shown on the top are used in obtaining negative taps, (b) corresponding RF filter responses measured (blue) and simulated using ideal (black) and measured (red) combs respectively, (c) The 2nd arm spectrum shaped to get the flat top profile chosen according to an equiripple filter design algorithm, and its corresponding filter response is shown in (d)

This technique can be used to easily change the bandwidth of flat top passband by programming amplitude and phase of the optical combs via pulse shaping. Fig. 3.5(a) shows an optical comb (left) shaped for a 3-dB bandwidth of 1.5 GHz when φ_n = [0 0 0 π π π π π 0 0 0 0 0 0 0 0 0 0 0 0 0 π π π π π 0 0 0], as well as the measured and simulated filter responses (right). The amplitude and the phase are shaped to match an impulse response with a sinc function envelope for 1.5 GHz ideal rectangular filter but apodized by a Kaiser window to limit the number of tabs to 32. The simulated filter

transfer function (dash line), obtained from Eq. (3.2) using the ideal impulse response, shows 31.5 dB sidelode suppression and 0.3 dB passband ripple. The measured response closely matches the predicted response with regards to 27.2 dB sidelode suppression and 0.45 dB passband ripple. Figs. 3.5(b), (c), and (c) also show the apodized spectra and corresponding filter transfer functions when 3dB bandwidths of flat-top filters are 2 GHz, 2.5 GHz, and 3 GHz, respectively. The comb of Fig. 3.5(b) is composed of 20 positive and 12 negative taps, and its measured filter response shows 27 dB sidelode suppression and 1.2 dB passband ripple. For Fig. 3.5(c), the measured filter transfer function shows 27.4 dB sidelode suppression and 1.7 dB passband ripple. Fig. 3.5(d) includes 18 positive and 14 negative taps and the measured filter transfer function shows 22.8 dB sidelode suppression and 1.6 dB passband ripple. The measured and the simulated passband shapes are in relatively close agreement in all four cases, although the experimental sidelobe levels are increased. Details of this will be discussed in chapter 3.6.

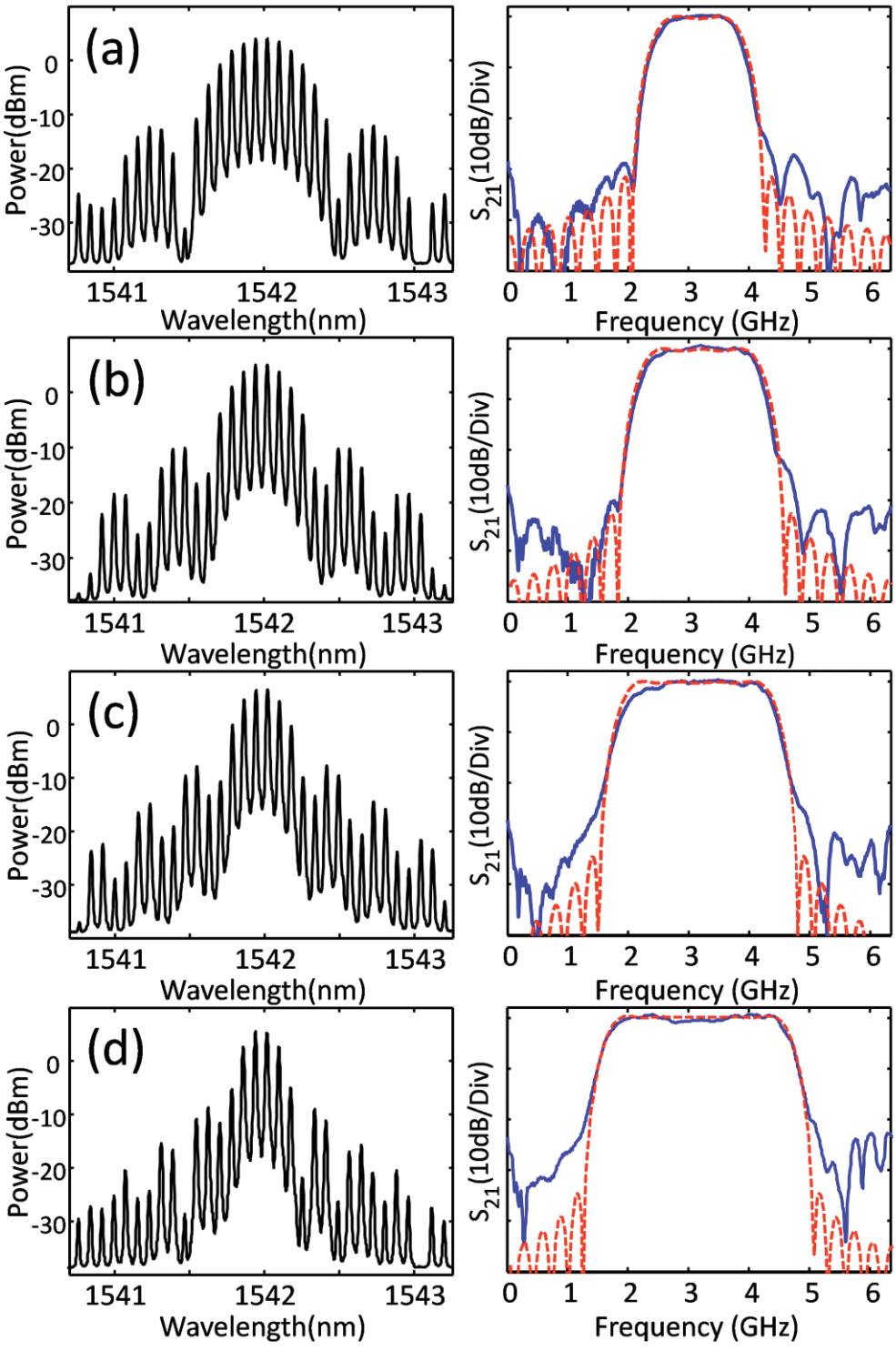

Fig. 3.5 Measured optical spectra (left) and corresponding filter responses measured (solid) and simulated (dash) (right) with 3dB bandwidths of flat-top filter equal to (a) 1.5GHz, (b) 2GHz, (c) 2.5GHz, and (d) 3GHz, respectively

3.5. Tunable Flat-top Microwave Photonic Filters

In this section we will demonstrate tunable flat top microwave photonic filter using a pulse shaper. Although tunable RF filters have been implemented in microwave engineering with a large tunble range and a reasonable loss, their orders usually do not exceed few poles and as a result the filter passband can not be configured to a great extent [21,61-63]. According to Eq. (3.2), tuning of the frequency response can be achieved by linear phase shifts given by $\Delta\omega\tau$ n or an optical delay stage given by τ [38]. We add 0 or π phase (generally, complex) to generate flat-top passband shape on the linear phase, in other words we applied additional 0 or π phase to the tap weights of the filter of which center frequency shifted by the time delay τ. More interesting and distinct method to obtain similar frequency tuning is to control φ_n to increase linearly as *n* increase.

The RF frequency shift is given by

$$\Delta f = -\frac{\tau}{2\pi\psi_2} \tag{3.4}$$

where ψ_2 is the fiber dispersion, and τ the relative delay between two paths. Because the comb light source is coherent (each frequency has a narrow linewidth, and the spacing between frequencies is rigidly fixed), it is not expected to suffer any phase noise degradations with such small delay detunings. This is what allows us to use delay variation as a means to tune the filter. The coherence property of the comb has been proven in our group's previous optical interferometry experiments, where we are able to use such a source to directly measure fiber dispersion by embedding the fiber under test in one arm of an interferometer [64].

Fig. 3.6 shows the programmable control of center frequency by controlling relative delay. The 2.5 GHz 3 dB bandwidth of flat top filter (red) occurs at 2.9 GHz which corresponds to a relative delay of *m*.100-28 ps, where *m* is an integer. The filter bandpass shifts by 4.2 GHz to higher frequency by reducing the delay in the delay path by 40 ps, resulting in the filter (blue) centered at 7.1 GHz without passband shape change.

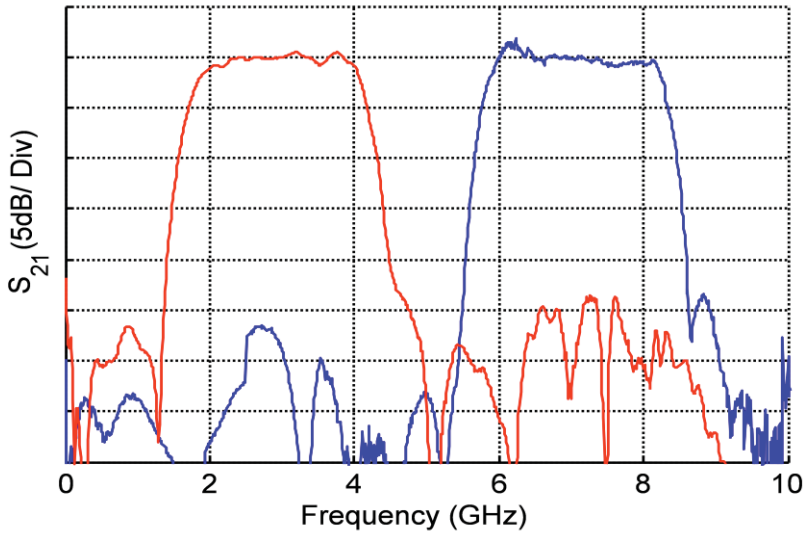

Fig. 3.6 The filter passband center shifts using delay stage. Measured filter transfer function for m.100-28 ps and m.100-68 ps relative delay in red and blue lines respectively. Other comb parameters are fixed to have a 2.5 GHz 3 dB bandwidth flat top filter

However, it is not easy to tune the filter by changing delay path. Here we apply a linear phase to the comb using a pulse shaper to achieve filter tuning. Fig. 3.7 shows the measured filter transfer functions. When no additional phase is applied, the passband is located at 3.2 GHz (corresponding to 30.7 ps). Then we program the pulse shaper to apply a linearly increasing phase (modulo 2π) in steps $\Delta\varphi = \pi/4$, $\pi/2$, and $3\pi/4$ per tap, respectively. The filter passband shifts to higher frequencies by 1.2, 2.3, and 3.6 GHz, which are close to the theoretical values of $FSR/(2\pi/\Delta\varphi)$=1.3, 2.6, and 3.9 GHz, respectively . The measured filter transfer functions, which show ~24.3 dB sidelobe suppression and ~1.3 dB passband ripple, remain approximately constant with relatively close agreement to the simulation result shown in Fig 3.5(b). These results verify that we can achieve tunable microwave photonic filters, with selectable passband profile and essentially without changing filter shape, via line-by-line pulse shaping.

In conclusion, we have demonstrated the implementation of programmable and tunable flat top microwave photonic filters based on optical frequency comb shaping. The amplitude and the phase of each comb lines are programmed by line-by-line pulse shaper.

We were able to vary filter bandwidths by changing the apodization function and to tune the filter center frequency by applying phase ramps across the comb lines. In the current experiment, we did an experiment using 32 flat comb lines but we believe that the extension of the number of comb line is possible, and it will be helpful to design better properties of arbitrary passband profile filters. For example, for flat top filters, we can achieve lower passband ripple, narrower transition band and stronger sidelobe suppression of flat top microwave photonic filters by increasing number of comb lines.

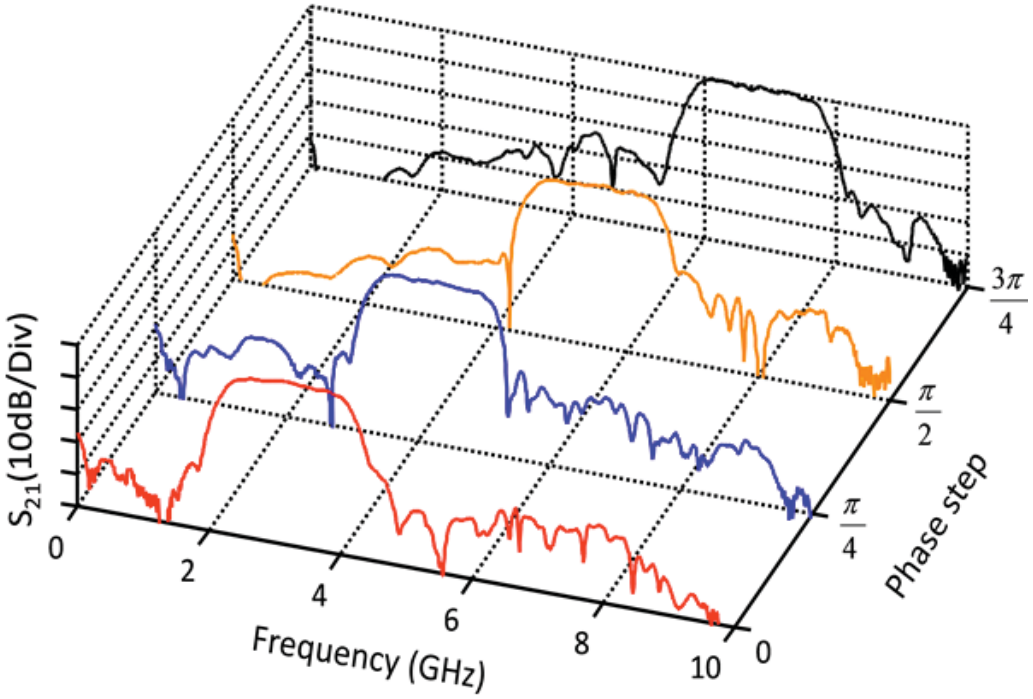

Fig. 3.7 The filter passband center shifts as the phase increases linearly at steps of 0 (not changed), π/4, π/2, and 3π/4 per tap. Other comb parameters are fixed to have a 2 GHz 3dB bandwidth flat-top filter

3.6. Sidelobe Suppression (SLS)

Finally, we do note that sidelobe suppression in the experiments is consistently several dB smaller than in simulation. This may be attributed to several practical issues. First, limited spectral resolution (comparable to the comb spacing) may introduce apodization and phase errors in pulse shaper control of the taps. Second, unwanted small

reflections in the interferometer structure are known to give rise to low amplitude replicas of the filter passband, which are shifted in frequency according to the delay of the reflection [38]. Finally, imperfect SSB modulation due to amplitude and phase imbalances of the modulator and the 90 degree hybrid coupler results in a small double sideband (DSB) modulation component, which is also known to cause a small, frequency shifted, passband replica [65]. Achieving improved sidelobe suppression will require attention to all of these factors.

The simulation results to show the importance of apodization accuracy are shown in Fig. 3.8. Although the combs in Fig. 3.4 and 3.5 have been apodized for the target profiles, the actual profiles have small deviations compared to the target apodization. The simulated filter transfer function obtained from Eq. (3.2) using the measured optical comb profiles shows the same passband shape and lower sidelobe suppression than the ideal sinc function impulse response apodized by Kaiser window is used for the simulation. This indicates that the sidelobes are more sensitive to the fluctuation of comb amplitude. Fig. 3.8 shows the simulated optical combs (left) when φ_n = [π 0 0 0 0 0 π π π π π 0 0 0 0 0 0 0 0 0 0 π π π π π 0 0 0 0 0 π] and the corresponding simulated filter transfer functions (right) when 3 dB bandwidth of passband is 2 GHz. According to our simulation, the extents of the comb fluctuations decide the limitation to the sidelobe suppression of filter responses. The ideal fit to our comb spectrum shown in dashed line would exhibit sidelobe suppression of more than 37 dB where the filter transfer function is shown in dashed line on the right. In Fig. 3.8(a), when 0.5 dB range random fluctuation shown in small bar is added to the comb, the filter response shows ~30 dB sidelobe suppression. The examples of the filter response with the random fluctuated combs are shown on the right (solid line). Figs. 3.8(b) and (c) also show the fluctuation range bar in spectra and corresponding filter transfer functions when fluctuation degrees are 1 and 2 dB. The filter responses of Fig. 3.8(b) and (c) show ~25 and ~20 dB SLS, respectively. This shows that exact filter shapes to the targets are possible via our technique, but very accurate apodization is essential for achieving the high quality filters with very low sidelobes.

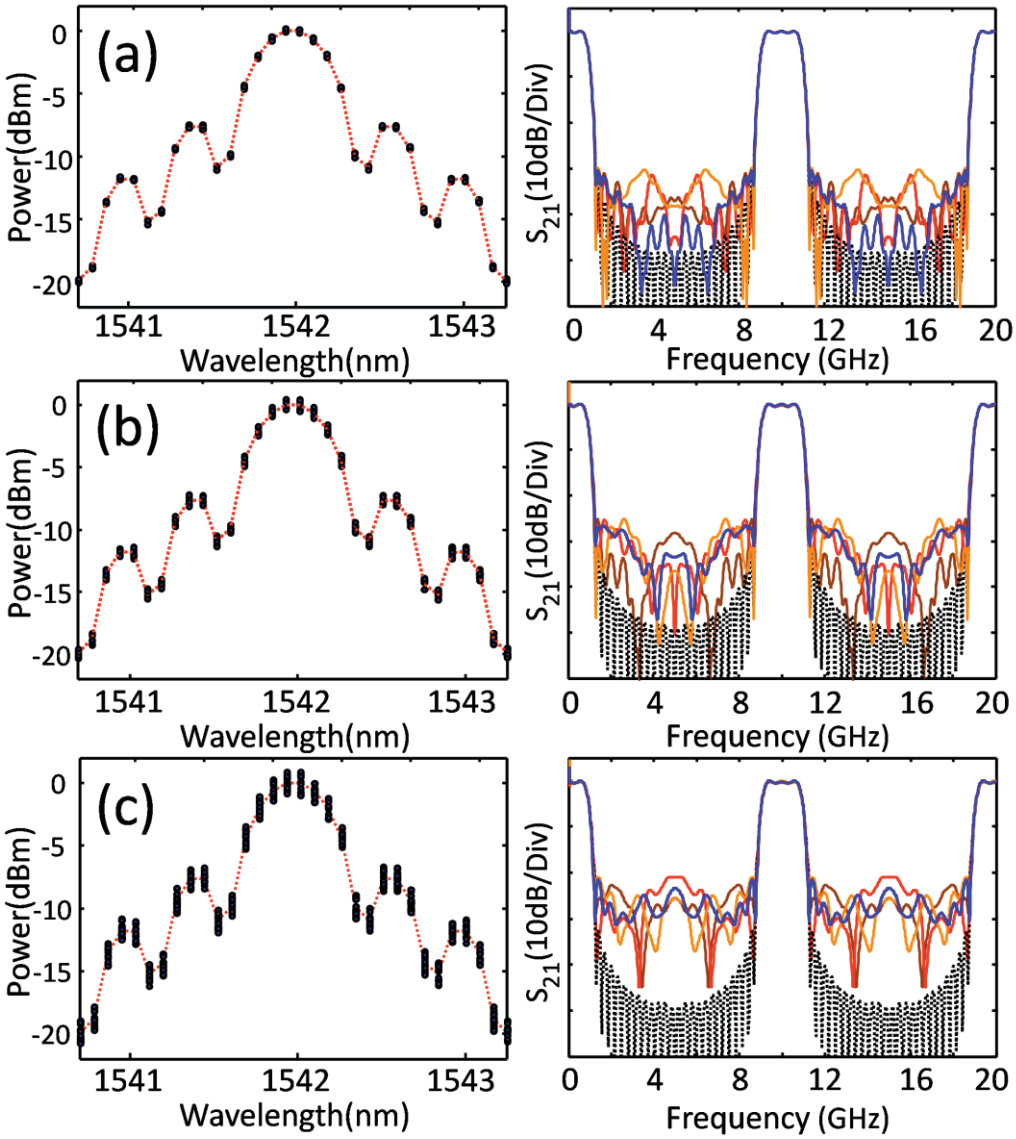

Fig. 3.8 Simulated optical spectra (left) and corresponding simulated filter responses (right) with random fluctuation of optical frequency combs equal to (a) 0.5 dB, (b) 1 dB, and (c) 2 dB, respectively. Ideal combs (dashed) are fixed to have a 2 GHz 3dB bandwidth flat-top passband as shown on the right (dashed). The small bars show the random fluctuation range of the combs, and the examples of the filter response with the random fluctuated combs are shown on the right (solid)

4. PROGRAMMABLE MULTI TAP MICROWAVE PHOTONIC PHASE FILTERS VIA OPTICAL FREQUENCY COMB SHAPING

4.1. Preface

In this chapter we demonstrate a fiber-optic coherent signal processing scheme to achieve a programmable multi-tap microwave photonic phase filter operating over an ultra-wide bandwidth. Complex programmability of tens or hundreds of taps is achieved by line-by-line pulse shaping on electro-optic frequency comb using an interferometric scheme shown in chapter 3. Through high-speed real-time measurement, we show programmable time domain chirp control of GHz-bandwidth microwave signals. In section 4.2 we will introduce the concept and applications of microwave photonic phase filter. In section 4.3 we will describe the experimental result to the amplitude and phase control in filter response contributed by optical phase control. In section 4.4 and 4.5, we will demonstrate the programmable multi-tap microwave photonic phase filters based on Gaussian shaped and flat optical frequency combs, respectively. We illustrate the potential of these MWP phase filters by performing a microwave-chirped-pulse generation experiment. In section 4.5, we will also show the compression of chirp waveform by applying programmable phase using microwave photonic phase filter. In section 4.6, we present the ultra-broadband optical frequency combs based on external non-linear broadening in a highly nonlinear fiber. The filter's achievable time-bandwidth product is related to the number of comb lines that can be individually manipulated. We show that this optical source can be used to achieve a programmable microwave photonic filter with large time-bandwidth product and long temporal aperture. The work relating to section 4.4 has been published in [66], the work in section 4.5 in [67] and the work in section 4.6 in [68].

4.2. Introduction

The implementation of MWP filters with complex coefficients would enable new signal processing applications in radar, ultra-wideband communications, and arbitrary waveform generation [69,70]. Several amplitude and phase filters, such as tunable and multiple passband complex filters and all-pass phase filters, can be easily designed by this approach. However, most of the research efforts in the literature to implement microwave photonic filters are focused on modifying the amplitude response without exploiting the phase characteristics with an exception of linear spectral phase [71-73]. The filters with non-constant group delay play a crucial role in applications which require a careful control over signal temporal characteristics. The realization of programmable arbitrary radio-frequency phase control is a more challenging task, yet with promising implications in modern radar systems [74] or compensation of antenna distortions [75]. One of the most promising applications of microwave photonics is the synthesis of broadband filters with programmable phase response [76]. Arbitrary ultra-broadband RF waveform can be generated by this technique [77]. This also enables processing based on phase-only matched filtering, where the filter cancels the nonlinear spectral phase components of the signal of interest [69,70].

Chirped filters typically present a flat magnitude with a certain coefficient of quadratic phase characteristic corresponds to the linear dispersion within the passband [78]. Here we apply multi-tap microwave photonic filter scheme to design programmable chirped filters, which are valuable components in applications such as radar and ultra-wideband communications [79,80]. As shown in Chapter 3, our group has demonstrated tunable and reconfigurable microwave photonic filter synthesis over tens of complex coefficient taps by implementing line-by-line pulse shaping in an interferometric scheme [45]. Here we extend this concept to demonstrate programmable microwave photonic filters with arbitrary phase response.

Figure 4.1 shows the programmable phase control microwave photonic filter previously implemented by our group using hyperfine resolution optical pulse shaping in an optical-to-electrical mapping configuration [76], which is proved through matched filtering [69]. In Fig. 4.1(a), the phase filter shows programmable quadratic phase

response (above) with flat passband shape (below) in filter response. The programmable phase filter allows us to perform a phase-matched filtering experiment (below) using a broadband chirped microwave signal (above) as show in Fig. 4.1(b). However, unlike with multi-tap dispersive FIR filter schemes, the time aperture of the filter was limited to <1ns as shown in Fig. 4.1(b) because of the finite spectral resolution of the pulse shaper. The time aperture of multi-tap microwave photonic phase filter is governed by the number of taps and the dispersion, and our scheme may be extended to a larger number of comb lines [8] which may be able to achieve large time aperture of phase filter. Highly chirped microwave photonic filters with bandwidth in excess of multi GHz have been implemented by incoherent photonic schemes [81,82], but the chirp coefficients are hard to be tuned in a continuous and convenient manner.

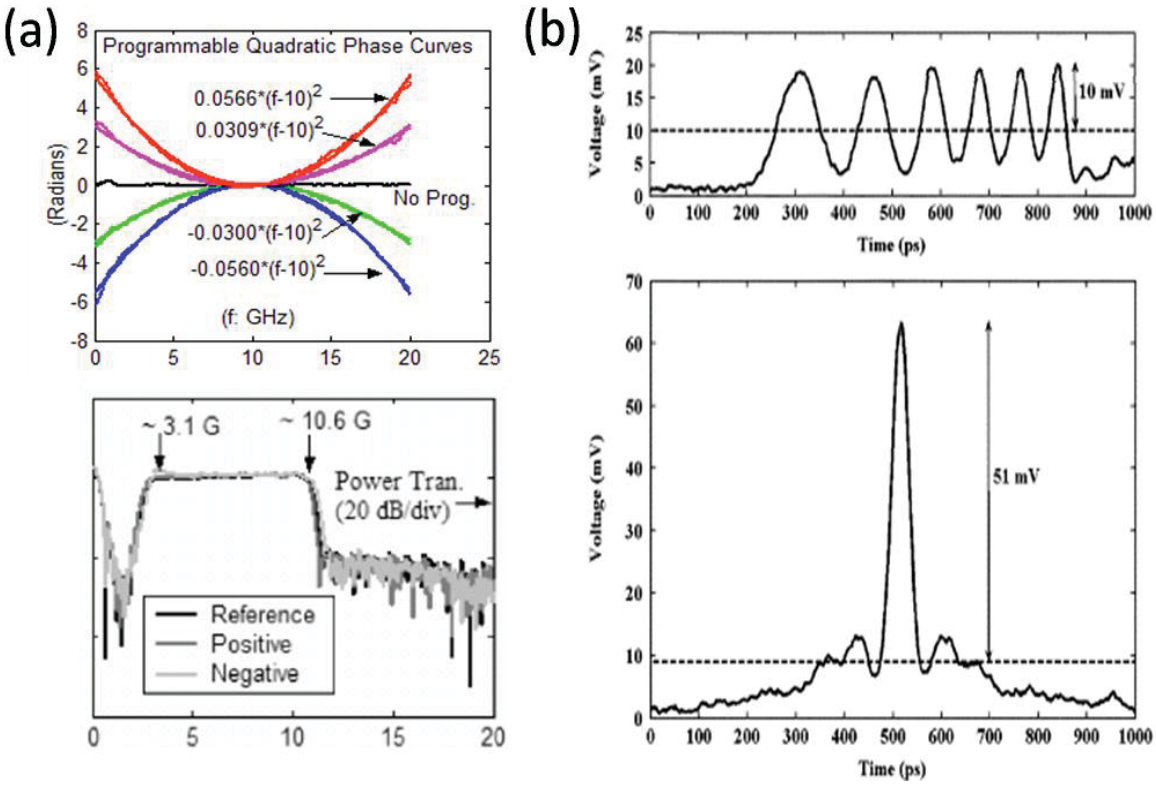

Fig. 4.1 (a) Programmable Microwave photonic phase filters based on direct electro-optical conversion of an optical filter into RF filter using hyperfine resolution optical pulse shaping (adapted from [76]), (b) matched filtering through phase filters shown in (a) (adapted from [69])

4.3. Amplitude and Phase Control in Filter Response by Optical Phase Control

Here for the first time we demonstrate programmable microwave photonic phase control filters based on multitap microwave photonic filter schemes with complex coefficients. We extend the concept shown in Chapter 3 and demonstrate that by implementing line-by-line pulse shaping in an interferometric scheme, we can synthesize complex FIR microwave photonic phase filters in a tap-by-tap basis. We apply the multi-tap complex-coefficient microwave photonic filter configuration introduced in Chapter 3 (Fig. 3.3), in which reconfigurable and tunable flat-top filter was implemented. However, here we program only phase of taps through a pulse shaper to implement phase filters. By engineering the phase of taps, both the amplitude and phase of the filter transfer function can be tailored.

Equation (3.2) shows the filter transfer function of the configuration shown in Fig. 3.3. However, since we program only phase of taps to implement phase filters, the filter transfer function for the MWP phase filters can be written as

$$H(\omega_{RF}) \propto \sum_n e_n^2 \exp[\, jnD\Delta\omega(\omega_{RF} + \tau/D) - j\Phi_n] \tag{4.1}$$

where e_n^2 is the optical intensity of the n^{th} original comb line, and Φ_n the additional phase applied to the n^{th} comb line by the pulse shaper.

Here we investigate microwave photonic filters with programmable quadratic spectral phase response over their passband. Fig. 4.2(a) shows our optical comb generated based on [83] which approximately have a Gaussian profile. The 10-GHz Gaussian-shaped optical frequency comb is implemented with the cascaded three intensity modulators (IMs) and two phase modulators (PMs). To generate Gaussian shape, the RF voltages of first 2 IMs are set to 0.5 V_π, and the RF voltage to the last IM is V_π [83]. When we program the optical pulse shaper to apply a programmable quadratic spectral phase to the Gaussian-shaped comb lines, we can write the filter transfer function as [84]

$$H(\omega_{RF}) \propto \sum_n \exp[-\alpha n^2 + j\beta n^2 + jnD\Delta\omega(\omega_{RF} + \tau/D)] \tag{4.2}$$

where α and β define the tap coefficients with Gaussian amplitude determined by our

comb generator and quadratic phase programmed by the pulse shaper, respectively. We can approximate this summation as an integral corresponding to Fourier transform and find the filter transfer function as [84]

$$H(\omega_{RF}) \propto \exp[-\frac{D^2\Delta\omega^2(\alpha+j\beta)}{4(\alpha^2+\beta^2)}(\omega_{RF}+\tau/D)^2] \tag{4.3}$$

From this equation, it is clear that line-by-line optical phase control offers the complex coefficients in an RF FIR dispersive filter in a tap-by-tap basis. The filter passband has a Gaussian spectral amplitude with programmable bandwidth and programmable quadratic spectral phase by applying optical quadratic phase to Gaussian-shaped combs.

Fig. 4.2(c) shows the filter transfer function measured (solid) using the network analyzer and simulated (dash) when quadratic phase such that β equals to 0 (black), $\pi/98$ (blue), and $\pi/49$ (red) respectively. The corresponding quadratic phases applied to the comb lines are shown in circles, triangles, and squares respectively in Fig. 4.2(b). By fitting a quadratic polynomial to the peaks of the comb lines in Fig. 4.2 (a) we also calculate α which equals to 0.0437.

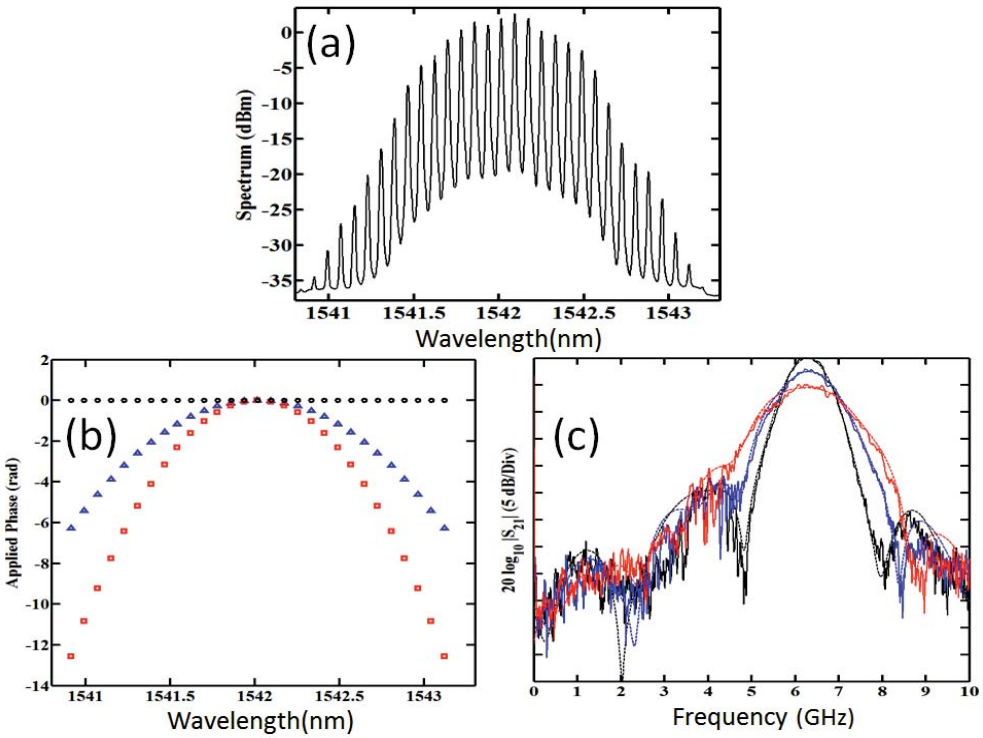

Fig. 4.2 (a) Measured optical spectra, (b) Applied quadratic spectral phases, (c) Corresponding filter responses measured (solid) and simulated (dash)

4.4. Programmable MWP Phase Filters based on Gaussian shaped OFCs

By applying optical quadratic phase ($\Phi_n = \beta n^2$), the Eq. (4.1) can be rewritten as

$$H(\omega_{RF}) \propto \sum_n e_n^2 \exp[\, jnD\Delta\omega\left(\tilde{\omega}_{RF} - \frac{\beta n}{D\Delta\omega}\right)] \tag{4.4}$$

where $\tilde{\omega}_{RF}$ (= $\omega_{RF} + \tau/D$) is offset from center of the filter passband, and β the quadratic phase programmed by the pulse shaper. Here the relation between $\tilde{\omega}_{RF}$ and n can be obtained as

$$\tilde{\omega}_{RF} = \frac{\beta n}{D\Delta\omega}, or\ n = \frac{D\Delta\omega\,\tilde{\omega}_{RF}}{\beta} \tag{4.5}$$

The corresponding delay for tap n is simply expressed as [24]

$$\tau_n = n D \Delta\omega \tag{4.6}$$

Hence

$$\tau(\tilde{\omega}_{RF}) = n D \Delta\omega = \left(\frac{D\Delta\omega \tilde{\omega}_{RF}}{\beta} \right) D \Delta\omega = \frac{(D\Delta\omega)^2}{\beta} \tilde{\omega}_{RF} \tag{4.7}$$

As shown in Section 4.3, by applying optical quadratic phase ($\Phi_n = \beta n^2$), the filter transfer function will also have a quadratic spectral phase response as

$$\psi(\omega_{RF}) = \arg\left[H(\omega_{RF}) \right] \approx -\frac{\psi_2 \omega_{RF}^{\ 2}}{2} \tag{4.8}$$

The relation between frequency dependent delay $\tau(\omega_{RF})$ and RF spectral phase response can be written as [24]

$$\tau(\omega_{RF}) = -\frac{\partial \psi(\omega_{RF})}{\partial \omega_{RF}} = -\psi_2 \omega_{RF} \tag{4.9}$$

From Eqs. (4.7) and (4.9), ψ_2 is obtained as

$$\psi_2 = -\frac{(D\Delta\omega)^2}{\beta} \tag{4.10}$$

As a result, the calculated dispersion in ns/GHz is

$$2\pi\psi_2 = -\frac{2\pi(D\Delta\omega)^2}{\beta} \tag{4.11}$$

As we notice, the quadratic spectral phase response predicted to accompany the increased bandwidths should allow us to impose programmable linear chirps onto bandwidth limited input RF bursts, or conversely to compress frequency-modulated RF bursts. The real-valuated coefficient ψ_2 establishes the amount of linear dispersion (in ns/GHz) over the designed bandpass. To prove spectral phase response in the filter, we implement the time domain measurements.

Here we first investigate the microwave photonic phase filter introducing a programmable optical quadratic phase on a Gaussian comb, which is investigated in the Section 4.3. We explore the phase characteristics of the synthesized electrical filter using a time-domain technique. Figure 4.3 shows the experimental setup. A pulse whose bandwidth lies within the band of the filter shape is synthesized with an arbitrary waveform generator (Tektronix AWG 7122B). The AWG is capable of generating signals

up to 1 volt peak-to-peak at a sampling rate of 12 GS/s. The microwave photonic phase filter modifies the spectral amplitude and introduces the desired spectral phase on the electrical pulse. Then, after amplification and filtering (4 GHz low-pass filter), the received signal is measured with a real-time sampling scope (Tektronix DSA 72004B) with 20 GHz analog bandwidth and 50 GS/s sampling rate. Average acquisition mode is used to effectively reduce the additive noise in the received signal.

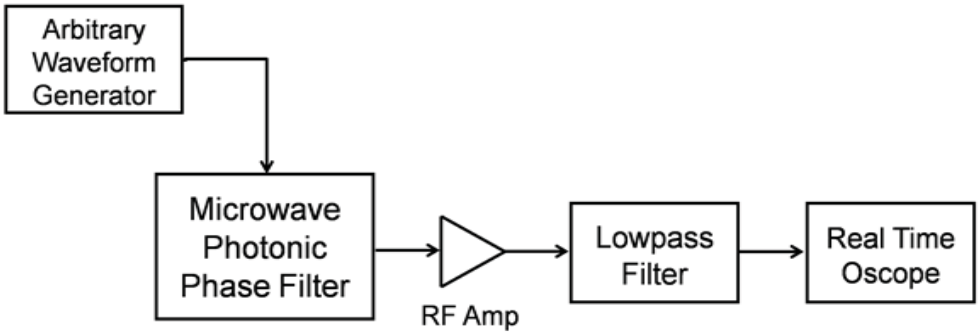

Fig. 4.3 Experimental setup for the time domain measurement of multi-tap microwave photonic phase filters

Figure 4.4(a) shows the 32-tap directly generated Gaussian shaped optical comb [83] measured by an optical spectrum analyzer with 0.01 nm resolution. The envelope (blue) is fit to a Gaussian curve (red), from which we obtained the coefficient $\alpha = 0.023$. The maximum coefficient of RF quadratic phase can be obtained when the Gaussian coefficient α is equal to the coefficient of the optical quadratic phase β. It is derived by differentiating the coefficient of RF quadratic phase shown in Eq. (4.3). Figure 4.4 (b) shows the corresponding filter transfer function measured by a network analyzer when the quadratic phase coefficient $\beta = \alpha$ is applied by the pulse shaper. The center frequency of the band-pass is 2.75 GHz, which is carefully selected by adjusting the relative delay between the two paths in the interferometer. As can be seen, the filter amplitude shape shows 21.4 dB side-lobe suppression and 1.35 GHz bandwidth measured at the 3-dB level.

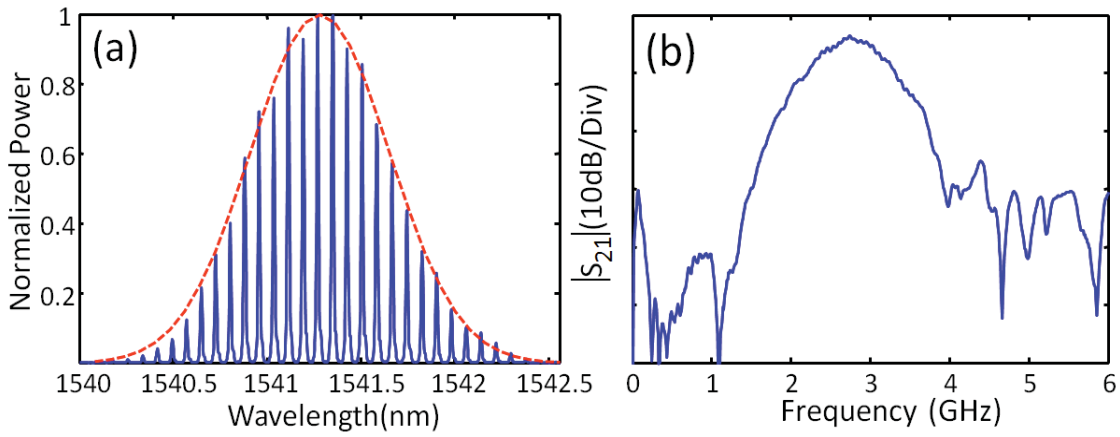

Fig. 4.4 (a) Direct Gaussian shaped comb on a linear scale (solid line) and numerical Gaussian fit (dashed line), (b) Corresponding amplitude filter transfer function of microwave photonic filter on dB scale

Figure 4.5 (a) shows the measured input pulse generated by the AWG whose frequency response corresponds to the filter. The corresponding radio-frequency spectrum, measured with an RF spectrum analyzer with 16.7 MHz resolution, is shown in Fig. 4.5 (b). As can be seen, the pulse spectrum matches the center frequency of the filter shown in Fig. 4.4(b).

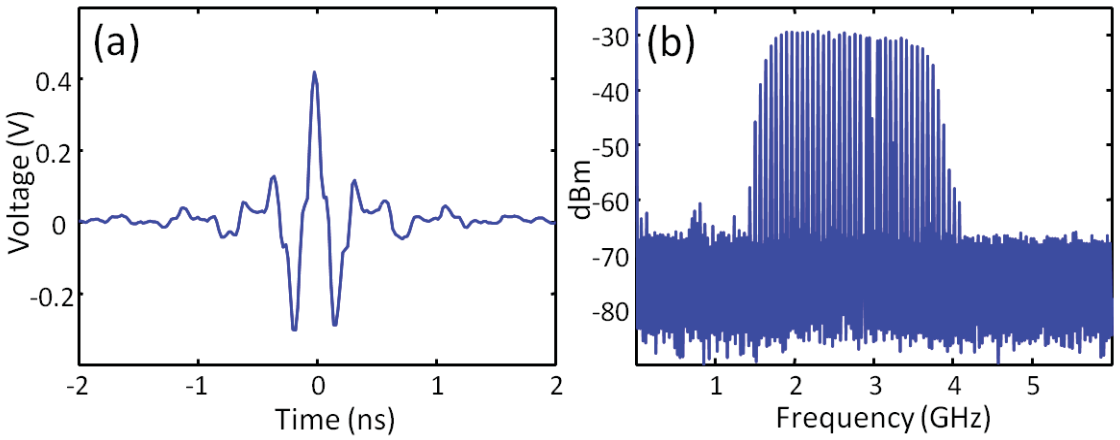

Fig. 4.5 Characteristics of the synthesized input pulse, (a) Temporal profile, (b) Radio-frequency spectrum

Figure 4.6 (a)-(c) show the output pulse measured by the real-time sampling scope and the corresponding numerically calculated spectrograms (for which we used a 0.4 ns Gaussian gating function) [24] when the coefficients of the optical quadratic phases implemented with the pulse shaper are $\beta = 0$, $\beta = \alpha$, and $\beta = -\alpha$, respectively. In Fig. 4.6 (a), the output pulse is broader than the input due to the filter's spectral amplitude modulation. We observe from Fig. 4.6 (b) a linearly down-chirped pulse with a measured chirp coefficient ~ - 1.7 ns/GHz. When we reverse the sign of the applied optical phase, we achieve a linearly up-chirped pulse with ~ 1.8 ns/GHz chirp, as is shown in Fig. 4.6 (c) and the corresponding angle change in the spectrogram. These results clearly show the ability to reprogram the chirp coefficient of the present microwave photonic phase filter.

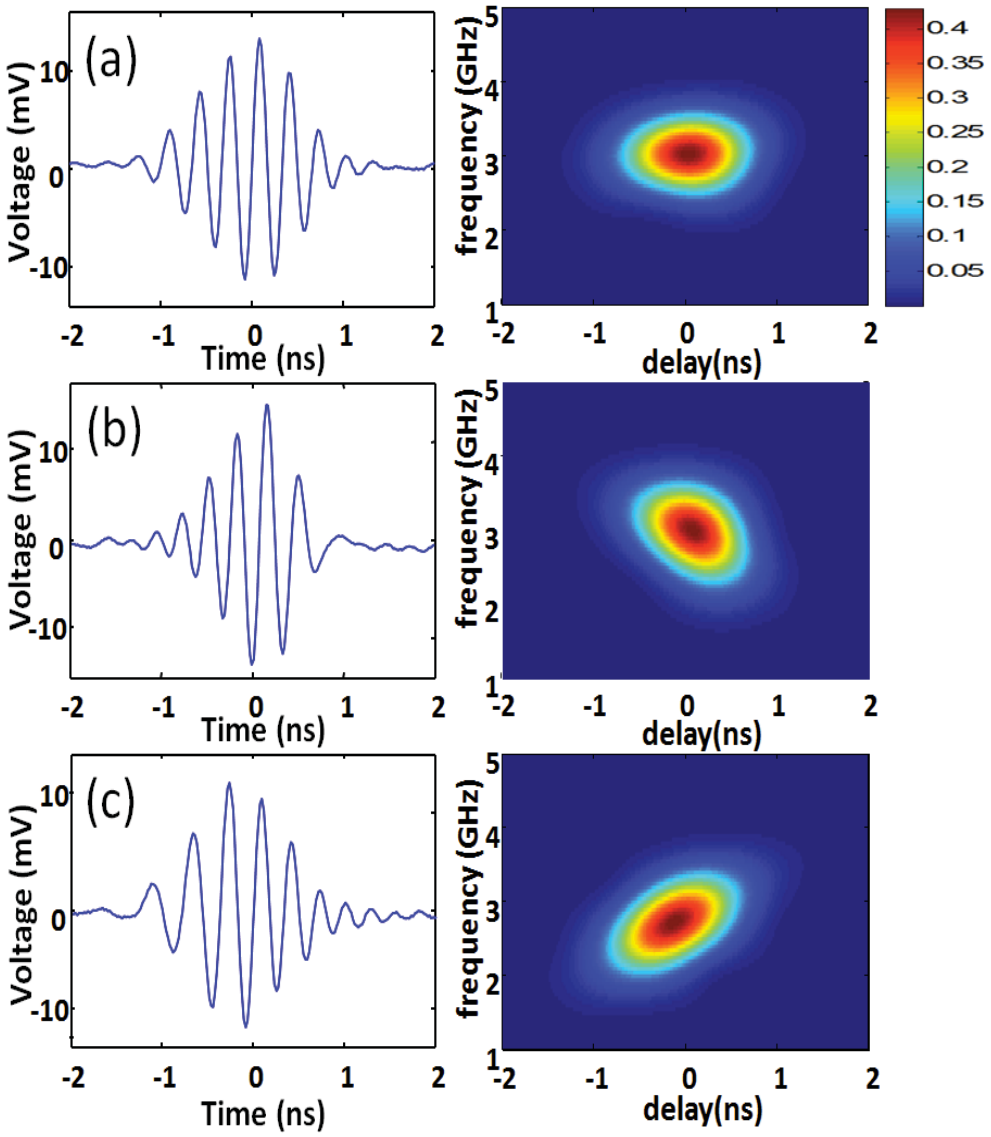

Fig. 4.6 Measured output pulses (left column) and corresponding calculated spectrograms (right column). The achieved chirp values are: (a) 0, (b) -1.7 ns/GHz, and (c) 1.8 ns/GHz, respectively

4.5. Programmable MWP Phase Filters Based on Flat OFCs

In Section 4.4, the Gaussian shaped passband derived by Gaussian apodized comb shows the broader pulse at the output (Fig. 4.6 (a)) compared to the input pulse (Fig. 4.5(a)), which is due to the filter's spectral amplitude modulation. The ideal phase filter's transfer function can be written as

$$H(\omega_{RF}) = \exp[j\psi(\omega_{RF})] \tag{4.12}$$

Hence, the ideal microwave phase filter's amplitude should be constant in passband. Since $|H(\omega_{RF})|$ will introduce filtering noise, the flat-topped bandpass filter is desirable.

Here we investigate microwave photonic filters with programmable quadratic spectral phase response over flat-top passband. When we program the optical pulse shaper to apply a programmable quadratic spectral phase to the flat comb lines, we can obtain broad bandwidth quasi-flat passband as shown in Fig. 4.7. Figure 4.7 shows the simulated filter transfer functions obtained from Eq. (4.1) using the 21 taps ideal flat comb profile when the amount of quadratic phase $\beta = 0$ (black), $\beta = 0.05$ (blue), and $\beta = 0.1$ (red) rad., respectively. The center frequency of the bandpass is set to ~3.1 GHz to clearly show the passband shape changes. By increasing the coefficient of optical quadratic phase, the bandwidth of passband will be increased, resulting in broadband quasi-flat passband.

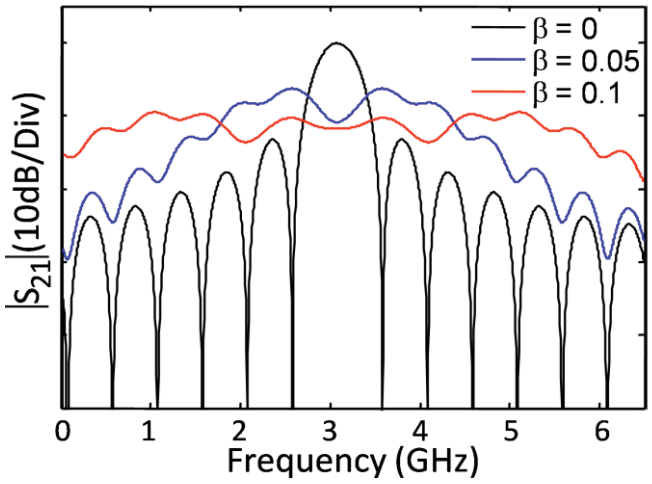

Fig. 4.7 (a) Simulated filter responses with the applied coefficients of quadratic phase to the comb equal to 0 (black), 0.05 (blue), and 0.1 (red), respectively

Figure 4.8(a) shows our optical comb which approximately has a flat profile, as well as measured and simulated filter response in Fig. 4.8(b) when β equals to 0.096. This

value is chosen to maximize the ψ_2 parameter, according to a numerical analysis based on Eq. (4.1). The simulated filter transfer functions (dash lines) obtained from Eq. (4.1) using the measured comb profile are close to the measured filter transfer function (solid lines). The filter gain is -45dB, and the center is selected at 3.4 GHz (corresponding to τ = 32.6 ps tuned with the delay stage). The flat passband bandwidth is ~3.7 GHz in 3 dB bandwidth from the filter passband peak.

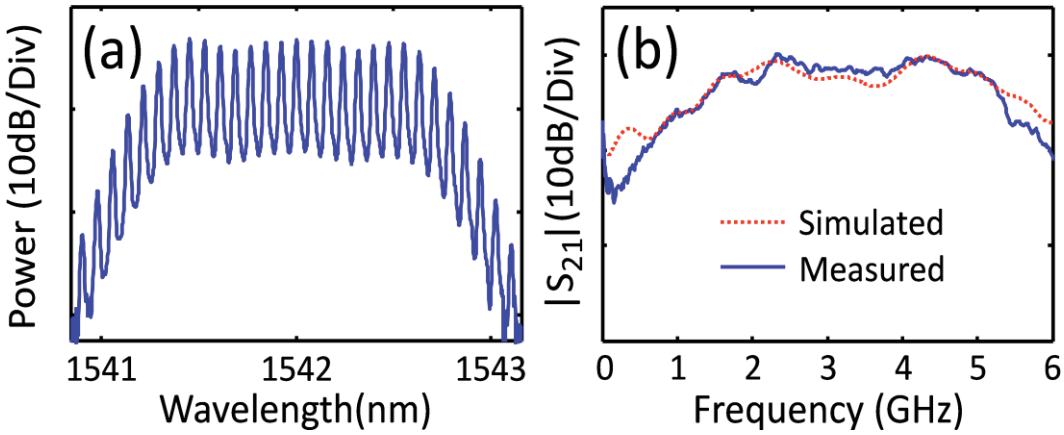

Fig. 4.8 (a) Measured optical spectra of the flat comb, (b) Corresponding filter response measured (solid line) and simulated (dashed line) with the applied coefficients of quadratic phase to the comb equal to 0.096 rad

As shown in Section 4.4, the quadratic spectral phase responses which accompany the increased bandwidths should allow us to impose programmable linear chirps onto the input RF signals. To verify this effect in the flat-topped bandpass filter, we explored the phase characteristics of the synthesized electrical filter in time-domain using the set up shown in Fig. 4.3.

Fig. 4.9(a) shows the applied transform-limited microwave pulse (i.e., a broad-bandwidth pulse with constant spectral phase) generated by the AWG, and its corresponding radio-frequency spectrum measured by an RF spectrum analyzer, which shows 2.8 GHz flat passband at 3-dB level and the 3.4 GHz of center frequency which is matched to the filter paasband center frequency. The input waveform repeats periodically

every 11 ns, which is synthesized with an arbitrary waveform generator operating at 12 GS/s. From Fig. 4.3, the output waveform is amplified, filtered, and finally measured with a real-time sampling scope with 20 GHz analog bandwidth and 50 GS/s sampling rate. 200 traces are averaged together to enhance the signal-to-noise ratio (SNR). Figure 4.9(b) shows the measured (solid) and simulated (dash) output pulses (left) when β equals to – 0.096 rad, and the corresponding calculated spectrogram with 0.4 ns Gaussian gating function (right). Through Fourier analysis of the measured electrical signal, the dispersion is calculated to be ψ_2 = +0.6 ns/GHz. As expected, a measured chirp coefficient of the linearly up-chirped pulse is close to theoretical result calculated using Eq. (4.1) (+0.61 ns/GHz). The slight linear deviation is attributed to small errors in the programmed optical phase. When we reverse the sign of the applied optical phase (β = +0.096 rad), we achieve a linearly down-chirped pulse (left) with –0.56 ns/GHz dispersion, as shown in Fig. 4.9(c). The corresponding angle change in the spectrogram (right) also can be confirmed in Fig. 4.9(c). As expected, the measured pulses are close to the simulated waveforms, and this result clearly shows the ability to reprogram the chirp coefficient of the microwave photonic phase filter.

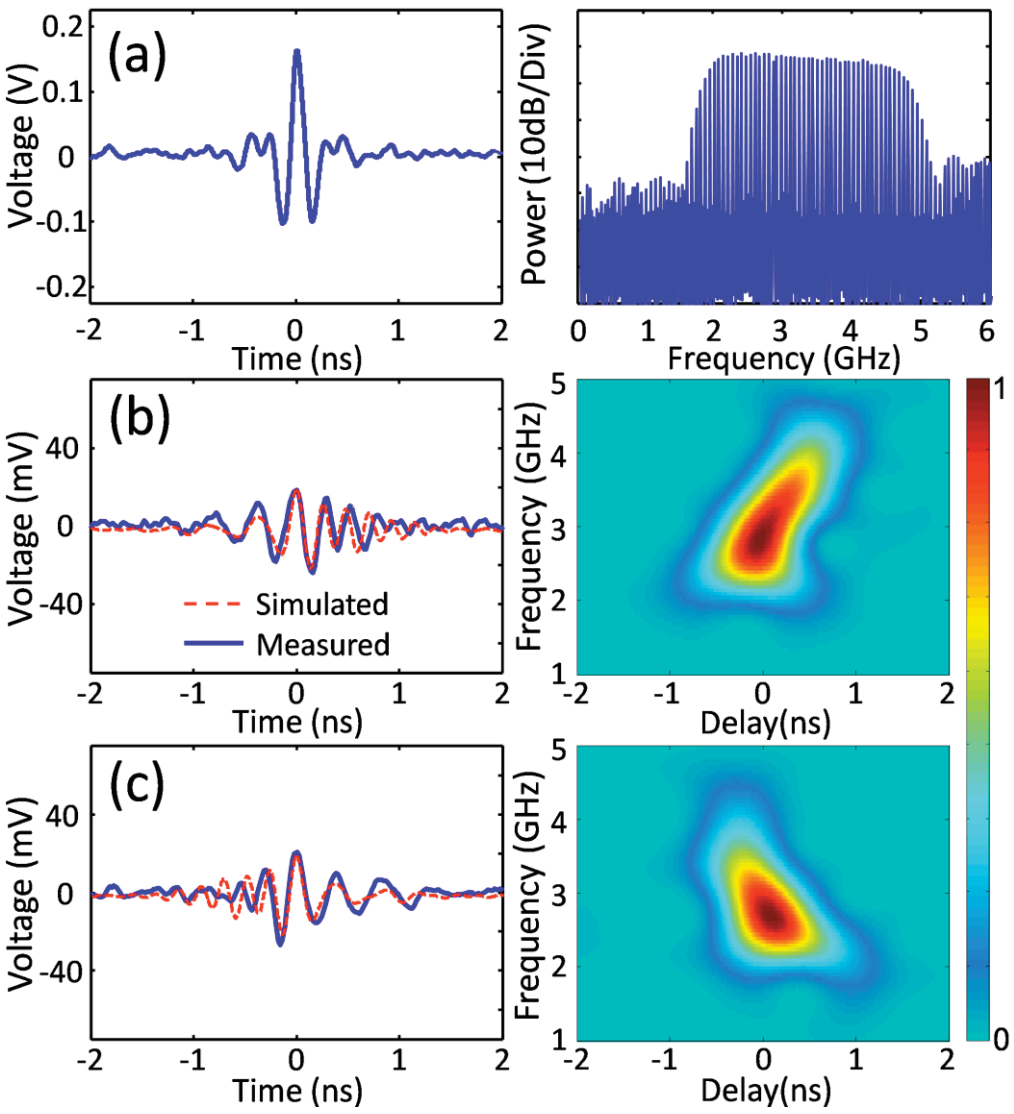

Fig. 4.9 (a) Measured temporal profile (left) and RF spectrum of the synthesized in phase input pulse. Measured (solid line) and simulated (dashed line) output temporal profile (left) and corresponding calculated spectrogram (right) with a 0.4 ns Gaussian gating function when β equals to (b) -0.096 rad. and (c) 0.096 rad.

These programmable MWP phase filters constitute a convenient platform to implement phase-only matched filtering over nanosecond temporal windows. Matched filtering of electrical waveforms is one of the commonly used applications of spectral phase filtering in communication system [85,86]. A matched filter is a linear time-invariant filter whose impulse response is a time-reversed version of the specified signal,

which corresponds to conjugate of the signal spectral phase. The operation of this filter causes a linear spectral phase due to multiplication in frequency domain, resulting in the compressed output waveform to its bandwidth limited duration [86].

Figures 4.10(a) and (c) show the applied linearly chirped input pulse generated by the AWG with the same spectral amplitude characteristics as the one in Fig. 4.9(a) but with a quadratic spectral phase corresponding to a dispersion of either -0.58ns/GHz and + 0.56ns/GHz, respectively. After sending either of these waveforms to the synthesized microwave photonic phase filters corresponding to Figs. 4.9(c) and (d), respectively, we compensate for the input dispersion and obtain at the output the transform-limited waveforms illustrated in Figs. 4.10(b) and (d). The measured waveforms (solid) are very close to the simulated results (dash) as shown Figs. 4.10(b) and (d), indicating exact compression of input chirped waveforms to theirs bandwidth limited pulse duration. We also show a typical single-shot waveform in the inset of Fig. 4.10(d). After 6 GHz low-pass digital filtering, this waveform exhibits an SNR of ~20dB.

The variation in output pulse arises from the variation in the responses of the MWP filter mainly caused by an interferometer. To check the fluctuations on a longer temporal scale, we measured the variation of phase in compressed output pulse. Since pulses have well defined maximum, the time corresponding the maximum voltage at each pulse can be found and recorded easily. Fig. 3.10 (a) shows the phase variation performance for filter output pulses (single-shot measurements of a sequence of ~9000 compressed pulses, one every 11 ns, over a 100 μs span), which shows less than 0.8 rad in 100 μs time range.

In conclusion, the flat-topped bandpass filter including optical quadratic phase can be obtained with the flat OFCs and a pulse shaper in our interferometric scheme. It enabled us to synthesize linear electrical chirps to ~ ns/GHz without filter's spectral amplitude modulation, and it is utilized to compress the linearly chirped broad microwave pulses with nanosecond temporal apertures to their bandwidth-limited duration. Longer temporal aperture could be achieved either by using higher repetition-rate optical frequency combs, larger dispersion amounts, or more comb lines, which will be introduced in Section 4.6.

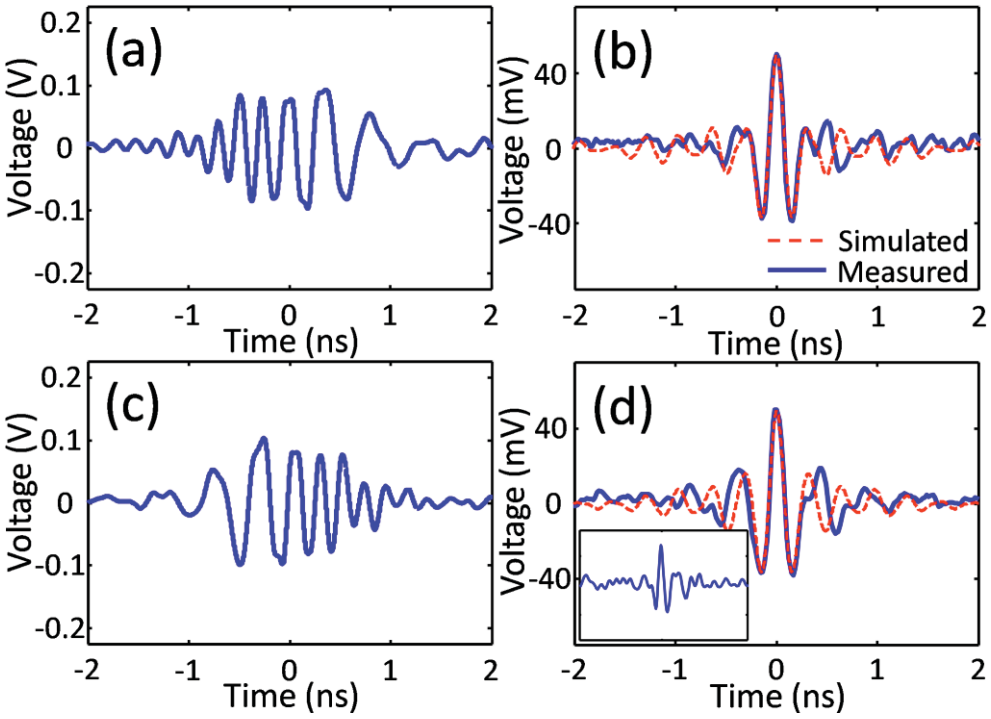

Fig. 4.10 (a) (c) Applied linearly chirped input pulses (temporal profile) with – 0.58 ns/GHz and + 0.56 ns/GHz chirp respectively, and (b) (d) corresponding measured (solid line) and simulated (dashed line) compressed pulses after the matched filter is applied when β equals to –0.096 and 0.096, respectively. Inset of (d), single-shot waveform with same x and y axis scale as (d)

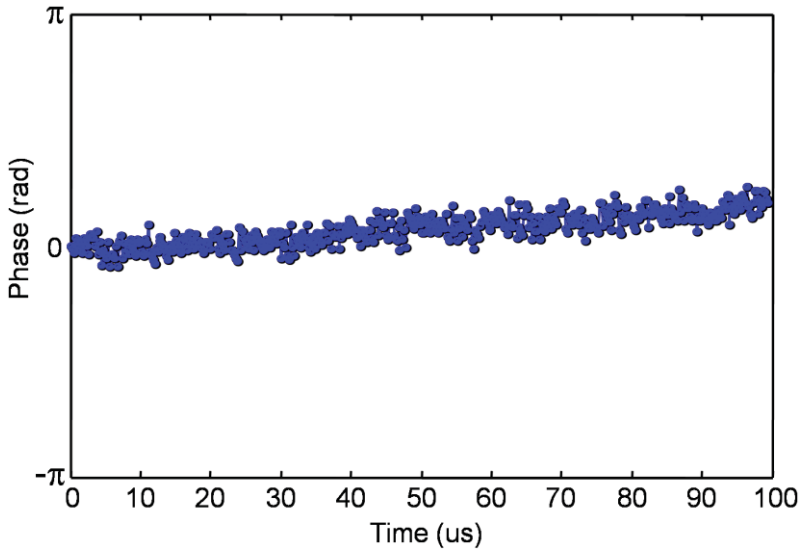

Fig. 4.11 The phase fluctuation measurement of compressed pulse in time range of 100 us

4.6. Programmable MWP Phase Filters Based on Ultra-Broadband OFCs

The flat-topped bandpass MWP phase filter has been implemented as shown in Section 4.5. However, practical filters must have a large time-bandwidth product (TBWP) and operate over long temporal apertures. In other words, it must manipulate the spectral components over the bandwidth of interest with very fine resolution. In [76], a programmable phase filter based on a hyperfine resolution optical pulse shaper was reported with a ~30 TBWP and 20 GHz bandwidth. Although such large TBWP was unprecedented, the temporal aperture of the filter is limited by the resolution of the pulse shaper, resulting in the sub-nanosecond range [80]. To achieve programmable phase control over longer temporal apertures, different configurations that make use of optical dispersion have been recently reported [81,87]. In [81], a chirped single-bandpass microwave photonic reconfigurable filter is presented. This type of structure can achieve large quadratic spectral phase factors over high-frequency carriers, but it lacks the programmability necessary to implement different than quadratic spectral phase profiles, as required by phase-matched filtering. Another interesting configuration is presented in [87], which uses a commercially available optical pulse shaper (Finisar WaveShaper 4000s) to apodize a multi-wavelength laser light source with ~40 taps. This configuration allows for matched filtering operation over a pre-defined band. However, the setup presents an unwanted baseband and it lacks band-pass tuning capabilities.

Preliminary results shown in Section 4.5 demonstrated programmable phase control with ~20 complex-coefficient taps using a simple 10 GHz opto-electronic frequency comb generator. In this contribution, we use such a microwave photonic filter scheme with a ultra-broad band flat-topped optical frequency comb based on seeding a highly nonlinear fiber with transform-limited Gaussian-shaped pulse directly generated by Gaussian-shaped comb generator [88]. It enables to overcome the limitation of TBWP and temporal aperture fundamentally caused by the limited number of available optical taps.

4.6.1. Ultra-broadband Optical Frequency Comb Generation

Few tens of taps at high repetition rate have been implemented by optical frequency combs generated by strong phase modulation while being fed by a single CW laser [13].

More taps (i.e. >100 taps) can be achieved by either more cascaded phase modulators or nonlinear spectral broadening [89]. Among them, the nonlinear spectral broadening technique is a relatively simple solution due to the broad range of highly nonlinear platforms and the availability of high-power optical amplifiers. The 10 GHz flat-topped frequency comb generator with 38 taps in 1 dB power variation have implemented in our group [11]. However, the ultra-broadband frequency comb generators based on nonlinear broadening is difficult to simultaneously achieve the degree of flatness and power stability as required by the particular application. In [90], it was theoretically demonstrated that by pumping a highly nonlinear fiber (HNLF) in the normal dispersion regime a flat, relatively broad and stable supercontinuum can be generated, but the seed pump pulse must be close to a Gaussian-shaped pulse.

Figure 4.12 shows the experimental scheme to generate supercontinuum flat-toped comb, and the first part in the figure is to generate Gaussian pulse based on directly generated Gaussian-shaped comb [91]. Recently, a directly generated Gaussian-shaped opto-electronic frequency comb generator based on the notions of time-to-frequency mapping theory [12] was implemented in our group [91]. As shown in Fig. 4.12, the Gaussian shaped comb is achieved by placing 3 intensity modulators (IMs) and two phase modulators (PMs). The 10 GHz RF signal is transmitted into the IM's ($V\pi$ = ~9 V) and the PM's ($V\pi$ = ~3 V). IM1 and IM2 are both biased at 0.5 $V\pi$, and IM3 is biased at 0 (maximum transmission) to generate Gaussian-shaped pulse. The two cascaded PMs driven at their maximum allowed RF power (30 dBm) enable to be used as time-to-frequency mapping stage, where the generated periodic quasi-quadratic phase by two PMs causes the spectral envelope to mimic the input Gaussian intensity profile.

Figure 4.13(a) shows the optical spectrum of the output directly generated Gaussian comb from the first part in Fig. 4.12, which has 40 lines close agreement to simulated Gaussian fit. Figure 4.13(b) shows the spectral phase of the comb (blue) measured using a linear optical implementation of spectral shearing interferometry [92], and it agrees very well with the quadratic fit (red). The quadratic phase in the combs can be compensated by the appropriate length of SMF. The measured intensity autocorrelation trace after passing the comb in Fig. 4.13(a) through 740 meter of SMF is shown in Fig.

4.13(c) (blue), which is correspond to the simulated autocorrelation trace (red) taking into account the measured comb spectrum and assuming a flat phase (bandwidth limited duration). The measured autocorrelation trace has 4.35 ps FWHM, corresponding to a 3.1 psec Gaussian pulse.

The phase compensated Gaussian shaped optical frequency comb is used as seed to achieve an ultra-broad flat frequency comb generation in an external highly nonlinear fiber. After amplification with an EDFA to 1.7 W, the Gaussian pulse is transmitted into 150 meter of highly nonlinear fiber with nominal dispersion -1.88 ps/nm/km. As shown in Fig. 4.13(d), we can achieve an ultra-broadband flat-topped optical frequency comb spectrum with 3.64 THz (28 nm or 365 lines) within 3.5 dB power variation region at 10 GHz repetition rate.

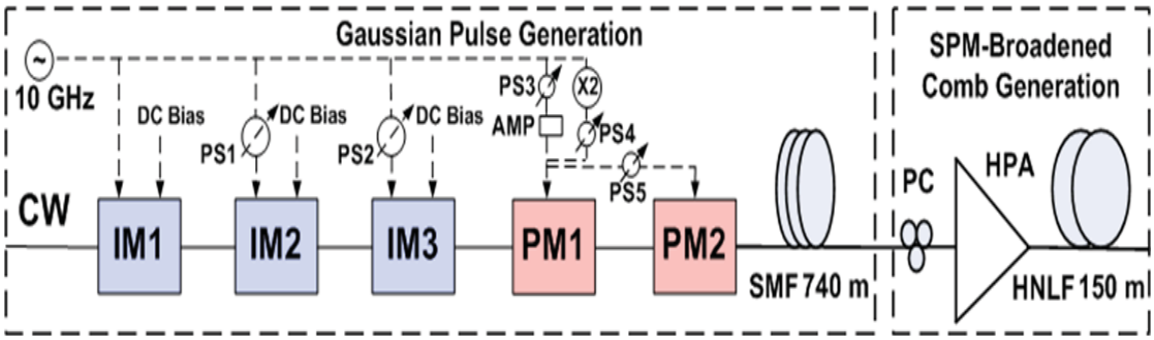

Fig. 4.12 Experimental scheme to generate 10 GHz supercontinuum flat-topped optical frequency combs. PS: phase shifter, SMF: single-mode fibers, X2: frequency doubler circuit, PC: polarization controller, HPA: high power amplifier, HNLF: highly nonlinear fiber

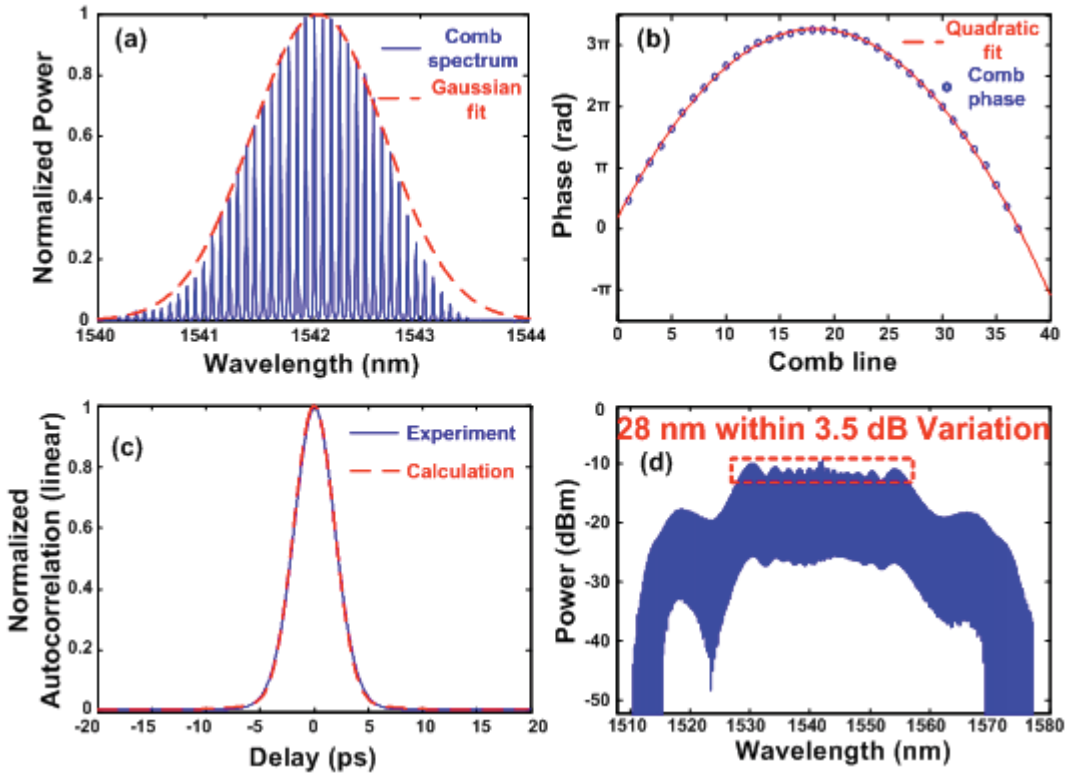

Fig. 4.13 (a) Optical spectrum of directly generated Gaussian frequency comb (blue) and Gaussian fit (red), (b) Experimentally measured comb phase (blue) and quadratic fit (red), (c) Normalized intensity autocorrelation measured (blue) and calculated (red), (d) ultra-broad flat-topped optical frequency comb (adapted from [88])

4.6.2. MWP Phase Filter with Large TBWP and Long Time Aperture

Figure 4.14 shows the microwave photonic phase filter configuration based on ultra-broadband OFCs, a line-by-line pulse shaper, and single-sideband carrier-suppressed modulation in an interferometric scheme. To provide a smooth spectrum, we use an optical band-pass filter (8nm at 10 dB) at the input of the interferometer, which also helps to suppress part of the ASE from the high-power optical amplifier. Besides the smoothing, the filter truncates the optical bandwidth to ~80 optical taps as shown in Fig. 4.15 (a). As introduced in Fig. 3.3, the interferometric scheme enables us to program the phase of the individual comb lines via optical pulse shaper. The corresponding measured amplitude and phase microwave filter response when an optical quadratic phase corresponding to $\beta = -0.032$ is programmed in a line-by-line manner with the shaper

are shown in Fig. 4.15(b) and (c), respectively. In Fig. 4.15(b), the center frequency of the band-pass is 2.75 GHz (corresponding to τ = 26.4 ps tuned with the delay stage), and the achieved bandwidth is ~2.5 GHz at -3 dB. Figure 4.15(c) shows the measured group delay in passband (solid) obtained by differentiating the measured phase response by VNA and its fitting line (dotted line). As expected, it shows linear dispersion in passband, and the chirp rate is 1.7 ns/GHz, as obtained by the fitting line. Both, the number of comb lines and achieved dispersion coefficient are ~4x larger than previously demonstrated in Section 4.5.

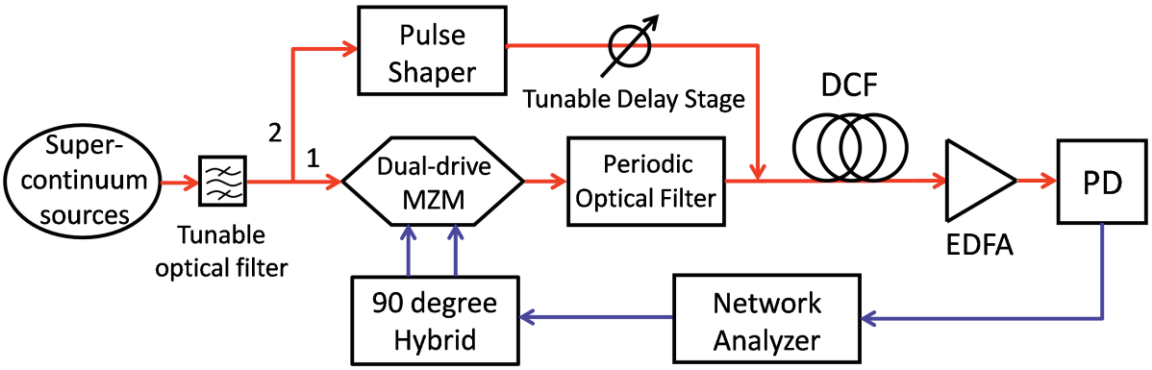

Fig. 4.14 Experimental setup for the complex coefficient taps MWP phase filters based on supercontinuum flat-topped optical frequency comb sources

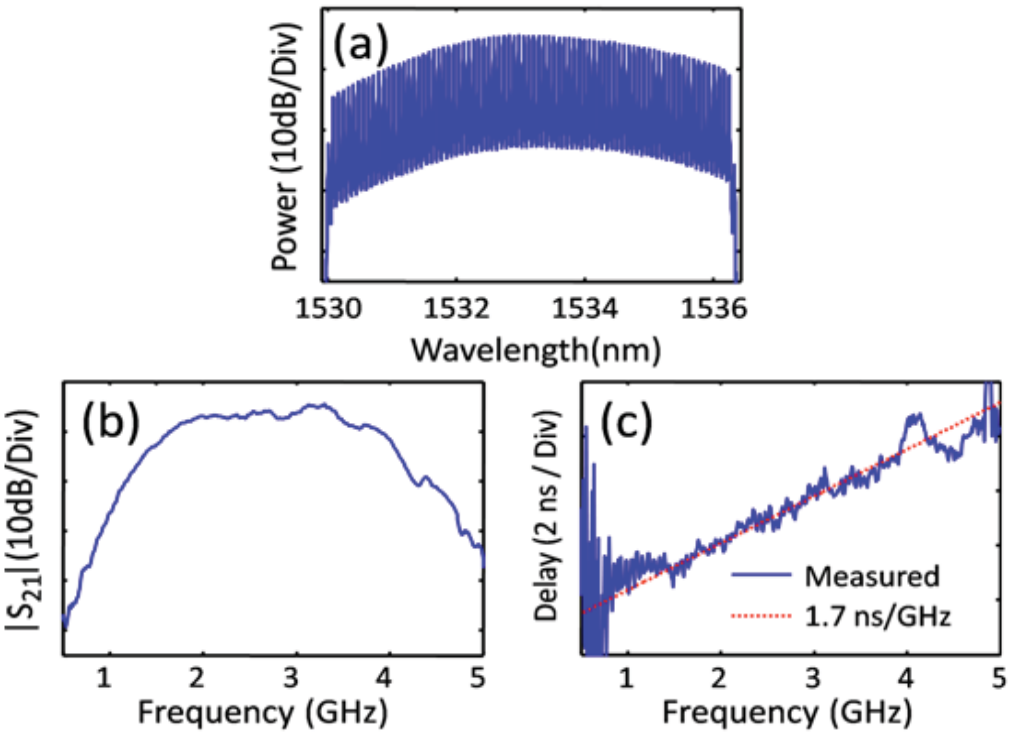

Fig. 4.15 (a) Gaussian shaped comb; (b) Corresponding measured amplitude filter transfer function of MWP filter on dB scale; (c) Measured (solid line) group delay of the filter and its linear fitting line (dotted line)

The large TBWP of the above programmable phase filter constitute a convenient platform to implement a phase-matched filtering experiment using a broadband chirped microwave signal with temporal duration spanning several nanoseconds. We investigate the phase characteristics of the synthesized electrical filter by using the experimental setup in Fig. 4.3. Figure 4.16(a) shows the measured linearly down-chirped input pulse generated by the AWG and its frequency response measured by RF spectrum analyzer, which has a chirp coefficient ~-1.7ns/GHz and ~8 ns temporal aperture. After sending the waveforms to the synthesized MWP phase filters corresponding to Figs. 4.15, we compensate for the input dispersion and obtain at the output the transform-limited waveforms shown in Fig. 4.16(b). The measured waveform (left) very close to simulated result and the corresponding spectrogram (for which we used a 0.4 ns Gaussian gating function) (right) indicate high fidelity spectral phase control. We also show a typical single-shot waveform in the inset of Fig. 4.16(b), which exhibits a signal to background

ratio of ~15 dB. To clearly show the ability to reprogram the chirp coefficient of the microwave photonic phase filter, the linearly chirped input waveform with a chirp coefficient ~+1.7 ns/GHz is applied as shown in Fig. 4.16(c), which has almost same time aperture and frequency response as Fig. 4.16(a). It is exactly compressed to its bandwidth limited duration as shown in Fig. 4.16(d) when coefficient of quadratic phase $\beta = 0.038$. The single-shot waveform in the inset of Fig. 4.16 (d) shows a signal to background ratio of ~20 dB.

In conclusion, we have demonstrated MWP phase filters using an ultra-broadband optical frequency comb as the light source. With this platform, we have shown compression of linearly chirped broad microwave pulses with ~ 8 ns temporal apertures and ~ 3.5 GHz bandwidth at 10 dB to their bandwidth-limited duration. There have been several researches about microwave photonic phase filters as shown in Table 4.1, and our phase shows outstanding temporal aperture and time bandwidth product compared to other results. This work opens a new route for ultra-broad RF phase filtering in large TBWP and long temporal apertures, compatible with the strong demands of modern wireless communication systems.

Table. 4.1 Comparison of a time aperture, a time-bandwidth product, and a chirp rate of our MWP phase filter to the other implementations.

	Time aperture	ΔTB	Chirp rate
E. Hamidi *et al*, *J.Lightw.Tech.*, (2008)	0.7 ns	10.5	0.05 ns/GHz
M. Bolea *et al*, *Opt. Exp.*, (2011)	0.4 ns	2.3	17.2 ns/GHz
M. Li *et al*, MWP, (2011)	3.3 ns	3.9	1 ns/GHz
M. Song *et al*, Opt. Lett., (2012)	2 ns	7	0.6 ns/GHz
M. Song *et al*, MWP, (2012)	**8 ns**	**28**	**1.7 ns/GHz**

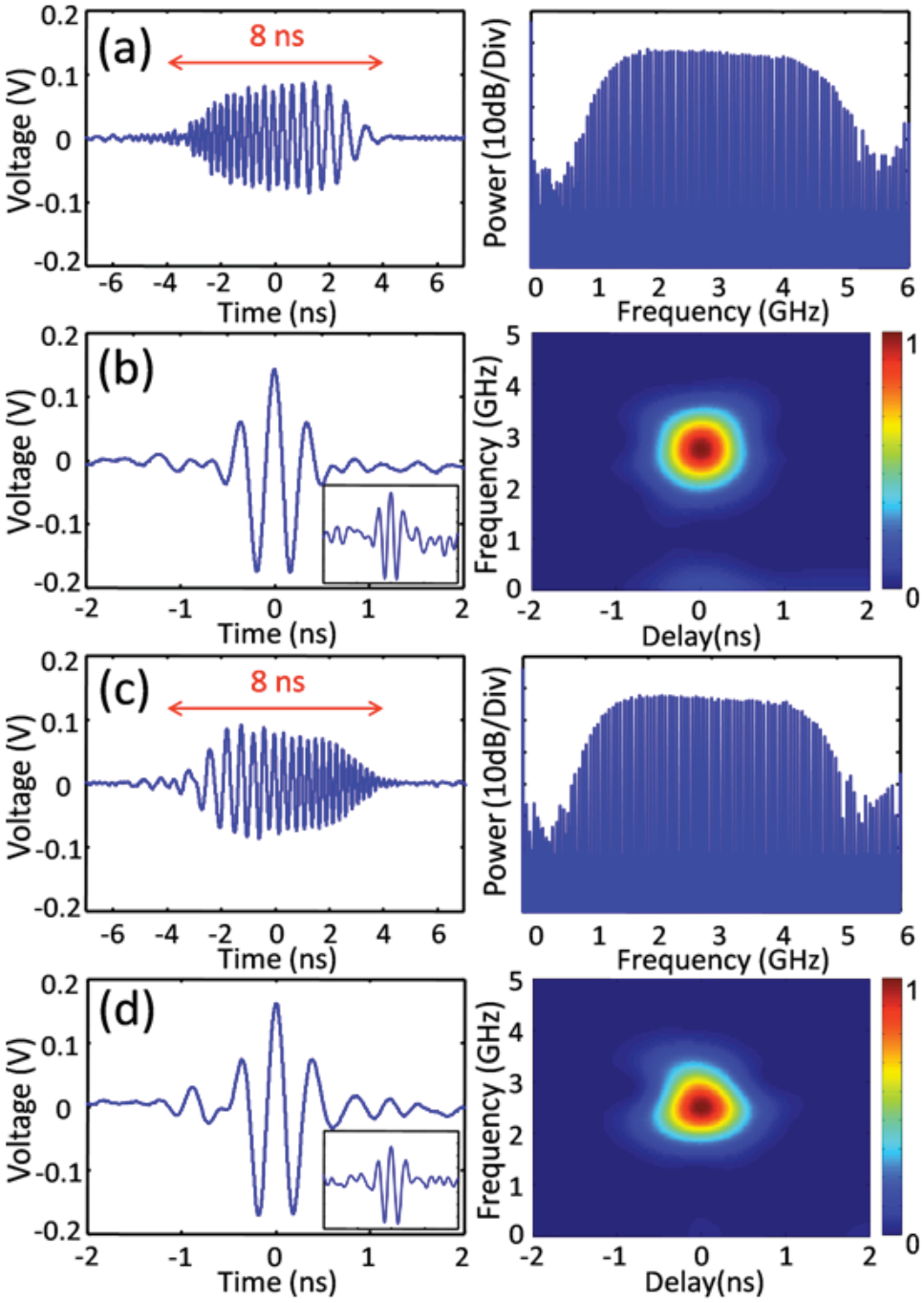

Fig. 4.16 (a) (c) Input linear chirp pulses (left) and corresponding RF spectra of synthesized input pulses (right) with -1.7 ns/GHz and +1.7 ns/GHz chirp respectively, and (b) (d) corresponding measured compressed pulses (left) and their spectrogram (right) after the matched filter is Inset of (b) and (d), single-shot waveforms with same x and y axis scale as (b) and (d) respectively

5. GROUP DELAY RIPPLE (GDR) COMPENSATION OF CHIRPED FIBER BRAGG GRATING (CFBG) VIA PULSE SHAPING

5.1. Preface

In this chapter we will demonstrate a group delay ripple (GDR) compensation of linearly chirped fiber Bragg grating (CFBG) through a phase modulation implemented by pulse shaping. The MWP filter employs a dispersive fiber of order 10 km in length, which leads to a delay or latency of order 50 μsec, which may be too long for certain applications. Our photonic filter may be tuned or scanned in frequency on time scale of 1 μsec or below [40], but this very rapid filter frequency agility will be useful only if the filter delay can be reduced accordingly. One possibility is to substitute a chirped FBG for the long dispersive fiber. Since chirped FBGs offer large accumulated chromatic dispersion in small volumes with low loss, it has used in long haul, high bit rate communication systems as a dispersive medium. However, due to the fabrication error of fiber Bragg grating (FBG), it causes GDR resulting in a substantial degradation in communication systems. We implement the GDR compensation by applying pulse shaper to modulate the phase (i.e. the delay), and we prove it in MWP filter. In section 5.2 we will introduce a principle of CFBG and a GDR of the CFBG mainly caused by stitching error during fabrication. Simulation results for the GDR compensation via phase programming show that the pulse shaping techniques enables us to reduce GDR from the CFBG. In section 5.3 we first introduce a method to measure dispersion of a dispersive medium. We describe the experimental set up of dispersion measurement based on an automated program to conduct the measurement, and we show the experimental result to the group delay and GDR of the CFBG. In section 5.4 we will describe the experimental result to the GDR compensation through phase control via pulse shaping. GDR degrades

filter properties especially for sidelobe suppression, and GDR compensation is proved by improving sidelobe suppression in filter response.

5.2. Introduction

Over the last decades, fiber Bragg gratings (FBGs) constructed in a short optical fiber that reflects particular wavelengths of light and transmits all others have been investigated [93,94]. Therefore, FBGs type of distributed Bragg reflector can be used as an optical filter to block or transmit certain wavelengths. Among them, a chirped fiber Bragg grating (CFBG) has been considered as a promising candidate of a dispersion compensator to replace dispersion compensating fiber (DCF) in optical communication systems [95,96]. It also found use in many applications which require a large dispersive element with an accurate linear relationship between frequency and time delay such as optical pulse shaping [97], optical frequency-domain reflectometry [98,99], and arbitrary electrical waveform generation [100,101].

Fig. 5.1 shows the linearly chirped FBG structure with reflective index profile. The periodic variation of refractive index into the core is written by an intense ultraviolet (UV) source such as a UV laser [95], resulting in the reflection depending on wavelength (i.e. a wavelength specific dielectric mirror). A chirped FBG can provide a total dispersive delay of 10 nsec in approximately 1 meter of grating length.

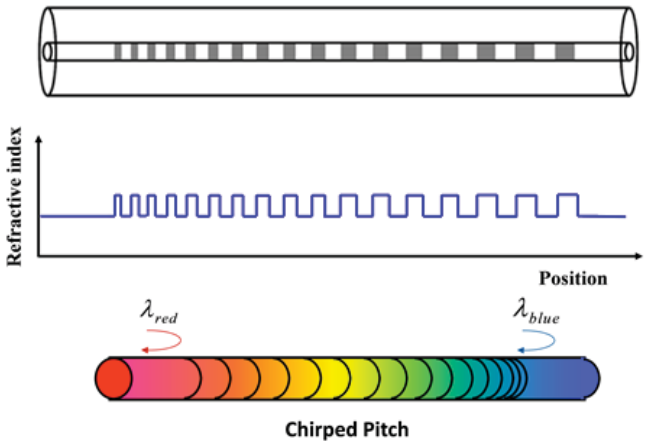

Fig. 5.1 A linear chirped fiber Bragg grating (CFBG) structure with reflective index profile

CFBGs offer substantial advantages compared to a long optical fiber as highly dispersive medium [95]. They can provide large accumulated chromatic dispersion in significantly compact forms with small insertion loss. They also can be designed to have independently customized dispersion and bandwidth in a convenient manner [102,103]. It allows scaling the technique for operation throughout over the C-band [104]. As another advantage, linearly CFBGs provide linear chirp without the third and higher phase distortions which cause serious degradation in transmission system. The conventional dispersive mediums have significant higher order terms which can be only compensated by post-processing [105,106], and the representative technological solution is a CFBG to set all higher order terms to zero.

However, it is well known that CFBGs typically have significant group delay ripple (GDR) which gives rise to substantial degradation to CFBG-based all-fiber applications [107]. A primary cause of such group delay ripple is random and systematic errors as well as imperfection introduced during fiber grating fabrication, and it is defined as a deviation of the group delay from the target (usually linear) behavior. Fig. 5.2 shows an example of group delay ripple and its corresponding group delay ripple of a CFBG (Proximion 1200 ps/nm DCM-PC over 6nm) [108]. The measured group delay (GD) (blue) shows close agreement to the ideal linear plot (red) whose slope is 1200 ps/nm. By subtracting ideal linear slope to the measured group delay, group delay ripple which is deviation of group delay from the target will be given as shown in Fig. 5.2 (right) indicating ~45 picoseconds peak-to-peak ripple over 6 nm.

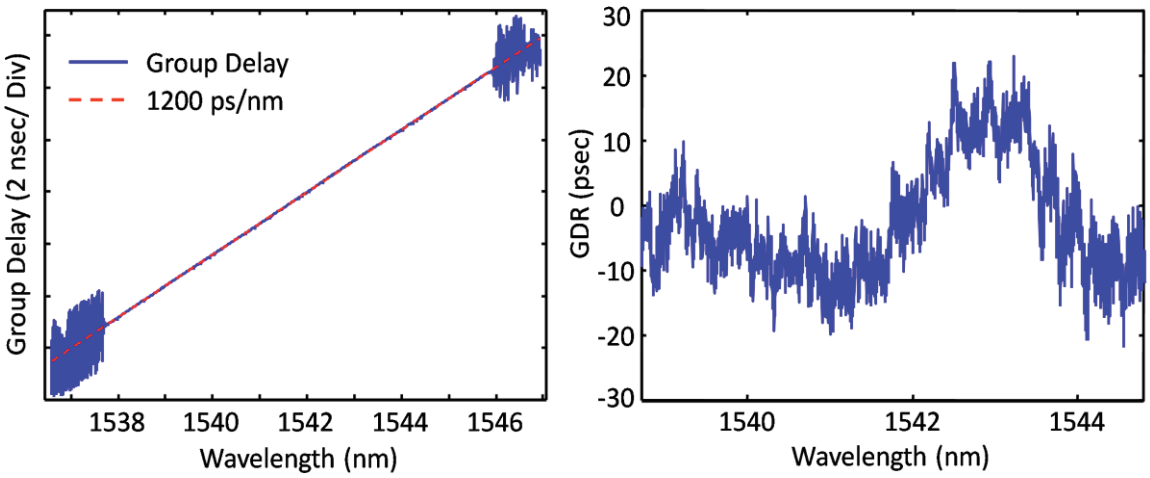

Fig. 5.2 An example of group delay (left) and the corresponding group delay ripple of a chirped fiber Bragg grating (right) [108] provided by Proximion.

The mitigation of GDR in fiber Bragg gratings have been implemented modification of the fiber grating fabrication process [109-111]. Although these works allow for significant reduction of GDR, they did not deal with random errors introduced in fiber grating fabrication. Several research groups also have reported methods to correct the GDR such as dispersion balanced out pairs [112], a digital post-processing routine [113], optical finite and infinite impulse response equalizer structures [114], and a generically initialized transversal filter [115]. However, these techniques typically translate into complicated configurations and relatively long processing time. Here we introduce the simple and powerful method to correct random GDR by using optical spectral phase shaping to equalize the Bragg grating GDR characteristic. Synthesis of a spectral phase equalizer based on a programmable pulse shaper has been reported using such an approach [105,106]. We extend this concept to compensate the GDR of CFBGs through arbitrary spectral phase control. Even if the GDR compensation method based on pulse shaping was recently demonstrated [116], it only covers the fixed systematic errors. Here we show the method to correct the phase ripple (i.e. group delay ripple) including all the flexible random and systematic errors by applying directly and automatically measured GDR. The GDR correction by a pulse shaper is proved by a microwave photonic filter sidelobe suppression improvement.

The phase errors caused by GDR can be obtained by integrating the GDR. The resulting phase characteristic can be written as

$$\delta\psi(\omega) = -\int \delta\tau(\omega)\, d\omega \tag{5.1}$$

where $\delta\tau$ is group delay ripple and $\delta\psi$ is the phase error caused by GDR. By applying opposite sign of phase error using a pulse shaper, phase error can be compensated, resulting in correcting GDR. Even if a high resolution pulse shaper can resolve and control phase error precisely, it requires a spectral disperser with enough resolution to resolve and a spectral mask that can manipulate [18]. Figure 5.3 shows the simulation correction results of group delay ripple shown in Fig. 5.2 using a phase control pulse shaper when its spectral resolution is either 5 GHz or 10 GHz. The peak-to-peak of phase error by GDR is ~4.3 radians over 6nm bandwidth (not shown), and it can be reduced by > 0.2 and > 0.3 radians by applying the 5 GHz and 10 GHz spectral resolution of pulse shaper respectively as shown in Fig. 5.3. They also show 0.04 and 0.06 radians of root-mean-square (RMS) respectively.

According to our simulations, GDR will degrade filter properties especially for sidelobe suppression. The filter transfer function with GDR can be written as

$$H(\omega_{RF}) \propto \sum_n a_n \exp[\, j(nD\Delta\omega + \delta\psi)\, \omega_{RF}\,] \tag{5.2}$$

where a_n is the powers of the n^{th} comb line, D the fiber dispersion, $\Delta\omega$ the repetition frequency of optical frequency comb. Figure 5.4 shows the simulated filter responses with 30 taps of Gaussian apodized combs to see the effects of GDR. Ideal filter without GDR is shown in black, and the red line shows the filter response when the GDR shown in Fig. 5.2 is applied to the filter. It shows about 21 dB sidelobe suppression. However, by correcting GDR through a 10 GHz resolution pulse shaper, the sidelobe suppression approached to its ideal filter response as shown in blue. It shows ~50 dB sidelobe suppression when a 10 GHz spectral resolution pulse shaper is used to correct GDR.

In section 5.3, we first present experiment results for the simple and automatic measurement of the group delay (including group delay ripple) of CFBG by applying tunable laser and arbitrary waveform generator (AWG). In section 5.4, we compensate

the GDR of CFBGs by applying a pulse shaper, and it is demonstrated by sidelobe suppression improvement in MWP filters.

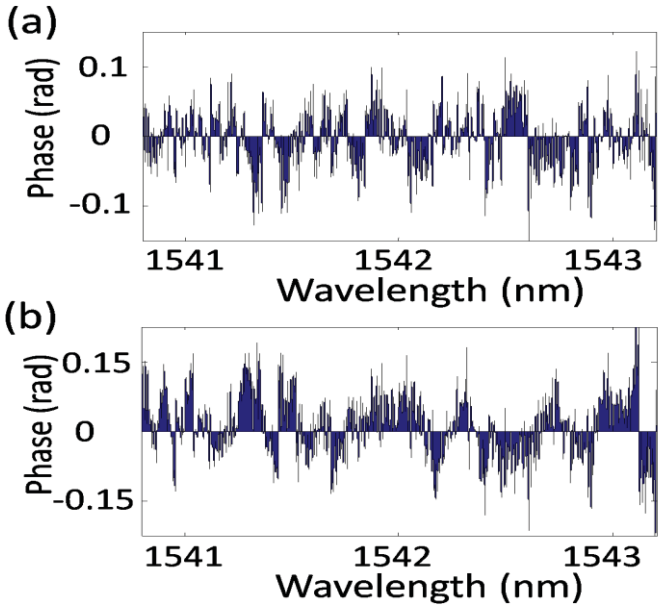

Fig. 5.3 Group delay ripple correction using a phase control pulse shaper with spectral resolution of pulse shaper equal to (a) 5 GHz and (b) 10 GHz, respectively

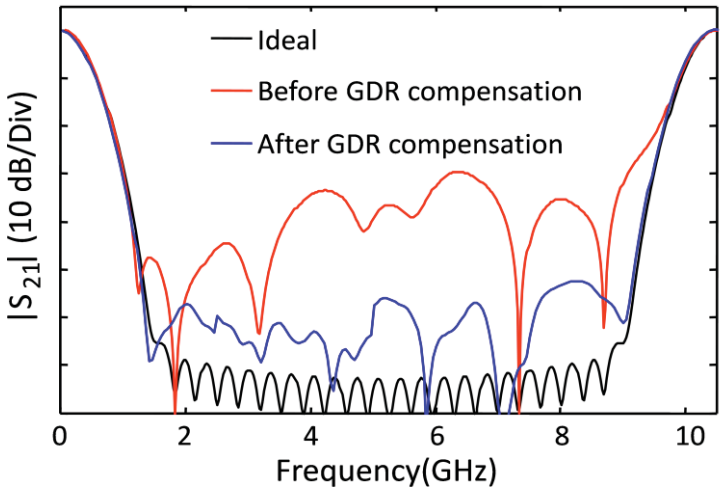

Fig. 5.4 Simulated filter responses with Gaussian apodized combs when there is no group delay ripple (black), and when group delay ripple shown in Fig. 5.2 is applied to the filters (red), and when it is corrected by a 10 GHz spectral resolution pulse shaper (blue)

5.3. Group Delay and Group Delay Ripple Measurement

It is obvious that the precise characteristic of GDR in CFBGs is a critical task to compensate it. Methods for measuring the group delay (including GDR) characteristics of dispersive components include, among others: Frequency-to–time mapping interferomery [117], Phase reconstruction using optical ultrafast differentiation [118], and scanning interferometric techniques: low-coherence interferometric methods [119], phase-shift techniques [120], and swept-wavelength interferometry (SWI) [121,122].

We present monitoring of the group delay ripple of a 10 m long linearly CFBG with dispersion of 1200 ps/nm over 6 nm bandwidth through wavelength sweep scheme based on the use of a wavelength-tunable laser [121] with an arbitrary waveform generator. By running a Matlab program to make the tunable laser moves wavelength steps after a certain time interval, and taking a trace from the sampling scope at each wavelength after the short pulse generated by AWG is passed through CFBGs, we can easily and automatically measure and analyze the delay of the output pulse (i.e. group delay and GDR).

Figure 5.5 shows the schematic of our experiment setup to measure the group delay and group delay ripple profile of a CFBG. After adjusting the polarization of carriers before modulation by a polarization controller (PC), the tunable laser source (Agilent 8163) is modulated by a short input pulse generated by synthesized with an arbitrary waveform generator (Tektronix AWG 7122B) through a dual-drive Mach-Zehnder modulator biased at quadrature point. The AWG is capable of generating signals up to 1 volt peak-to-peak at a sampling rate of 24 GS/s. After amplification through an EDFA (Erbium Doped Fiber Amplifier), the modulated light is sent to a dispersive medium (a CFBG that has 1200 ps/nm dispersion at 1550 nm with 6 nm bandwidth) and subsequently detected by a 22 GHz bandwidth photodiode (PD). The changing output pulse delay is measured using the 60-GHz sampling oscilloscope (Tektronix DSA 8200), and the wavelength sweep of the tunable laser is monitored by optical spectrum analyzer with 0.01 nm resolution. The sampling oscilloscope is triggered by the AWG's digital output sent by a RF cable. It is synchronized with the waveform generated by AWG, and its timing jitter is below 30 ps.

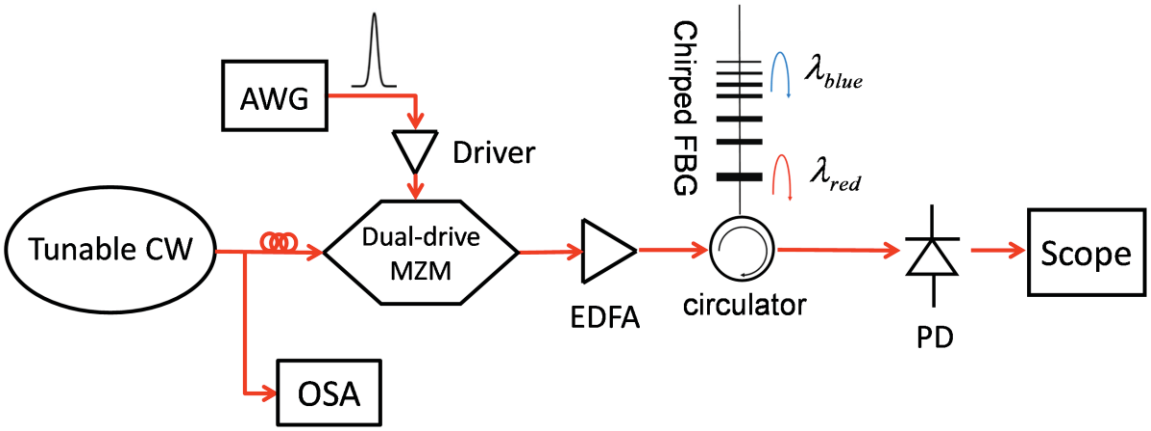

Fig. 5.5 Schematic of the experiment setup for measuring the group delay and the group delay ripple profile of a CFBG

The group delay and group delay ripple of a fiber link under test (i.e. a CFBG) is measured by sweeping the tunable laser (from 1538.72 nm to 1544.80 nm with 0.04 nm steps) and measuring the changing pulse delay using the sampling oscilloscope. Fig. 5.6(a) and (b) show the optical spectrums measured by optical spectrum analyzer (OSA) and the output pulses measured by sampling oscilloscope when the wavelengths of a CW laser are 1540 nm (blue), 1542 nm (red), and 1544 nm (black), respectively. When a 40 sec time interval is taken between measurements in order to allow the oscilloscope to average (here 100 traces are averaged), the output waveforms show clear voltage peaks by applying short input pulse using AWG. Since waveforms have well defined maximum, the time corresponding the maximum voltage at each wavelength can be found and recorded easily, resulting in delay vs. wavelength vector. Figure 5.6(c) shows the analyzed GDR (red) when the laser is scanned from 1538.72 nm to 1544.80 nm with 0.04 nm steps, and the measurement is repeated 10 times to prove the stability and precision of our proposed measurement setup. The standard deviation as low as ~4 ps (a maximum standard deviation of 6 ps) is shown in vertical bars of the plot.

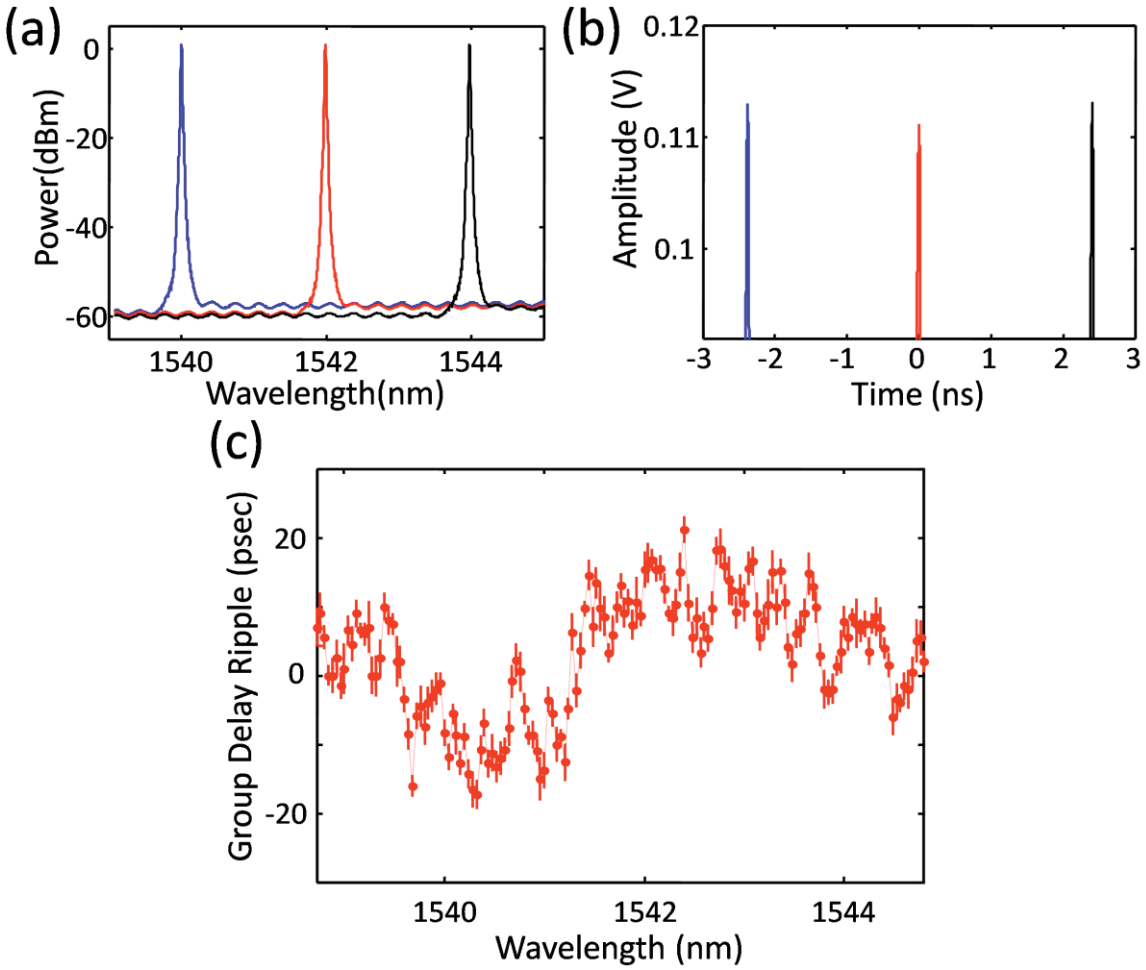

Fig. 5.6 (a) Measured tunable CW laser sources and (b) corresponding output waveforms when the wavelengths equal to 1540 nm (blue), 1542 nm (red), and 1544 nm (black), respectively, (c) GDR of the tested CFBG

5.4. Group Delay Ripple Compensation

Here we demonstrate a method to correct random GDR by applying optical spectral phase shaping. Figure 5.7 shows the MWP filter configuration to prove the GDR compensation of a CFBG. A 10 GHz repetition rate comb composed by cascading an intensity and phase modulator driven by a 10 GHz clock signal is amplified and polarized by an EDFA and a PC, respectively. The comb is then modulated by the electrical signal given by a network analyzer through a dual-drive Mach-Zehnder modulator. The two input RF ports have 90 degree phase difference, featuring optical single-sideband (OSSB)

modulation [42]. The modulated light is sent to a tested CFBG and the spectrum is then phase modulated and further Gaussian apodized in the optical pulse shaper (Finisar Waveshaper, Model 1000s) to remove the GDR and get a Gaussian shaped passband in the filter [38] to clearly show the sidelobe suppression improvement through GDR compensation. The filter transfer function (S21 parameter) is measured by a network analyzer after photodetection from a 22 GHz bandwidth photodiode (PD).

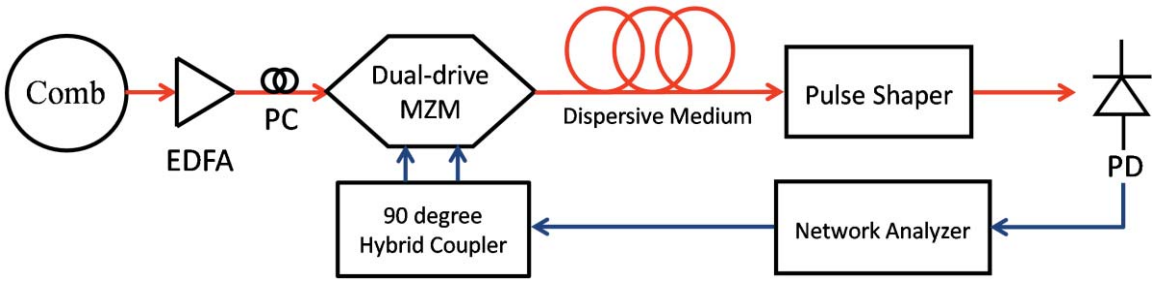

Fig. 5.7 Experimental setup for group delay ripple correction using a amplitude and phase control pulse shaper

As shown in Fig. 5.4, GDR degrades the sidelobe suppression in microwave photonic filters. First, we demonstrate the degradation through a comparative study of the sidelobe suppression in two microwave photonic filter links based on a dispersion compensating fiber (DCF) and a CFBG.

Figure 5.8(a) shows Gaussian shaped combs which have 21 taps with ~ 40 dB of extinction ratio. Figure 5.8(b) shows the corresponding measured (solid) and simulated (dashed) filter responses when the filter is implemented with a CFBG (red) and a DCF (black), respectively. As observed from Fig. 5.8(b), microwave photonic filters implemented with a CFBG have significantly worse sidelobe suppressions when compared to a DCF based filter links. The measured responses closely match the predicted filter transfer functions obtained from Eq. (4.1) using the measured optical comb profiles (in Fig. 5.8(a)) and the GDR (in Fig. 5.6(c)), and the filters based on a CFBG and a DCF show similar passband shapes, but differ in the sidelobe suppression (~ 17.5 dB). By applying a pulse shaper to generate the phase that is opposite to the phase

error induced by GDR of the CFBG, the sidelobe suppression is improved by ~ 10 dB (blue) than the filter without GDR correction (red). The simulated filter response (blue dashed) is obtained by applying simulated residual phase caused by the limited resolution of pulse shaper (10 GHz spectral resolution) with the measured comb, which is relatively close agreement to the measured response. The experiment sidelobe levels in blue are several dB larger than simulation, and it may be attributed by phase errors and worse spectral resolution than simulation in pulse shaper.

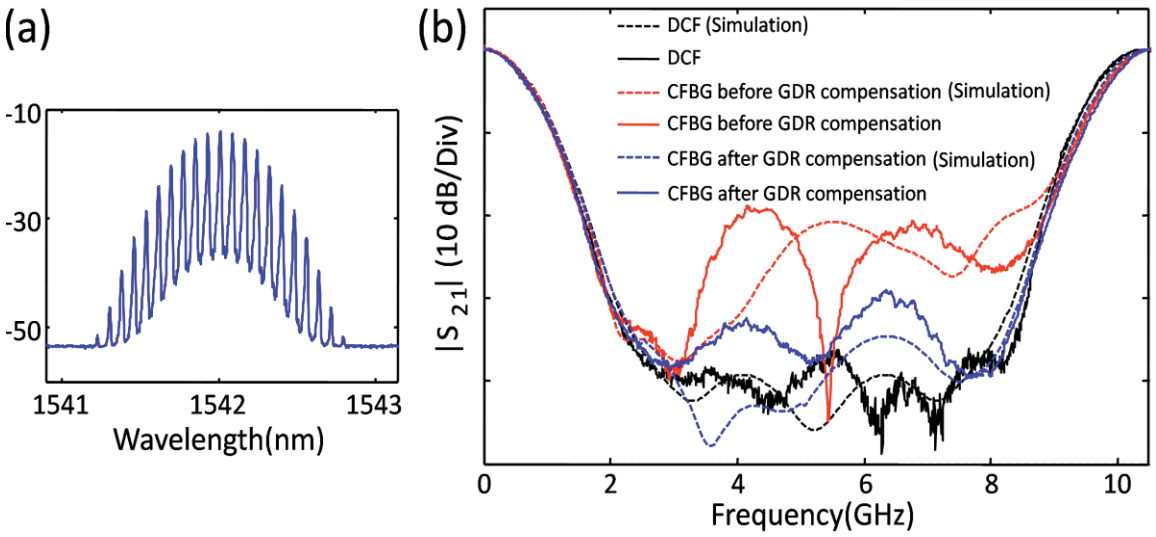

Fig. 5.8 (a) Measured optical spectra of the Gaussian shaped combs, (b) Corresponding filter response measured (solid) and simulated (dashed) when DCF (black) or CFBG (red) is applied as dispersive medium without phase programming, and when GDR of the CFBG is corrected by pulse shaper (blue)

In summary, we have demonstrated a simple and powerful method to measure and correct random GDR through optical spectral phase shaping by a pulse shaper. By running a program to make the tunable laser moves certain wavelength steps, and taking a trace from the sampling scope at each wavelength when the short pulse is passed through CFBGs, we can easily and automatically measure the delay of the output (i.e. group delay and GDR). The measured GDR is integrated and applied to a pulse shaper to compensate the GDR, and the GDR correction is proved by sidelobe suppression

improvement in microwave photonic filters. We have performed a comparative study of the sidelobe suppression of two microwave photonic filter links based on a CFBG and a DCF. The CFBG based filter link including GDR effect shows worse sidelobe suppression than the DCF based filter link. However, by correcting the GDR using a pulse shaper, it shows clear improvement in sidelobe suppression. These results highlight the potential of this technique as a higher order dispersion and/or phase error monitor and compensator in radio-over-fiber communications. Without GDR, the unique features of CFBGs will be attractive for several applications where high acquisition speeds and large accumulated chromatic dispersion are required.

6. SUMMARY AND FUTURE WORK

In this thesis, we presented comprehensive theoretical, simulational, and experimental studies for microwave photonic filters based on optical frequency combs shaping. The main accomplishments of this thesis are the following:

1) In Chapter 2, we experimentally investigated noise characteristic of two MWP filter links using two different multi-wavelength sources: a spectrally coherent opto-electronic frequency comb and a spectrally sliced incoherent ASE source. Although both multi-wavelength sources can be precisely tailored to generate identical MWP filter transfer functions, our experimental results (eye diagram, bit-error-rate (BER), and single-sideband (SSB) spectrum) show that their noise characteristics are completely different. When compared to alternative spectral slicing techniques, MWP filter links based on optical frequency combs support the transmission of wideband microwave signals with a sufficiently high SNR. Although the SNR of MWP filters links can be increased with broader bandwidth ASE sources, this comes at the expense of an inefficient use of bandwidth to keep a sufficiently high SNR. These results show the potential of optical frequency combs as multi-wavelength light sources for MWP applications in radio-over-fiber communications.
2) In Chapter 3, we demonstrated the implementation of reconfigurable tunable flat top microwave photonic filters based on an optical frequency comb shaping. The amplitude and the phase of each comb lines were programmed by line-by-line pulse shaper in interferometric configuration to implement complex tap weights. The versatility of the comb source and the pulse shaper allowed successful demonstration of arbitrary bandpass profile and tunable filters. Arbitrary bandpass (3 dB bandwidth from 1.5 to 3 GHz) of flat-topped filters are

demonstrated by applying 32 positive or negative taps. We also apply a linear phase to the comb using a pulse shaper to achieve filter tuning without changing filter shape. We can further achieve lower passband ripple, narrower transition band and stronger sidelobe suppression of flat top microwave photonic filters with the extension of the number of comb line and the further precise programming of amplitude and phase in pulse shaping.

3) In Chapter 4, we implemented microwave photonic phase filters with complex coefficient taps using an optical frequency comb as the light source in an interferometric configuration. Optical quadratic phase programmed by a pulse shaper has enabled us to synthesize programmable linear electrical chirps in the ~ ns/GHz range, and it is utilized to compress the linearly chirped pulse to its bandwidth limited pulse. Higher chirping rates and large time aperture could be easily achieved by using higher repetition-rate optical frequency combs, larger dispersion amounts, or more comb lines. By applying an ultra-broadband optical frequency comb as the light source, we have shown compression of linearly chirped broad microwave pulses with ~ 8 ns temporal apertures and ~ 4 GHz bandwidth at 10 dB to their bandwidth-limited duration. This work opens a new route for ultra-broad RF phase filtering in large TBWP and long time apertures, compatible with the strong demands of modern wireless communication systems.
4) In Chapter 5, we investigated a GDR compensation of linear CFBG through a phase modulation by a pulse shaper. GD and GDR of a linearly CFBG with dispersion of 1200 ps/nm over 6 nm bandwidth were measured by automated wavelength sweep scheme based on the use of a wavelength-tunable laser. The measured GDR was compensated by phase control via pulse shaping, and the GDR compensation is proved by sidelobe suppression improvement in MWP filters and auto correlation trace. CFBGs without GDR will be attractive for several applications as large accumulated dispersive medium.

There are some possible future improvements and/or directions to extend the work shown from this dissertation.

1) In Chapter 3 and 4 we discussed the construction of complex coefficient taps MWP filters based on a pulse shaper and a DPSK demodulator in an optical interferometer. However, regular pulse shapers based on diffraction grating have resolution typically limited to ~10 GHz, and an interferometric configuration with couplers and a DPSK demodulator increases the filter loss and noise. These limitations can be overcome by using hyperfine 2D pulse shaper based on a VIPA and a 2D LCOS (liquid crystal on silicon) display spatial light modulator. A Fourier transform pulse shaper in a 2D configuration was previously devised by combining a VIPA [123] and a grating in a cross dispersion configuration [124]. Because the fixed mask used in [124] is an amplitude only mask, it causes limitations of programmability and spectral phase control. This limitation was overcome by using a 2D LCOS spatial light modulator [125]. The programmable phase and amplitude modulation using a phase only spatial liquid modulator was implemented by creating super-pixels which are much larger in size to the focused spot size to control the amount of light diffracted, therefore allowing us to modulate also amplitude of the light beam [126]. This novel 2D shaping configuration incorporating a programmable 2D LCOS can be utilized to achieve high resolution complex coefficient taps microwave photonic filters. Instead of using a 1D line-by-line pulse shaper, an optical filter (DPSK demodulator), and an interferometer to generate the complex taps, a 2D line-by-line pulse shaper is only used to implement complex coefficient taps [57]. Apodization and phase errors in pulse shaper caused by limited spectral resolution will be reduced by applying the VIPA spectral disperser. A 2D line-by-line pulse shaper may be also employed for MWP filter channelizer. A single row of SLM pixels in the pulse shaper can generate a complex coefficient taps MWP filter, and ~1000 rows of the shaper enable the generation of complex coefficient taps MWP filter bank. Multichannel RF arbitrary waveform generation based on 2D pulse shaper was implemented in our group [127], and the versatility of 2D shaper will be able to be applied to the generation of RF filter channelizer systems.

2) In Chapter 2 we showed the one path MWP filter scheme, and in Chapter 3 and 4 the two paths MWP filter configuration was introduced to generate complex coefficient taps. According to our measurement, these two MWP filter scheme shows >20dB and >30dB filter insertion loss respectively. The insertion loss of the filter links cause the poor noise figure leading to the degradation of SNR. There are some possible methods to reduce the insertion loss. First, it can be improved by decreasing the half wave voltage of the electro-optic modulator. The link gain is inversely proportional to the square of the half wave voltage, which enables the realization of a lossless modulator (or further increasing the link of the gain) link when it is <1 volt [128,129]. The insertion loss is also can be improved by increasing the power of optical sources. As the optical source power limited by the power handling of the modulator is increased, the optical link can be implemented with low optical link loss, low noise figure, and high spurious-free dynamic range (SFDR) [130]. We also can achieve high power RF output resulting in decrease of the RF photonic link loss [131] by applying the high-current photodetectors with high linearity and large bandwidth. Finally, in Chapter 5, we introduced CFBGs as a highly dispersive medium in optical links. By applying a CFBG which provide large amount of dispersion while having low loss (e.g. CFBG (Proximion): ~1.3dB vs. DCF (OFS): ~4dB of insertion loss over ~±1200 ps/nm dispersion), the insertion loss will be able to be decreased in the optical links.
3) The MWP filter configurations shown in this dissertation were composed of several expensive bulk optical components such as a CW laser source, an optical frequency comb generator, a pulse shaper, optical amplifiers, an electro-optic modulator, and a photodetector. In order to be compatible with microwave filters in cost, loss, size, and so on, the photonic devices should be realized in on-chip level. There have been a lot of challenges to achieve such integrated devices on silicon wafer, which is referred as silicon photonics [132]. The photonic devices such as lasers, modulators, beam splitter, (de)multiplexers, photo-detectors, etc. have been integrated onto small-size chips [133-137]. Our group

also has adopted a silicon photonic scheme to design integrated optical devices such as a microresonator frequency comb generator and an optical diode [138,139]. Although the design, fabrication, and the integration of the different units in one single platform is still a challenge, they provide the building blocks to potentially enable to fully integrate these techniques into silicon photonics.

LIST OF REFERENCES

LIST OF REFERENCES

[1] J. Capmany, and D. Novak, "Microwave photonics combines two worlds," *Nature Photon.*, vol. 1, no. 6, pp. 319-330, Jun. 2007.

[2] J. P. Yao, "Microwave photonics," *J. Lightw. Technol.*, vol. 27, no. 3, pp. 314-335, Feb. 2009.

[3] J. Capmany, B. Ortega, and D. Pastor, "A tutorial on microwave photonic filters," *J. Lightw. Technol.,* vol. 24, no. 1, pp. 201-229, Jan. 2006.

[4] J. P. Yao, "Photonics for ultrawideband communications," *IEEE microwave magazine*, pp. 82-95, Jun. 2009.

[5] A. V. Oppenheim, and R. W. Schafer, Discrete-Time Signal Processing. 3rd Edition, *Prentice-Hall*, 2009.

[6] D. J. Jones, S. A. Diddams, J. K. Ranka, A. Stentz, R. S. Windeler, J. L. Hall, and S. T.Cundiff, "Carrier-envelope phase control of femtosecond mode-locked lasers and direct optical frequency synthesis," *Science*, vol. 288, no. 5466, pp. 635-639, Apr. 2000.

[7] T. Udem, R. Holzwarth, T. W. Hansch, "Optical frequency metrology," *Nature*, vol.416, no. 14, pp. 233-237, Mar. 2002.

[8] Z. Jiang, C.-B. Huang, D. E. Leaird and A. M. Weiner. "Optical arbitrary waveform processing of more than 100 spectral comb lines," *Nature Photon.*, vol. 1, pp. 463-467, Aug. 2007.

[9] T. Ohara, H. Takara, T. Yamamoto, H. Masuda, T. Morioka, M. Abe, and H. Takahashi, "Over-1000-channel ultradense WDM transmission with supercontinuum multicarrier source," *J. Lightw. Technol.,* vol. 24, no. 6, pp. 2311-2317, Jun. 2006.

[10] H. Murata, A. Morimoto, T. Kobayashi, and S. Yamamoto, "Optical pulse generation by electroopticmodulation method and its application to integrated ultrashort pulse generators," *IEEE J. Sel. Top. Quantum Electron.*, vol. 6, no. 6, pp. 1325-1331, Dec. 2000.

[11] R. Wu, V. R. Supradeepa, C. M. Long D. E. Leaird, and A. M. Weiner, "Generation of very flat optical frequency combs from continuous wave lasers using cascaded intensity and phase modulators driven by tailored radio frequency waveforms," *Opt. Lett.*, vol. 35, no. 19, pp. 3234-3236, Oct. 2010.

[12] V. Torres-Company, J. Lancis, and P. Andres, "Lossless equalization of frequency combs," *Opt. Lett.,* vol. 33, no. 16, pp. 1822-1824, Aug. 2008.

[13] C.-B. Huang, S.-G. Park, D.E. Leaird, and A.M. Weiner, "Nonlinearly broadened phase-modulated continuous-wave laser frequency combs characterized using DPSK decoding," *Opt. Exp.*, vol. 16, no. 4, pp. 2520-2527, Feb. 2008.

[14] P. Del'Haye, A. Schliesser, O. Arcizet, T. Wilken, R. Holzwarth and T. J. Kippenberg, "Optical frequency comb generation from a monolithic microresonator," *Nature*, vol. 450, pp. 1214-1217, Dec. 2007.

[15] D. E. Leaird and A. M. Weiner, "Femtosecond direct space-to-time pulse shaping," *IEEE J. Quantum Electron.*, vol. 37, no. 4, pp. 494-504, Apr. 2001.

[16] J. D. McKinney, D. Seo, and A. M. Weiner, "Direct space-to-time pulse shaping at 1.5um," *IEEE J. of Quantum Electron*., vol. 39, no. 12, pp.1635-1644, Dec. 2003.

[17] A. M. Weiner. "Femtosecond pulse shaping using spatial light modulators," *Rev. Sci. Instr.*, vol. 71, no. 5, pp. 1929–1960, May 2000.

[18] Z. Jiang, D. S. Seo, D. E. Leaird and A. M. Weiner. "Spectral line-by-line pulse shaping," *Opt. Lett.*, vol. 30, no. 12, pp. 1557-1559, Jun. 2005.

[19] Z. Jiang, D. E. Leaird and A. M. Weiner. "Optical arbitrary waveform generation and characterization using spectral line-by-line control," *J. Lightw. Techn.*, vol. 24, no. 7, pp. 2487-2494, Jul. 2007.

[20] G. Tsuzuki, S. Ye, and S. Berkowitz, "Ultra-selective 22-pole 10-transmission zero superconducting bandpass filter surpasses 50-pole Chebyshev filter," *IEEE Trans. Microw. Theory Techn*., vol. 50, no. 12, pp. 2924-2929, Dec. 2002.

[21] X. Liu, L. P. B. Katehi, W. J. Chappell, D. Peroulis, "Power handling of electrostatic MEMS evanescent-mode (EVA) tunable bandpass filters," *IEEE Trans. Microw. Theory Techn*., vol. 60, no. 2, pp. 270-283, Feb. 2012.

[22] H. Chen, A. W. Fang, J. D. Peters, Z. Wang, J. Bovington, D. Liang, and J. E. Bowers, "Integrated microwave photonic filter on a hybrid silicon platform," *IEEE Trans. Microw. Theory Techn*., vol. 58, no. 11, pp. 3213-3219, Nov. 2010.

[23] E. J. Norberg, R. S. Guzzon, J. S. Parker, L. A. Johansson, and L. A. Coldren, "Programmable photonic microwave filters monolithically integrated in InP-InGaAsP," *J. Lightw. Techn.*, vol. 29, no. 11, pp. 1611-1619,Jun. 2011.

[24] A. M. Weiner, Ultrafast Optics, 1st Edition. *New York: Wiley*, 2009.

[25] M. Song, V. Torres-Company, and A. M. Weiner, "Noise comparison of RF photonic filters based on coherent and incoherent multiwavelength sources," *IEEE Photon. Tech. Lett.*, vol. 24, no. 14, pp. 1236-1238, Jul. 2012.

[26] J. Capmany, D. Pastor, and B. Ortega, "New and flexible fiber-optic delay-line filters using chirped Bragg gratings and laser arrays," *IEEE Trans. Microw. Theory Techn.*, vol. 47, no. 7, pp. 1321-1326, Jul. 1999.

[27] D. B. Hunter, and R. A. Minasian, "High-quality online-reconfigurable microwave photonic transversal filter with positive and negative coefficients," *IEEE Microw. Guided Wave Lett.*, vol. 6, no. 2, pp. 103-105, Feb. 1996.

[28] J. H. Lee, Y. M. Chang, Y. G. Han, S. B. Lee, and H. Y. Chung, "Fully reconfigurable photonic microwave transversal filter based on digital micromirror device and continuous-wave, incoherent supercontinuum source," *Appl. Opt.*, vol. 46, no. 22, pp. 5158-5167, Aug. 2007.

[29] J. Mora, L. R. Chen, and J. Capmany, "Single-banpass microwave photonic filter with tuning and reconfiguration capabilities," *J. Lightw. Techn.*, vol. 26, no. 15, pp. 2663-2670, Aug. 2008.

[30] J. Capmany, J. Mora, D. Pastor, and B. Ortega, "High-quality online-reconfigurable microwave photonic transversal filter with positive and negative coefficients," *IEEE Photon. Tech. Lett.*, vol. 17, no. 12, pp. 2730-2732, Dec. 2005.

[31] X. K. Yi, and R. A. Minasian, "Noise mitigation in spectrum sliced microwave photonic signal processors," *J. Lightw. Techn.*, vol. 24, no. 12, pp. 4959-4965, Dec. 2006.

[32] J. Rutman and F. L. Walls, "Chracterization of frequency stability in precision frequency sources," *Proc. of the IEEE*, vol. 79, no. 6, pp. 952-960, Jun. 1991.

[33] A. Demir, A. Mehrotra, and J. Roychowdhury, "Phase noise in oscillators: a unifying theory and numerical methods for chracterization," *IEEE Trans. Circuits and Syst.*, vol. 47, pp. 655-674, May 2000.

[34] U. Gliese, S. Norskov, and T. N. Nielsen, "Chromatic dispersion in fiber- optic microwave and millimeter-wave links," *IEEE Trans. Microw. Theory Tech.*, vol. 44, no. 10, pp. 1716–1724, Oct. 1996.

[35] B. Pourbahri, P. A. Davies, D. S. George, and D. Wake, "The effects of fiber amplifier phase noise on radio over fibre signals," *in Proc. Broad-band commun*., pp. 89-91, Feb. 2000.

[36] G. Qi *et al.,* "Phase-noise analysis of optically generated millimeter-wave signals with external optical modulation techniques," *J. Lightw. Techn*., vol. 24, no. 12, pp. 4861-4875, Dec. 2006.

[37] X. Xue, X. Zheng, H. Zhang, and B. Zhou, "Noise reduction by balanced detection in microwave photonic filters based on optical broadband sources," *Conference of Lasers and Electro-Optics (CLEO)*, Baltimore, ML, May 2011.

[38] E. Hamidi, D. E. Leaird, A. M. Weiner, "Tunable programmable microwave photonic filters based on an optical frequency comb," *IEEE Trans. Microw. Theory Techn*., vol. 58, no. 11, pp. 3269-3278, Nov. 2010.

[39] A. Ortigosa-Blanch, J. Mora, J. Capmany, B. Ortega, and D. Pastor, "Tunable radio-frequency photonic filter based on an actively mode-locked fiber laser," *Opt. Lett*., vol. 31, no. 6, pp. 709-711, Mar. 2006.

[40] V. R. Supradeepa, C. M. Long, R. Wu, F. Ferdous, E. Hamidi, D. E. Leaird, and A. M. Weiner, "Comb-based radiofrequency photonic filters with rapid tenability and high selectivity," *Nature Photon.,* vol. 6, pp. 186-194, Feb. 2012.

[41] J. Capmany, B. Ortega, D. Pastor, and S. Sales, "Discrete-time optical processing of microwave signals," *J. Lightw. Technol.,* vol. 23, no. 2, pp. 702-723, Feb. 2005.

[42] K. Takano, Y. Naganuma, and K. Nakagawa, "Performance analysis of optical single sideband modulation based on Mach-Zehnder interferometers and its dispersive fiber transmission," *IEICE Trans. Commun*., vol. E88-B, no. 5, pp. 1994-2003, May 2005.

[43] G. J. Pendock and D. D. Sampson, "Transmission performance of high bit rate spectrum-sliced WDM systems," *J. Lightw. Technol*., vol. 14, no. 14, pp. 2141-2148, Oct. 1996.

[44] F. Grassi, J. Mora, B. Ortega, and J. Capmany, "Radio over fiber transceiver employing phase modulation of an optical broadband source", *Opt. Exp.,* vol. 18, no. 21, pp. 21750-21756, Sep. 2010.

[45] M. Song, C. M. Long, R.Wu, D. S. Seo, D. E. Leaird, and A. M. Weiner, "Reconfigurable and tunable flat-top microwave photonic filter utilizing optical frequency combs," *IEEE Photon. Tech. Lett*, vol. 23, no. 21, pp. 1618-1620, Nov. 2011.

[46] F. J. Harris, "On the use of windows for harmonic analysis with the discrete fourier transform," *Proc. IEEE*, vol. 66, no. 1, pp. 51-83, Jan. 1978.

[47] B. Ortega, D. Pastor, J. Mora, J. Capmany, and M. V. Andres, "Advanced optical processing of microwave signals," *EURASIP J. Appl. Signal Process,* vol. 2005, no. 10, pp. 1462-1484, Jun. 2005.

[48] T. Chen, X. Yi, T. Huang, and R. A. Minasian, "Multiple-bipolar-tap tunable spectrum sliced microwave photonic filter," *Opt. Lett*., vol. 35, no. 23, pp. 3934-3936, Dec. 2010.

[49] D. B. Hunter, "Incoherent bipolar tap microwave photonic filter based on balanced bridge electro-optic modulator," *Electon. Lett*., vol. 40, no. 14, pp. 856-858, Jul. 2004.

[50] Y. Dai, and J. P. Yao, "Nonuniformly-spaced photonic microwave delay-line filter," *Opt. Exp*., vol. 16, no. 7, pp. 4713-4718, Mar. 2008.

[51] F. Coppinger, S. Yegnanarayanan, P. D. Trinh, B. Jalali, and I. L. Newberg, "Nonrecursive tunable photonic filter using wavelength-selec true time delay," *IEEE Photon. Tech. Lett.*, vol. 8, no. 9, pp. 1214–1216, Sep. 1996.

[52] D. Norton, S. Johns, C. Keefer, and R. Soref, "Tunable microwave filtering using high dispersion fiber time delays," *IEEE Photon. Tech. Lett.*, vol. 6, no. 7, pp. 831–832, Jul. 1994.

[53] D. B. Hunter, R. A. Minasian, and P. A. Krug, "Tunable optical transversal filter based on chirped gratings," *Electron. Lett.*, vol. 31, no. 25, pp. 2205–2207, Dec. 1995.

[54] J. Mora, B. Ortega, M. V. Andres, J. Capmany, J. L. Cruz, D. Pastor, and S. Sales, "Tunable dispersion device based on a tapered fiber Bragg grating and nonuniform magnetic fields," *IEEE Photon. Tech. Lett.*, vol. 15, no. 7, pp. 951–953, Jul. 2003.

[55] M. Sagues, A. Loayssa, and J. Company, "Multi-tap complex-coefficient incoherent microwave photonic filters based on stimulated Brillouin scattering," *IEEE Photon. Tech. Lett*., vol. 19, no. 16, pp. 1194-1196, Aug. 2007.

[56] T. Mengual, B. Vidal, and J. Marti, "Continuously tunable photonic microwave filter based on a spatial light modulator," *Opt. Commun.*, vol. 281, no. 10, pp. 2746–2749, May 2008.

[57] X. Yi, T. X. H. Huang, and R. A. Minasian, "Tunable and reconfigurable photonic signal processor with programmable all-optical complex coefficients," *IEEE Trans. Microw. Theory Techn*., vol. 58, no. 11, pp. 3088-3093, Nov. 2010.

[58] M. Sagues, R. G. Olcina, A. Loayssa, S. Sale, and J. Company, "Multi-tap complex-coefficient incoherent microwave photonic filters based on optical single-sideband modulation and narrow band optical filtering," *Opt. Exp*., vol. 16, no. 1, pp. 295-303, Jan. 2008.

[59] P. Karivaratharajan, "Procedure for the generation of equiripple functions," *Electon. Lett*., vol. 9, no. 22, pp. 522-523, Nov. 1973.

[60] J. H. McClellan, T. W. Parks, and L.R. Rabiner, "FIR linear phase filter design program," *IEEE Press, New York, NY*, pp. 5.1-1-5.1-13, 1979.

[61] J. Lee, E. J. Naglich, H. H. Sigmarsson, D. Peroulis and W.J. Chappell, "Tunable inter-resonator coupling structure with positive and negative values and its application to the field-programmable filter array (FPFA)," *IEEE Trans. Microw. Theory Tech*., vol. 59, no. 12, pp. 3389-3400, Dec. 2011.

[62] H. Joshi, H. H. Sigmarsson, S. Moon, D. Peroulis, and W. J. Chappell, "High-Q fully reconfigurable tunable bandpass filters," *IEEE Trans. Microw. Theory Tech.*, vol. 57, no. 12, pp. 3525-3533, Dec. 2009.

[63] S. J. Park, I. Reines, C. Patel, and G. M. Rebeiz, "High-Q RF-MEMS 4-6-GHz tunable evanescent-mode cavity filter," *IEEE Trans. Microw. Theory Tech.*, vol. 58, no. 2, pp. 381-389, Feb. 2010.

[64] V. R. Supradeepa, C. M. Long, D. E. Leaird, and A. M. Weiner, "Fast characterization of dispersion and dispersion slope of optical fiber links using spectral interferometry with frequency combs," *IEEE Photon. Tech. Lett*, vol. 22, no. 3, pp. 155-157, Feb. 2010.

[65] E. Hamidi, R. Wu, V. R. Supradeepa, C. M. Long, D. E. Leaird, and A. M. Weiner, "Tunable radio frequency photonic filter based on intensity modulation of optical combs," *International Topical Meeting on Microwave Photonics*, Montreal, Canada, Oct. 2010.

[66] M. Song, V. Toress-Company, R. Wu, E. Hamidi, and A. M. Weiner, "Programmable multi-tap microwave photonic phase filtering via optical frequency comb shaping," *International Topical Meeting on Microwave Photonics*, Singapore, Oct. 2011.

[67] M. Song, V. Torres-Company, A. J. Metcalf, and A. M. Weiner, "Multitap microwave photonic filters with programmable phase response via optical frequency comb shaping," *Opt. Lett*., vol. 37, no. 5, pp. 845-847, Mar. 2012.

[68] M. Song, R. Wu, V. Toress-Company, and A. M. Weiner, "Programmable microwave photonic phase filters with large time-bandwidth product based on ultra-

broadband optical frequency comb generation," *International Topical Meeting on Microwave Photonics*, Noordwijk, Netherlands, Sep. 2012.

[69] E. Hamidi, and A. M. Weiner, "Phase-only matched filtering ultrawideband arbitrary microwave waveforms via optical pulse shaping," *J. Lightw. Technol*., vol. 26, no. 15, pp. 2355-2363, Aug. 2008.

[70] E. Hamidi, and A. M. Weiner, "Post-compensation of ultra-wideband antenna dispersion using microwave photonic phase filters and its applications to UWB systems," *IEEE Trans. Microw. Theory Techn*., vol. 57, no. 4, pp. 890-898, Apr. 2009.

[71] B. Ortega, J. L. Cruz, J. Capmany, M. V. Andres, and D. Pastor, "Variable delay line for phased-antenna based on a chirped fiber grating," *IEEE Trans. Microw. Theory Tech.*, vol. 48, no. 8, pp. 1352-1360, Aug. 2000.

[72] Y. Liu, J. Yang, and J. Yao, "Cotinuous true-time-delay beamforming for phased array antenna using a tunable chirped fiber grating delay line," *IEEE photon. Tech. Lett*., vol. 14, no. 8, pp. 1172-1174, Aug. 2002.

[73] D. B. Hunter, M. E. Parker, and J. L. Dexter, "Demonstration of a continuously variable true-time delay beamformer using a multichannel chirped fiber grating," *IEEE Trans. Microw. Theory Tech*., vol. 54, no. 2, pp. 861-867, Feb. 2006.

[74] P. Tortoli, F. Guidi, and C. Atzeni, "Digital vs SAW matched filter implementation for radar pulse compression," *Proc. IEEE Ultrason. Symp*., vol. 1, pp. 199-202, 1994.

[75] J. D. McKinney and A. M. Weiner, "Compensation of the effects of antenna dispersion on UWB waveforms via optical pulse shaping techniques," *IEEE Trans. Microw. Theory Tech*., vol. 54, no. 4, pp. 1681-1686, Apr. 2006.

[76] S. J. Xiao and A. M. Weiner, "Programmable photonic microwave filters with arbitrary ulra-wideband phase response," *IEEE Trans. Microw. Theory Techn.,* vol. 54, no. 11, pp. 4002-4008, Nov. 2006.

[77] S. J. Xiao and A. M. Weiner, "Coherent Fourier transform electrical pulse shaping," *Opt. Exp.*, vol. 14, no. 7, pp.3073-3082, Apr. 2006.

[78] M. A. G. Laso, T. Lopetegi, M. J. Erro, D. Benito, M. J. Garge, M. A. Muriel, M. Sorolla, and M. Guglielmi, "Real-time spectrum analysis in microstrip technology," *IEEE Trans. Microw. Theory Techn.*, vol. 51, no. 3, pp. 705-717, Mar. 2003.

[79] J. D. Schwartz, J. Azaña, and D. V. Plant, "A fully electronic system for the time magnification of ultra-wideband signals," *IEEE Trans. Microw. Theory Techn.*, vol. 55, no. 2, pp. 327-334, Feb. 2007.

[80] G. N. Saddik, R. S. Singh, and R. Brown, "Ultra-wideband multifunctional communications/radar system," *IEEE Trans. Microw. Theory Techn.*, vol. 55, no. 7, pp. 1431-1437, Jul. 2007.

[81] M. Bolea, J. Mora, B. Ortega, and J. Capmany, "Highly chirped single bandpass microwave photonic filter with reconfiguration capabilities," *Opt. Exp.*, vol. 19, no. 5, pp. 4566-4576, Feb. 2011.

[82] Y. Park and J. Azaña, "Ultrahigh dispersion of broadband microwave signals by incoherent photonic processing," *Opt. Exp.,* vol. 18, no. 14, pp. 14752-14761, Jul. 2010.

[83] R. Wu, C. M. Long, D. E. Leaird, and A. M. Weiner, "Directly generated Gaussian-shaped optical frequency comb for microwave photonic filtering and picoseconds pulse generation," *IEEE photon. Tech. Lett.*, vol. 24, no. 17, pp. 1484-1486, Sep. 2012.

[84] E. Hamidi, M. Song, R.Wu, V. R. Supradeeap, C. M. Long, D. E. Leaird, and A. M. Weiner, "Multitap Microwave Photonic Phase Filter," *Conference of Lasers and Electro-Optics (CLEO)*, Baltimore, ML, May 2011.

[85] G. L. Turin, "An introduction to matched filters," *IRE Trans. Inf. Theory*, vol. 6, no. 3, pp. 311-329, Jun. 1960.

[86] J. G. Proakis, Digital Communications, 4th ed. New York: McGraw-Hill, 2001.

[87] M. Li, A. Malacarne, N. Belhadj, S. LaRochelle, J. Yao, and J. Azana, "Reconfigurable optical fiber-based microwave dispersive line for single-shot chirped microwave pulse compression", *International Topical Meeting on Microwave Photonics*, Singapore, Oct. 2011.

[88] R. Wu, V. Torres-Company, D.E. Leaird, A.M. Weiner, "10-GHz Flat-topped Optical Frequency Comb with Ultra-broad Bandwidth", *Conference of Lasers and Electro-Optics (CLEO)*, San Jose, CA, May 2012.

[89] T. Inoue, and S. Namiki, "Pulse compression techniques using highly nonlinear fibers", *Las. Phot. Rev.*, vol. 2, no. 1-2, pp. 83-99, Mar. 2008.

[90] C. Finot, B. Kibler, L. Provost, and S. Wabnitz, "Beneficial impact of wave-breaking for coherent continuum generation in normally dispersive nonlinear fibers", *J. Opt. Soc. Am. B,* vol. 25, no. 11, pp. 1938-1948, Nov. 2008.

[91] R. Wu, C. M. Long, D. E. Leaird and A. M. Weiner, "Directly Generated Gaussian-shaped Optical Frequency Comb for Microwave Photonic Filtering and Picosecond Pulse Generation," *IEEE photon. Tech. Lett.*, vol. 24, no. 17, pp. 1484-1486, Sep. 2012.

[92] V. R. Supradeepa, C. M. Long, D. E. Leaird, and A. M. Weiner, "Self-referenced characterization of optical frequency combs and arbitrary waveforms using a simple, linear, zero-delay implementation of spectral shearing interferometry," *Opt. Exp.*, vol. 18, no. 17, pp. 18171-18179, Aug. 2010.

[93] K. O. Hill, Y. Fujii, D. C. Johnson, and B. S. Kawasaki, "Photosensitivity in optical fiber wave guides: Application to reflection filter fabrication," *Appl. Phs. Lett.*, vol. 32, no. 10, pp. 647-649, May 1978.

[94] K. O. Hill, and G. Meltz, "Fiber Bragg grating technology fundamentals and overview," *J. Lightw. Technol.*, vol. 15, no. 8, pp. 1263-1276, Aug. 1997.

[95] R. Kashyap, Fiber Bragg Gratings, *Academic*, 1999.

[96] B. J. Eggleton, A. Ahuja, P. S. Westbrook, J. A. Rogers, P. Kuo, T. N. Nielsen, and B. Mikkelsen, "Integrated tunable fiber gratings for dispersion management in high-bit rate systems," *J. Lightw. Technol.*, vol. 18, no. 10, pp. 1418-1432, Oct. 2000.

[97] R. E. Saperstein, N. Alic, D. Panasenko, R. Rokitski, and Y. Fainman, "Time-domain waveform processing by chromatic dispersion for temporal shaping of optical pulses," *J. Opt. Soc. Am. B*, vol. 22, no. 11, pp. 2427-1120, Nov. 2005.

[98] R. E. Saperstein, N. Alic, S. Zamek, K. Ikeda, B. Slutsky, and Y. Fainman, "Processing advantages of linear chirped fiber Bragg gratings in the time domain realization of optical frequency-domain refletometry," *Opt. Exp.,* vol. 15, no. 23, pp. 15464-15478, Nov. 2007.

[99] Y. Park, T. Ahn, J. Kieffer, and J. Azaña, "Optical frequency domain reflectometry based on real-time Fourier transformation," *Opt. Exp.,* vol. 15, no. 8, pp. 4597-4616, Apr. 2007.

[100] M. Abtahi, M. Dastralchi, S. LaRochelle, and L. A. Rusch, "Generation of arbitrary UWB waveforms by spectral pulse shaping and thermally-apodized FBGs," *J. Lightw. Technol.*, vol. 27, no. 23, pp. 5276-5283, Dec. 2009.

[101] R. E. Saperstein, and Y. Fainman, "Information processing with longitudinal spectral decomposition of ultra pulses," *Appl. Opt.,* vol. 47, no. 4, pp. A21-A31, Feb. 2008.

[102] M. A. Muriel, J. Azaña, and A. Carballar, "Real-time Fourier transformer based on fiber gratings," *Opt. Lett.,* vol. 24, no. 1, pp. 1-3, Jan. 1999.

[103] J. Azaña, and M. A. Muriel, "Real-time optical spectrum analysis based on the time-space duality in chirped fiber gratings," *IEEE J. of Quantum Electron.,* vol. 36, no. 5, pp. 517-526, May 2000.

[104] http://www.proximion.com/Technology/Fiber_Bragg_Grating_based_DCMs.

[105] C. C. Chang, H. P. Sardesai, and A. M. Weiner, "Dispersion-free fiber transmission for femtosecond pulses by use of a dispersion-compensating fiber and a programmable pulse shaper," *Opt. Lett*., vol. 23, no. 4, pp. 283-285, Feb. 1998.

[106] Z. Jiang, S. D. Yang, D. E. Leaird, and A. M. Weiner, "Fully dispersion-compensated ~500 fs pulse transmission over 5- km single-mode fiber," *Opt. Lett.*, vol. 30, no. 12, pp. 1449-1451, Jun. 2005.

[107] J. C. Cartledge, "Effect of modulator chirp and sinusoidal group delay ripple on the performance of systems using dispersion compensating gratings," *J. Lightw. Technol*., vol. 20, no. 11, pp. 1918-1923, Nov. 2002.

[108] http://www.proximion.com/Products/DCM-PC.

[109] A. V. Buryak and D. Y. Stepanov, "Correction of systematic errors in the fabrication of fiber Bragg gratings," *Opt. Lett.,* vol. 27, no. 13, pp 1099-1101, Jul. 2002.

[110] T. Komukai, T. Inui, M. Kurihara, S. Fujimoto, "Group-delay ripple reduction in step-chirped fiber Bragg gratings by using laser-beam written step-chirped phase masks," *IEEE Photon. Tech. Lett.,* vol. 14, no. 11, pp. 1554- 1556, Nov. 2002.

[111] P. I. Reyes, M. Sumetsky, N. M. Litchinitser, and P. S. Westbrook, "Reduction of group delay ripple of multi-channel chirped fiber gratings using adiabatic UV correction," *Opt. Exp.,* vol. 12, no. 12, pp. 2676-2687, Jun. 2004.

[112] N. Oguma, T. Kitoh, A. Mori, and H. Takahashi, "Ultrawide-passband tandem MZI-synchronized AWG and group delay ripple balancing out technique," *European conference and exhibition on optical communication*, Torino, Italy, Sep. 2010.

[113] J. A. Conway, G. A. Sefler, J. T. Chou, and G. C. Valley, "Phase ripple correction: theory and application," *Opt. Lett.,* vol. 33, no. 10, pp 1108-1110, May 2008.

[114] M. Westhäuser, M. Finkenbusch, C. Remmersmann, S. Pachnicke, "Optical filter-based mitigation of group delay ripple and PMD-related penalties for high-capacity metro networks," *J. Lightw. Technol*., vol. 29, no. 16, pp. 2350-2357, Aug. 2011.

[115] M. Westhäuser, C. Remmersmann, S. Pachnicke, B. Johansson, and P. M. Krummrich, "Reducing fiber Bragg-grating induced group delay ripples in 112 Gbit/s metro networks using generically initialized transversal filters," *ITG symposium on photonic networks*, Leipzig, Germany, May 2010.

[116] M. U. Piracha, D. Nguyen, and P. J. Delfyett, "A chirped fiber Bragg grating with ripple free group delay and its application in laser ranging," *Conference of Lasers and Electro-Optics (CLEO)*, San Jose, CA, May 2012.

[117] T. J. Ahn, Y. Park, and J. Azaña, "Fast and accurate group delay ripple measurement technique for ultralong chirped fiber Bragg grating," *Opt. Lett.,* vol. 32, no. 18, pp. 2674- 2676, Sep. 2007.

[118] F. Li, Y. Park, and J. Azaña, "Group delay characterization of dispersive devices using a pulse temporal intensity measurement setup," *IEEE Photon. Tech. Lett.,* vol. 20, no. 24, pp. 2042- 2044, Dec. 2008.

[119] S. D. Dyer, and K. B. Rochford, "Low-coherence interferometric measurements of fibre Bragg grating dispersion," *Electron. Lett.,* vol. 35, no. 17, pp. 1485- 1486, Aug. 1999.

[120] T. Niemi, M. Uusimaa, and H. Ludvigsen, "Limitations of phase-shift method in measuring dense group delay ripple of fiber bragg gratings," *IEEE Photon. Tech. Lett.,* vol. 13, no. 12, pp. 1334- 1336, Dec. 2001.

[121] D. K. Gifford, B. J. Soller, M. S. Wolfe, and M. E. Froggatt, "Optical vector network analzer for single-scan measurements of loss, group delay, and polarization mode dispersion," *Appl. Opt.,* vol. 44, no. 34, pp. 7282-7286, Dec. 2005.

[122] M. Froggatt, T. Erdogan, J. Moore, and S. Shenk, "Optical frequency domain characterization (OFDC) of dispersion in optical fiber Bragg gratings," *OSA Technical Digest Series (Optical Society of America, Washington, DC, 1999)*, paper FF2, 1999.

[123] M. Shirasaki. "Large angular dispersion by a virtually imaged phased array and it's application to a wavelength division multiplexer," *Opt. Lett*., vol. 21, no. 5, pp. 366–368, Mar. 1996.

[124] V. R. Supradeepa, Chen-Bin Huang, Daniel E. Leaird, and Andrew M. Weiner, "Femtosecond pulse shaping in two dimensions: Towards higher complexity optical waveforms," *Opt. Exp.*, vol. 16, no. 16, pp. 11878-11887, Aug. 2008.

[125] V. R. Supradeepa, Daniel E. Leaird, and Andrew M. Weiner, "Programmable high resolution broadband pulse shaping using a 2D VIPA grating pulse shaper with a liquid crystal on silicon (LCOS) spatial light modulator," *International Conference on Ultrafast Phenomena*, Snowmass Village, CO, Jul. 2010.

[126] J. C. Vaughan, T. Hotnung, T. Feurer, and K. A. Nelson, "Diffraction-based femtosecond pulse shaping with a two-dimensional spatial light modulator," *Opt. Lett.*, vol. 30, no. 3, pp. 323-325, Feb. 2005.

[127] V. Torres-Company, A. J. Metcalf, D. E. Leaird, and A. M. Weiner, "Multichannel radio-frequency arbitrary waveform generation based on multi-wavelength comb switching and 2-D line-by-line pulse shaping," *IEEE Photon. Tech. Lett*, vol. 24, no. 11, pp. 891-893, Jun. 2012.

[128] Y. Shi, C. Zhang, H. Zhang, J. H. Bechtel, L. R. Dalton, B. H. Robinson, and W. H. Steier, "Low (sub-1-volt) halfwave voltage polymeric electro-optic modulators achieved by controlling chromophore shape," *Science,* vol. 288, no. 5463, pp. 119-122, Apr. 2000.

[129] T. Baehr-Jones, B. Penkov, J. Huang, P. Sullivan, J. Davies, J. Takayesu, J. Luo, T. Kim, L. Dalton, A. Jen, M. Hochberg, and A. Scherer, "Nonlinear polymer-clad silicon slot waveguide modulator with a half wave voltage of 0.25V," *Appl. Phys. Lett.,* vol. 92, no. 16, pp. 163303-1-163303-3, Apr. 2008.

[130] R. DeSalvo, C. Middleton, M. Poulin, C. Latrasse, M. Morin, S. Ayotte, and F. Costin, "System impacts of modulation technology and phase noise on coherent analog optical links," *Optical Fiber Communication (OFC) Conference*, Los Angeles, CA, Mar. 2011.

[131] Z. Li, Y. Fu, M. Piels, H. Pan, A. Beling, J. E. Bowers, and J. C. Campbell, "High-power high-linearity flip-chip bonded modified uni-traveling carrier photodiode," *Opt. Exp.*, vol. 19, no. 26, pp. 385-390, Dec. 2011.

[132] B. Jalali and S. Fathpour, "Silicon photonics," *J. Lightw. Technol.*, vol. 24, no. 12, pp. 4600-4615, Dec. 2006.

[133] H. Rong, S. Xu, Y. Kuo, V. Sih, O. Cohen, O. Raday, and M. Paniccia, "Low-threshold continuous-wave Raman silicon laser," *Nature,* vol. 1, pp. 232-237, Apr. 2007.

[134] Y. Li, L. S. Stewart, and P. D. Dapkus, "High speed silicon microring modulator employing dynamic intracavity energy balance," *Opt. Exp.,* vol. 20, no. 7, pp. 7404-7414, Mar. 2012.

[135] D. Dai, J. Bauters, and J. E. Bowers, "Passive technologies for future large-scale photonic integrated circuits on silicon: polarization handlind, light non-reciprocity and loss reduction," *Nature,* vol. 1, pp. 1-12, Mar. 2012.

[136] F. Horst, W. M. J. Green, B. J. Offrein, and Y. A. Vlasov, "Silicon-on-insulator echelle grating WDM demultiplexers with two stigmatic points," *IEEE Photon. Tech. Lett*, vol. 21, no. 23, pp. 1743-1745, Dec. 2009.

[137] S. Assefa, F. Xia, and Y. A. Vlasov, "Reinventing nanophotonic avalanche photodetector for on chip optical interconnects," *Nature,* vol. 464, pp. 80-84, Mar. 2010.

[138] F. Ferdous, H. Miao, D. E. Leaird, K. Srinivasan, J. Wang, Lei Chen, L. T. Varghese, and A. M. Weiner, "Spectral line-by-line pulse shaping of on-chip microresonator frequency combs," *Nature Photon.,* vol. 9, pp. 770-776, Oct. 2011.

[139] L. Fan, J. Wang, L. T. Varghese, H. Shen, B. Niu, Y. Xuan, A. M. Weiner, and M. Qi, "An all-silicon passive optical diode," *Science,* vol. 335, pp. 447-450, Jan. 2012.

VITA

VITA

Minhyup Song was born in Seoul, Korea in 1981. He received his BS degree in Electrical Engineering from Korea University, Seoul, Korea, in 2006. Since 2008, he has been pursuing his Direct Ph.D. degree at Purdue University, West Lafayette, IN, USA. He has performed researches in the Ultrafast Optics and Optical Fiber Communications Laboratory on microwave photonic filter design based on optical frequency comb source.

During the course of his graduate study, Minhyup has authored/co-authored over 10 publications in conferences and journals. He is a student member of the Optical Society of America and IEEE Photonics Society. He has served as a reviewer for Journal of Optics Express and Journal of the Optical Society of America B.